Model-based Development of Thermoelectric Energy Harvesting Systems

Modellbasierte Entwicklung von thermoelektrischen Energy Harvesting Systemen

Dissertation

zur Erlangung des Grades

des Doktors der Ingenieurwissenschaften

der Naturwissenschaftlich-Technischen Fakultät

der Universität des Saarlandes

von

Dipl.-Ing. Marco Nesarajah

Saarbrücken

2017

Tag des Kolloquiums:	26.09.2017
Dekan:	Univ.-Prof. Dr. rer. nat. Guido Kickelbick
Mitglieder des	
Prüfungsausschusses:	
Vorsitzender:	Univ.-Prof. Dr.-Ing. Michael Vielhaber
Gutachter:	Univ.-Prof. Dr.-Ing. Georg Frey
	Univ.-Prof. Dr.-Ing. Jürgen Köhler
Akademischer Mitarbeiter:	Dr. rer. nat. Tilman Sauerwald

Acknowledgments

I have worked on my dissertation for more than four years and now I am very proud of having finished it. Of course, this would not have been possible without the help, support and understanding of many people. Therefore, I would like to thank these persons very much for having been a good support in this phase of my life.

First of all, I would like to thank my doctoral advisor Professor GEORG FREY, who offered me the opportunity to join his team, the Chair of Automation and Energy Systems at Saarland University. He helped me to find the promising subject of this thesis and always gave me guidance, advice and encouragement during my work. I thank him for the trust and intellectual freedom he has provided to me, from which I learned proper and independent research.

Besides Professor GEORG FREY, I would like to thank the other members of the evaluation board: Professor JÜRGEN KÖHLER from the Technische Universität Braunschweig, chairman Professor MICHAEL VIELHABER, and DR. TILMAN SAUERWALD, both from Saarland University.

I warmly thank the complete staff of the Chair of Automation and Energy Systems for allowing it to be a second home for me during my PhD. I shared a wonderful time and wonderful moments with you all. Thank you for your friendship, your honesty and the enjoyable moments we spent together. Particularly noteworthy is my roommate LUKAS EXEL, who was always ready with advice and support.

I would like to offer my thanks to the (former) student workers and assistants FLORIAN SCHWITZGEBEL, ROMAN WALETZKE, RAJA REHAN KHALID, MAXIMILIAN BERNAT and THOMAS KREIS for their contribution to this work; and to DR. FELIX FELGNER, whose basic work made my dissertation possible in the first place. Moreover, I am deeply grateful to our institute's technician MANFRED RACHOR, who gives me a lot of support building up my hardware projects.

To DR. FELIX FELGNER, DANNY JONAS, and LEANDER REINERT: Many thanks for proofreading the manuscript and hinting at a considerable number of flaws I was able to eliminate with your help. Moreover, I thank KATE RAU for checking the English language of this work.

Last but not least, my sincerest thanks go to my family: My dear PARENTS, for their love, their support and the opportunities they have given me and my TWO SISTERS, who are always there for me. Finally I want to thank my lovely partner KATHI for her understanding and support, especially in the final phase of this work.

Saarbrücken, December 2017 Marco Nesarajah

Abstract

The motivation of this work is the study of thermoelectric energy harvesting systems (EHS). The main research focus in the scientific community is on the development of new, more efficient, cheaper and environmentally friendly thermoelectric materials. But besides the material research, the complete development, build-up and optimization of thermoelectric EHSs are also necessary points to be studied. For this reason, this work deals with the **model-based development of thermoelectric EHSs**. The first objective is the modeling and simulation as well as design and controlling of these systems. For this purpose, a library should be developed and published to provide end-users with an easy tool to configure and build-up these systems in a simulation environment (Modelica/Dymola). The second objective is the elaboration and presentation of a development process to support the setup of a thermoelectric EHS. Finally, to show the usefulness of the developed scheme and library, three real application examples will be presented. These are an EHS at a radiator to supply an electronic thermostat valve in an office, the green barbecue and an EHS at a heating mockup of an oil-fired heater.

Diese Arbeit befasst sich mit thermoelektrischen Energy Harvesting Systemen (EHS). Der aktuelle Forschungsschwerpunkt in der Wissenschaft liegt vor allem in der Entwicklung neuer thermoelektrischer Materialien. Diese sollen effizienter, kostengünstiger und umweltfreundlicher sein. Neben der Materialforschung sind jedoch auch die komplette Entwicklung, der Aufbau sowie die Optimierung der thermoelektrischen Gesamtsysteme von hoher Bedeutung. Aus diesem Grund beschäftigt sich diese Arbeit mit der **modellbasierten Entwicklung thermoelektrischer EHS**. Eine erste Zielsetzung dabei ist die Modellierung und Simulation sowie Auslegung und Regelung solcher Systeme. Zu diesem Zweck soll eine Modellbibliothek entwickelt und veröffentlicht werden. Diese soll einem Endnutzer als einfaches Werkzeug dienen um die Systeme in einer Simulationsumgebung (hier: Modelica/Dymola) zusammenzusetzen und konfigurieren zu können. Die zweite Zielsetzung besteht in der Ausarbeitung und Präsentation eines Entwicklungsprozesses zur Unterstützung des Aufbaus eines thermoelektrischen EHS. Zur Demonstration des entworfenen Entwicklungsprozesses sowie der entwickelten Modellbibliothek, werden abschließend drei reale Anwendungsbeispiele vorgestellt. Dabei handelt es sich um ein EHS, welches an einem Heizkörper in einem Büro angebracht wurde um ein elektronisches Thermostatventil zu versorgen, den „grünen Schwenker“ sowie ein EHS an einem Heizungsnachbau einer ölbefeuerten Heizungsanlage.

Contents

1 Introduction

1.1 Problem Definition

The increasing shortage of fossil fuels and a growing environmental awareness lead to a rethink of politics and society. Today, a lot of effort and money are invested in environmentally friendly energy production. In addition to completely replacing the fossil fuels, which is currently still not possible, a further focus is placed on the increase in efficiency of existing processes. This is a very important point and essential for a successful energy transition. As demonstrated in [Quas2010], in Chapter 3.1, nearly 35% of the inserted primary energy is already lost in the energy sector as waste heat or as a transport loss. So, only 65% of the inserted energy reaches the end-user, whereas here again high energy losses, mainly in the form of waste heat, are documented, e.g. in bulbs or in combustion engines of automobiles. Up to this point, only 34% of the primary energy is used reasonably. In addition to this, the effective energy is not used meaningfully in all cases, e.g. the illumination of an empty room. In total, [Quas2010] comes to the conclusion that only 20% of the original inserted primary energy is used wisely. In all three of these areas, namely the energy production, the energy conversion and the wise energy usage, big potentials of energy saving exist. In this work, the first two areas are considered as they can relate to thermoelectric energy harvesting systems (EHSs). The German Federal Government has also recognized the importance of energy efficiency to support the "Energiewende" (energy transition) and has launched a national action plan on energy efficiency (NAPE) with the objective of reducing the primary energy consumption by 20% by 2020 (compared with 2008) and by 50% by 2050 [BMWi2014].

Thermoelectric EHSs can help to achieve these targets by using a temperature difference to generate electrical power. Thus, part of the wasted heat energy of manmade processes can be made useful again. Moreover, as yet unused heat sources can be made useable. Also the point of energy production on the spot, e.g. for wireless sensors or for hard-to-reach places, forces the research in the field of thermoelectricity. The main advantages of thermoelectric EHSs are the high life expectancy and low maintenance, but they still face low efficiency. Thermoelectricity is a red-hot topic, which is currently confirmed with the publication of [Kö++2016] in the BINE information portal, which is sponsored by the German Federal Ministry for Economic Affairs and Energy to support the transfer of information from research to practice. Also the expertise of the market research company IDTechEx has shown that the market for thermoelectric energy harvesters will reach over $1.1 billion by 2026, [Zerv2016].

1.2 Motivation and Goals

The motivation of this contribution is the study of thermoelectric EHSs. The main research focus in the scientific community is on the development of new, more efficient and cheaper thermoelectric

materials. But besides the materials research, the complete development, build-up and optimization of thermoelectric EHSs are also necessary points to be studied. For this reason, this work deals with the **model-based development of thermoelectric energy harvesting systems**.

The first objective is the modeling and simulation as well as design and controlling of these systems. For this purpose, a library should be developed and published to provide end-users with an easy tool to configure and build-up these systems in a simulation environment. Therefore, the typical approach of software development is used, a V-model [BrDr1995] and [MeLi2000], as shown in Figure 1.1. From left to right, the time axis of the development process is shown and top down the decomposition of the process. It is normally a model for software development and shows different stages of the software development process, but applies here for the building of the library. In the modeling chapter, more details of the V-model will be shown. The final library, called `EHSTEG` (Energy Harvesting Systems based on Thermoelectric Generators), is developed in Chapter 3 and finally described in Chapter 3.6. Control concepts are shown in Chapter 5.

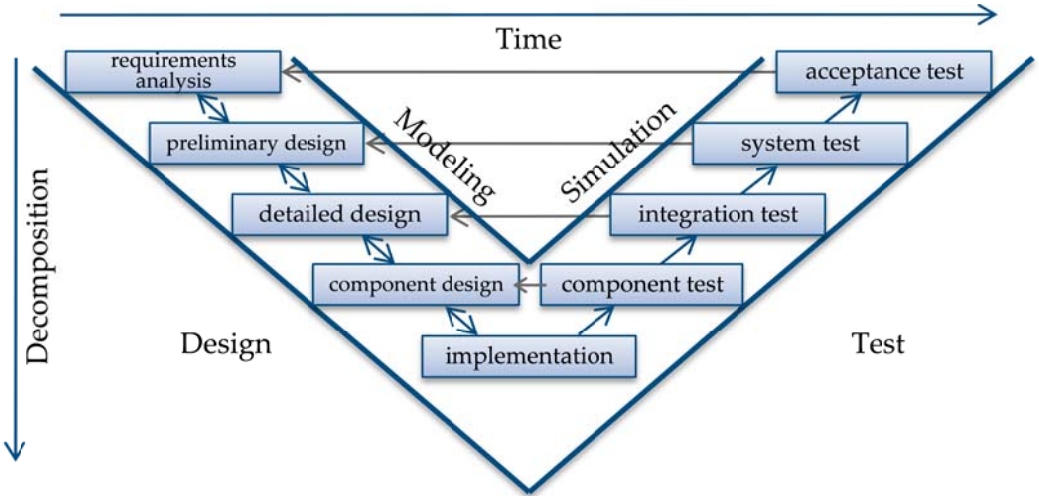

Figure 1.1: The V-model of the system development process.

The second objective is the elaboration and presentation of a development process to support the setup of a thermoelectric EHS. Figure 1.2 shows a scheme of the developed process, which will be explained in detail in Chapter 4. Obviously, the main steps can be done within a multi-physics simulation [NeFr2016b], which is possible with the previously developed `EHSTEG` library. The scheme of the development process is a guide to get the optimal thermoelectric EHS for a concrete application and this is also shown for three real application examples—small systems for private users—in this contribution, cf. Chapter 6.

It should be noted, that here the model-based development concept should not be confused with model-based design and model-driven engineering. The latter two produce an executable code or an executable software from formal models, whereas the model-based development process

introduced here provides as a result a real working system or more exact, an assembly plan for a real system.

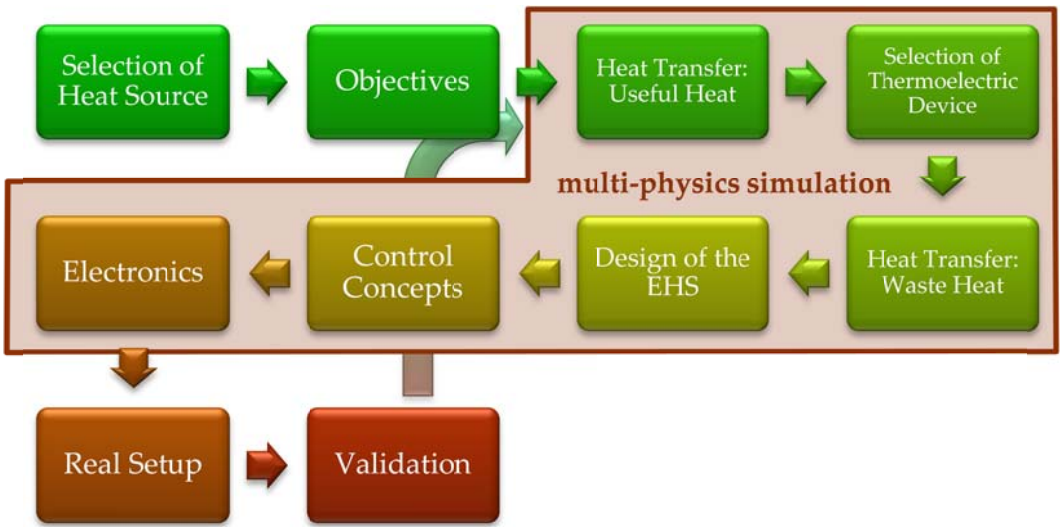

Figure 1.2: Model-based development process for thermoelectric EHSs, [NeFr2016b].

The idea of model-in-the-loop (MIL) simulation at one of the first stages and hardware-in-the-loop (HIL) simulation at a later date are also realizable with the `EHSTEG` library during the development process, which will be shown later.

1.3 Demarcation of the Work

This subchapter gives an overview of the state of the art of thermoelectricity, more precisely of thermoelectric EHSs, and serves to demarcate the content of this contribution to other work. The area of thermoelectricity which concerns the topic of this thesis is the modeling and simulation of thermoelectric energy harvesting applications and the setup of these systems, as mentioned in Chapter 1.2.

The first topic of this thesis, the modeling and simulation of thermoelectric EHSs, has already been done by different researchers. The most important to mention is the work of Andreas Bitschi, Min Chen and Christine Junior. In the PhD thesis of Andreas Bitschi—modeling of thermoelectric devices for electric power generation—tools for the evaluation of thermoelectric power generation units are developed. For this purpose, the method of the finite elements and the software COMSOL are used to model firstly the thermoelectric modules, and subsequently an array of a multitude of them into a cross flow heat exchanger system. The goal of this simulation model is to optimize the properties of a thermoelectric generator, e.g. the thermoelectric leg length [Bits2009]. Min Chen published his dissertation—design, modeling and utilization of thermoelectrical materials and devices in energy systems—in 2009 [Chen2009], and has done further publications since then on the same topic. The modeling of thermoelectric devices here is usually performed with the SPICE software and also some control strategies are taken into account, [Chen2014a].

Therefore, the behavior of the thermoelectric devices has to be transferred to equivalent electrical circuits. In the PhD thesis of Christine Junior—analysis of thermoelectrical modules and systems—Modelica is used to model the thermoelectric modules. The developed simulation model displays the performance of thermoelectric heat pumps and thermoelectric generators on the basis of two real examples [Juni2010]. With their simulation models, they all have shown that thermoelectric EHSs can be promising for some application fields and that there are different modeling methods for thermoelectric devices. Nevertheless, their models are not really comfortable or understandable for end-users and are often limited to specific cases. This dissertation delivers in addition to an easy to understand library, for all components of a thermoelectric EHS and not only for the thermoelectric device, also a guideline for building such systems in reality.

With the second thesis topic, the setup of thermoelectric EHSs, the Fraunhofer IPM deals especially in their public funded projects [Köni2016], e.g. TeWab (increased efficiency of CHP with thermoelectric heat exchanger), RExTEC (thermoelectric generator to increase the efficiency of range extender vehicles), HEATRECAR (thermoelectric waste heat recovery in light duty trucks) and TEG2020 (development of modular high-performance and flexible application of thermoelectric generators). Here, the main focus lies primarily on big systems in the automotive sector and the power station sector. In contrast, this work deals more with smaller systems for private users, including the usage of commercially available elements and not of prototypes, but can also be made scalable for bigger systems.

1.4 Structure of the Thesis

There are seven main chapters in this thesis. Thermoelectric EHSs are the core of the thesis and so Chapter 2 starts with the basics of thermoelectric EHSs. Therefore, EHSs are described in general, followed by thermoelectric EHSs. Further, this chapter deals with thermoelectricity, describes thermoelectric effects and deals with thermoelectric devices. The main focus is on thermoelectric generators, the used thermoelectric material, the fabrication of the generators, the fields of application, the commercially available thermoelectric generators and the sources of failure.

The multi-physics simulation of thermoelectric EHSs is represented in Chapter 3. There is a short introduction in the used modeling language Modelica and the simulation environment Dymola. Then, a description of the model of a thermoelectric device is given. Afterwards, a description of further system components like heat source, heat transfer and cooling elements as well as the presentation of the developed heat pipe library is given. The final developed `EHSTEG` library, containing everything necessary to build up a thermoelectric EHS, is depicted subsequently.

Chapter 4 deals with the development process. For this purpose, an overview is given first and then the single steps of the developed scheme are illustrated. This starts with the thermal design,

followed by the selection of the thermoelectric device, the mechanical design, the electrical design and ends up with the control design of the developed EHS.

Different controlling concepts for thermoelectric EHSs are presented in Chapter 5. These include the controlling of the cooling elements, either air or liquid cooling, and the possibility of system reconfiguration during operation mode. The controlling concepts are necessary for the following chapter.

To exemplify the knowledge gained in the previous chapters, Chapter 6 gives three real application examples which are built up at the Chair of Automation and Energy Systems at Saarland University. These are an electronic thermostatic valve in an office, a green barbecue and a heating mockup of a real oil-fired heater.

The conclusions of this work as well as an outlook are given in Chapter 7.

2 Basics of Thermoelectric Energy Harvesting Systems

This chapter explains the basics of energy harvesting systems (EHS) in general, and of thermoelectric EHSs in particular. This contains a general definition of EHSs themselves and an explanation of how the systems are understood in this context. Furthermore, the different physical effects are presented and different challenges are fleshed out before thermoelectric EHSs are considered. Afterwards, the thermoelectricity is depicted. First, a short timeline of the development of thermoelectricity is shown and, after that, the thermoelectric effects are explained as well as the structure of thermoelectric devices followed by their usage as thermoelectric generator in EHSs.

2.1 Energy Harvesting

Energy harvesting, also known as energy scavenging or power harvesting, is the transformation of ambient energy sources in small amounts of electrical energy, which are mostly buffered in an accumulator or a super capacitor [Stei2008] and [Br++2015]. This gained electrical energy can be used to supply low-power devices like sensors or mobile devices. A great advantage is the fact that the used energy sources are free of charge and freely available. The left side of Figure 2.1 shows different possible energy sources for EHSs. These include for example light, vibration, radio frequency, water flow or heat. EHSs are often added to the sustainable energy sector depending on the energy source used, or at least as systems which enhance the energy efficiency of existing processes. If the converted energy comes from a non-exhaustible source, the EHS really produces green and sustainable energy. But also if it is a manmade, exhaustible energy source, the waste energy would normally be remain unused and consequently be lost. So, it is definitely beneficial to use the waste energy with an EHS. However, it is not advisable to create an energy source especially for an energy harvesting usage due to the low efficiency of such systems. There is no official definition of an EHS, but a very common understanding of EHS is like the definition of the integrated circuit seller company Maxim Integrated, [Maxi2015]:

Energy harvesting (…) is the process in which energy is captured from a system's environment and converted into usable electric power. (…). An energy harvesting system generally includes circuitry to charge an energy storage cell, and manage the power, providing regulation and protection.

In this work, the understanding of EHS also means the complete system from the transformation of the ambient energy source until the supply of an electrical device. Consequently, the EHS consists of an energy converter, electrical energy storage and very often an energy management system as well as the electronics which produces a regulated output voltage for the power supply of electrical devices, see Figure 2.1. Thus, the EHS also includes the electrical part and this means for the end-user, that by installing an EHS, it is possible for him to directly use the gained electrical energy.

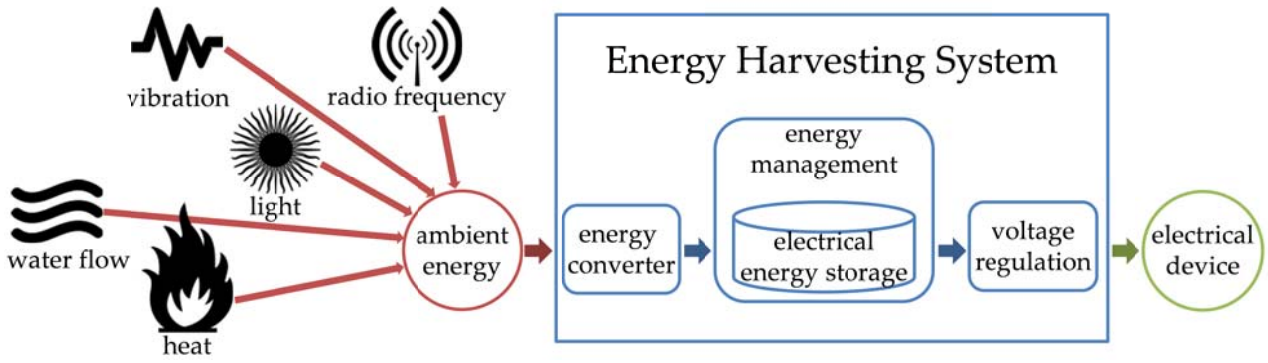

Figure 2.1: Different possible energy sources for EHSs and the schematic structure of an EHS

The biggest advantage of an EHS is the use of normally unused and thus, wasted energy sources. Though they produce only a small amount of electrical energy with rather low efficiency, they are useful and can help contribute to a better exploitation of the primary energy carrier. That is the reason why a typical application for EHSs is in long-lived applications, where for example a regular exchange of batteries should be prevented. Normally, a battery delivers a high power (milliwatts to watts) in a short time period, e.g. to collect sensor values and send them during a time slot of a few seconds. In contrast to this, the EHS loads the battery continuously over a longer time period, but only in the range of microwatts. The electrical energy gained fluctuates a lot due to the fluctuation of the converted ambient energy and so, an electronic circuit which regulates the voltage output, is obligatory. Consequently, the usage of EHSs supports the energy transition by increasing the energy efficiency [VDE2016], by making parts of the waste energy reusable. A further advantage is the energy production and consumption on the spot. This means there is no need for external energy supply via long cable lines or batteries. In industry for example, this fact can be used for sensors which are located in hard-to-reach places.

To produce electrical energy from ambient energy sources, different physical effects can be used depending on the kind of source [Schw2014], [Dono2013] and [Miks2011]. In Table 2-1 possible ambient energy sources and the associated physical effects, which are used to convert the energy, are shown. Also mentioned are some application examples which are already existent. Moreover, the need of an electrical buffer is also visible, as many of the energy sources only arise temporarily and not exactly when they are required.

The fields of application for EHSs are far reaching. Especially with the upcoming Internet of Things (IoT), more and more applications emerge. The idea of the IoT is that physical objects are equipped with intelligence and can collect data as well as communicate with each other. Thereby, they should facilitate and support human life. As all of the components need electrical energy and in the best case are self-sufficient, EHSs are very important for the success of the IoT.

Table 2-1: Possible ambient energy sources, the physical effects used and exemplary applications for EHSs.

ambient energy sources	description	physical effect	exemplary applications/products
mechanical energy	kinetic energy (translation, rotation), vibration, stress, flow energy (water flow, wind)	piezoelectric, electrostatic (capacitive), electromagnetic (inductive), triboelectric	EHS in the heel of a running shoe [BaAs2009]
thermal energy	temperature difference, heat flux	thermoelectric, pyroelectric	Seiko Thermic (wrist watch) [Seik2012], iTRV EnOcean (electrical thermostat) [Micr2015], BioLite (CampStove) [BioL2016]
radiant energy	electromagnetic radiation (radio waves), solar radiation	electromagnetic (inductive), photoelectric	RFID (radio-frequency identification), solar cells, wireless RF-powered wall clocks [Br++2015]
chemical energy	energy in chemical compound, chemical reaction	osmosis	osmotic power plant [Reut2009]

The examples of EHSs in Table 2-1 already show the scattered fields of applications. In addition, there are some further application areas, e.g. in the building automation sector (keywords smart home and smart meter). There are many devices which only need a small amount of energy. One example is an electrical thermostat, which can obtain its electrical energy from the temperature difference between radiator and ambient temperature (cf. Chapter 6.1). An example from the medicine sector is a piezoelectric EHS for a pacemaker, which produces the necessary electrical energy by the vibrations of the beating heart [Br++2015]. In the industry sector, very different application fields for EHSs can be found, e.g. in power stations. In operation mode, a generator provides at the same time two different possible ways of connecting an EHS. One is the usage of the vibration and the other the usage of the waste heat. The main interest in the automotive sector is on thermoelectric EHSs at the exhaust pipe of vehicles. But also piezoelectric EHSs as tire pressure sensors are of interest [Kü++2010]. Even in the leisure sector EHSs can be used, e.g. for sensors to measure vital signs. Thus, it is obvious that the range of applications for EHSs, no matter what kind of physical effect is used, is very large.

A lot of research is presently being done in the area of waste heat recovery, because every combustion process delivers quantities of waste heat [Quas2010]. Thereby considerable progress was made in the last few decades, e.g. the use of the waste heat for warm water production for

domestic or industrial purposes. Nevertheless, there remains a big potential for efficiency enhancement. In addition to the warm water production, waste heat can be used to produce electrical power for example with a Stirling engine, an Organic Rankine Cycle (ORC) or a thermoelectric EHS. In [FeEF2012], the two options ORC and thermoelectric EHS are compared.

2.2 Thermoelectric Energy Harvesting Systems

A special case of EHSs are thermoelectric EHSs, which are considered in the following. A thermoelectric EHS uses a temperature difference to generate electrical energy with thermoelectric generators (TEG), see Chapter 2.4.1. The underlying physical effects are the thermoelectric effects (cf. Chapter 2.3). The advantages of the thermoelectricity are the free availability of the waste heat, which is also given for a Stirling engine or an ORC, but in contrast to them, thermoelectricity is quiet, needs neither working fluid nor has moving parts, is maintenance free and does not pollute the environment. One application for example is to use the temperature of the exhaust gas line in automobiles with TEG-based EHSs, see [AnKu2012] and [Hs++2011]. Another application is the more efficient use of solar energy, in addition to use only the visible light; the authors in [Da++2014] use the invisible, infrared light of the sun. As more than half of the energy coming from the sun is thermal energy, this seems reasonable. Other researchers consider thermoelectric EHSs in combination with phase change materials, see [El++2013] and [Ki++2014]. In [Zh++2011] an experimental study of a thermoelectric generation system for application in exhaust heat of kilns is developed. In addition to this small-scale thermoelectric EHSs (which produce only a few watts of electrical energy), there are also large-scale thermoelectric EHSs producing a few hundred watts of electrical energy. They are mostly based on radioisotope thermoelectric generators (RTG) and are applied in satellites, e.g. Apollo 14-17 (ca. 75 W), Galileo (287 W) or Voyager 1 and 2 (ca. 160 W). RTGs involve radioactive material and convert the heat released by the decay. They are especially used in space applications beyond the planet Mars, because the sunlight there is too weak and thus the photovoltaics are not usable. Therefore, the radioactive material delivers the heat and the outer space the cold, which results in a very high temperature difference and thus, in a high power yield. A detailed summary can be found in [Benn1995]. Some satellites have been running over 30 years now, and the TEGs still deliver electrical energy. A well-known representative in current time is the Mars rover Curiosity, which runs with a multi-mission radioisotope thermoelectric generator (MMRTG).

The main parameter for a thermoelectric EHS is the given hot side temperature and thus, the resulting temperature difference. The theoretical highest possible efficiency of a system, using a temperature difference is given by Carnot's theorem, see Equation (2.1).

$$\eta_{\max} = \eta_{\text{Carnot}} = \frac{T_{\text{high}} - T_{\text{low}}}{T_{\text{high}}} = 1 - \frac{T_{\text{low}}}{T_{\text{high}}}, \tag{2.1}$$

where η_{max} is the maximum efficiency, η_{Carnot} the Carnot efficiency, T_{high} the higher temperature and T_{low} the lower temperature, both in K. The Carnot efficiency corresponds to the maximum useful work in the conversion of heat into mechanical energy in an ideal thermodynamic cycle. The temperature difference delivers the potential (voltage based on the Seebeck effect) for an efficient energy conversion; whereas the heat flux delivers the power (forces the electrical current). The rejected heat has to be dissipated by a heat sink. The heat energy input is given by Equation (2.2), with $\dot{Q}$ as the rate of heat flow, λ the heat conductivity, A the area, ΔT the temperature difference ($T_{high} - T_{low}$) and d as the distance:

$$\dot{Q} = \lambda A \frac{\Delta T}{d} . \tag{2.2}$$

It follows that the maximum electrical power that can be gained from a rate of heat flow with Equation (2.3):

$$P_{el,\,max} = \dot{Q} \cdot \eta_{Carnot} , \tag{2.3}$$

where $P_{el,\,max}$ is the maximum electrical power (Equation (2.1), (2.2) and (2.3) are from [Snyd2008]). However, also with big heat fluxes, the extractable power is low due to the low Carnot efficiency and the low efficiency of the currently existing thermoelectric materials. The efficiency of the thermoelectric material is determined with a dimensionless parameter ZT (figure of merit), which will be explained in Chapter 2.4.1. Consequently, the actual electrical power gained is given by,

$$P_{el} = \dot{Q} \cdot \eta_{TEG} = \dot{Q} \cdot \eta_{Carnot}\, \eta_{TE} = P_{el,\,max}\, \eta_{TE} = P_{el,\,max}\, \frac{\sqrt{1+ZT}-1}{\sqrt{1+ZT}+\frac{T_{low}}{T_{high}}} , \tag{2.4}$$

where P_{el} is the actual gained power, η_{TEG} the efficiency of the TEG and η_{TE} the efficiency of the thermoelectric material. It is evident that for a $ZT \to \infty$, $\eta_{TE} = 1$ and thus, the power will be maximal, as shown in Equation (2.3). Unfortunately, purchasable TEGs have only a ZT between 0.8 and 1.2 [Vini2009] and thus, typical values for η_{TE} for low temperature applications (between room temperature and 200°C) are between 15% and 23%. Simplified, one can say that the efficiency of TEGs increases almost linearly with the temperature difference, which is valid for good bismuth telluride devices and small temperature differences [Snyd2008]. It is approximately:

$$\eta_{TEG} \approx \eta_1 \cdot \Delta T;\ \eta_1 \approx 0.05\ \%/K . \tag{2.5}$$

In addition to those limitations given by the temperatures and the thermoelectric materials used, there are also losses due to the electrical connections, thermal and electrical contact resistances as well as further thermal losses. Despite all of these facts, there are still enough possibilities to apply thermoelectric EHSs. In Chapter 6, three real application examples will be shown.

For a better understanding of thermoelectric EHSs and their physical effects, the basics of thermoelectricity are described in the following section.

2.3 Thermoelectricity

Thermoelectricity deals with the relations between temperatures and electricity. It is based on three effects, which will be explained in this section. Thomas Seebeck laid the foundation of thermoelectricity in 1821 with the discovering of the "Seebeck Effect" named after him. The Seebeck effect is the key factor for the functionality of thermoelectric generators. In 1834, Jean Peltier discovered the so-called "Peltier Effect," which is crucial for Peltier elements, used for thermoelectric cooling and heat pumps. The third effect was discovered by William Thomson (Lord Kelvin) in 1856. Already in 1854, he found a relation between the Seebeck and Peltier effects, the "Thomson-Relation" named after him, which brought him finally two years later to the last thermoelectric effect, the "Thomson Effect." The first correct calculation of the maximum efficiency of a TEG and the performance of a thermoelectric cooler was done in 1909 and 1911 by Edmund Altenkirch, which later ends in the thermoelectric figure of merit ZT (cf. Equation (2.23)). In 1949, the modern theory of thermoelectricity was developed by Abram Fedorovich Ioffe and the first devices powered (Maria Telkes, 1947; first thermoelectric power generator with an efficiency of 5%) or cooled (H. Julian Goldsmid, 1954; cooled a surface to 0°C with a thermoelectric cooler) by thermoelectric elements were constructed. In 1959 the first RTG was built, which launched two years later in the satellite Transit 4A. Afterwards, more and more satellites featuring RTG were sent into outer space. Between 1970 and 2000, the thermoelectric applications eked out a niche existence. Thereby, the Peltier elements (thermoelectric coolers (TECs)) had a better status as they were used for many cooling systems like small refrigerators, ice boxes, seat cooling and heating systems and so on. In contrast, TEGs only found their applications in some niche fields, where a reliable, long-lived power source was more important than the investment costs. These were and are mainly space and military applications. Also the Mars rover Curiosity is powered by TEGs. Here, a MMRTG is used. But since 2000, there is increasing interest in the idea of thermoelectric power generation due to the development and knowledge in nanotechnology and the efforts to reduce the CO_2 emissions, to enhance the electrical efficiency of existing systems and to push the energy transition. Therefore, the focus for new thermoelectric materials is on a higher efficiency (higher ZT value), more cost-effective production and environmentally-friendly materials. A more detailed timeline can be found in [Alph2014] and [Snyd2016].

The three aforementioned thermoelectric effects are well described in [Poll1995] and in [Gold2010], Chapter 1. The first discovered effect, the **Seebeck Effect**, predicates that an electrical field occurs in a (semi)conductive material, when a temperature gradient is applied. Due to the different temperature levels on both sides of the material, the electrons have different energies and thus, thermo-diffusion currents arise. As a result, there is the appearance of an electrical field. This is the absolute Seebeck Effect. For a better illustration of this phenomenon, the usage of a

thermoelement, as shown in Figure 2.2a, is advantageous. A thermoelement consists of two different materials which are electrically connected at their ends. If there is a temperature difference between these ends, a voltage can be measured over the open terminals. Thus, the Seebeck Effect is an electromotive force (EMF), which originates from the temperature difference between the junctions of two different conductive materials. Equivalent to the electrochemical series, it is possible to give a thermoelectric voltage series, at which the Seebeck coefficient α is given relative to platinum for a temperature difference of 100 K. These Seebeck coefficients are normally valid for 273 K and an overview is given in Table 2-2. The higher the distance of the Seebeck coefficients of the two used materials, the larger is the thermoelectric voltage for a thermoelement.

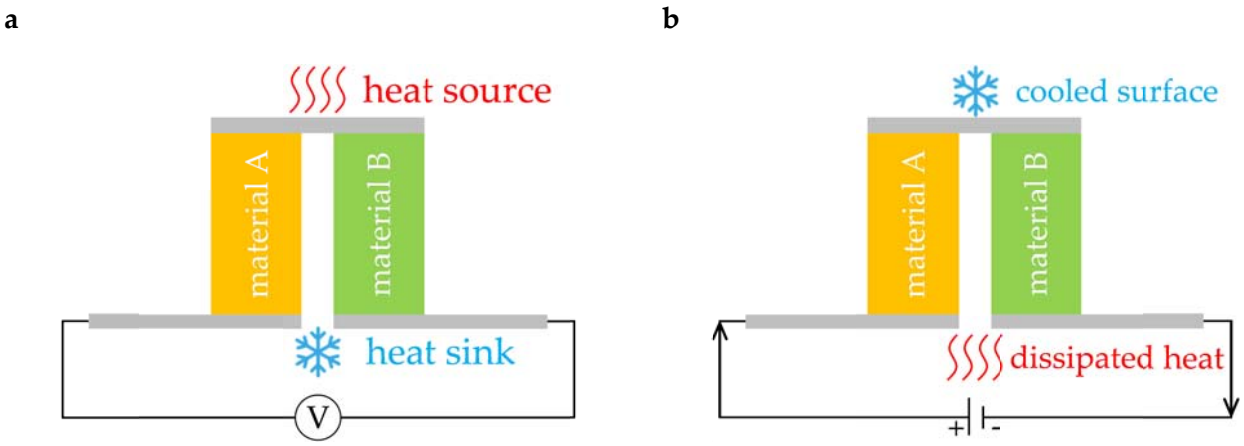

Figure 2.2: a: Illustration of the Seebeck effect; b: Illustration of the Peltier effect.

With the discovery of the **Peltier Effect**, it was shown that heat can be absorbed or emitted when an electrical current flows through a junction of two different conductors. A connection of a voltage source drives a current through the conductor and thus changes the heat transport, see Figure 2.2b. Colloquially, the Peltier effect is often called reverse Seebeck effect, but in effect, they are two different phenomena. The Peltier effect is a result of the change of entropy of the electrical charge carrier when it crosses a junction.

The **Thomson Effect** is defined as the degree of warming per unit length and results from the current density through the conductor, in which a uniform temperature gradient is present. The Thomson relation gives the relation of Peltier coefficient to Seebeck coefficient.

The Seebeck Effect is independent of the Thomson and the Peltier effects. The latter two effects only occur under an electrical current and are no voltages. An applied voltage (Seebeck voltage or normal voltage source) is the driving force for the current flow, which is then responsible for the Peltier and the Thomson effects.

Furthermore, in addition to the thermoelectric effects there are also thermogalvanomagnetic effects. Thermoelectric effects can be changed when a magnetic field is applied and even new phenomena occur. These phenomena can influence the performance of thermoelectric devices, for more information see Chapter 1.3 in [Gold2010]. A detailed physical description of the thermoelectric transport theory (electron distribution, Boltzmann equation and Fermi energy) can be found in [Bhan1995] and is not necessary here. The physical effects and equations described in the next section are completely sufficient to consider thermoelectric EHS in this context.

Table 2-2: Thermoelectric voltage series and Seebeck coefficient in μV/°C of some materials at a temperature of 0°C (273.13 K), [eFun2016].

Material	Seebeck coefficient	Material	Seebeck coefficient	Material	Seebeck coefficient
Bismuth	-72	Aluminum	3.5	Tungsten	7.5
Constantan	-35	Lead	4.0	Iron	19
Nickel	-15	Tantalum	4.5	Nichrome	25
Potassium	-9.0	Rhodium	6.0	Antimony	47
Sodium	-2.0	Copper	6.5	Germanium	300
Platinum	**0**	Gold	6.5	Silicon	440
Mercury	0.6	Silver	6.5	Tellurium	500
Carbon	3.0	Cadmium	7.5	Selenium	900

The thermoelectric effects are reversible in principle, but in reality they are accompanied by irreversible effects like the electrical resistance (see Equation (2.6)) and the thermal conduction (see Equation (2.7)).

$$I = \frac{\sigma U A}{d}, \tag{2.6}$$

$$\dot{q} = -\frac{\lambda \Delta T}{d}, \tag{2.7}$$

with I as the electrical current, σ as the electrical conductivity, U as the voltage and $\dot{q}$ as the heat flux density.

2.4 Thermoelectric Device

2.4.1 Thermoelectric Generator

A thermoelectric device (TEG or TEC) consists of a multiplicity of thermocouples, in which a thermocouple consists of two legs which are linked by a metal bridge. One leg consists of an n- or p-doped thermoelectric material and the outer ending of the thermoelectric device is enclosed with ceramic plates, see Figure 2.5. When the thermoelectric device is exposed to a temperature

difference and thus generates electrical energy, it is called a thermoelectric generator (TEG). Applying a voltage source and thus generating a forced heat transfer is called thermoelectric cooler (TEC) or Peltier element and can be used for cooling applications or as a heat pump. In reality, there are some differences between TECs and TEGs due to the different field of application. However, in some cases it can be wise to replace a TEG with a cheaper TEC. This is an important fact for the setup of affordable thermoelectric EHSs. A detailed comparison between TEGs and TECs will be done in Chapter 4.4 and was also done in [NeFr2016a].

In the following, only thermoelectric devices working as voltage sources are considered, regardless of whether they are TECs or TEGs. For simplicity TEGs are used.

Figure 2.3 shows an illustration of one thermocouple, which is sufficient to explain the physical effects occurring in a TEG during operation mode. It will be assumed that there is a steady-state, temperature-independent parameters and the heat only flows in $\mathbf{e}_x$ direction through the legs. These are very common assumptions to describe the principal behavior of TEGs, [LiBe2007], [Su++2015] and [Fa++2016].

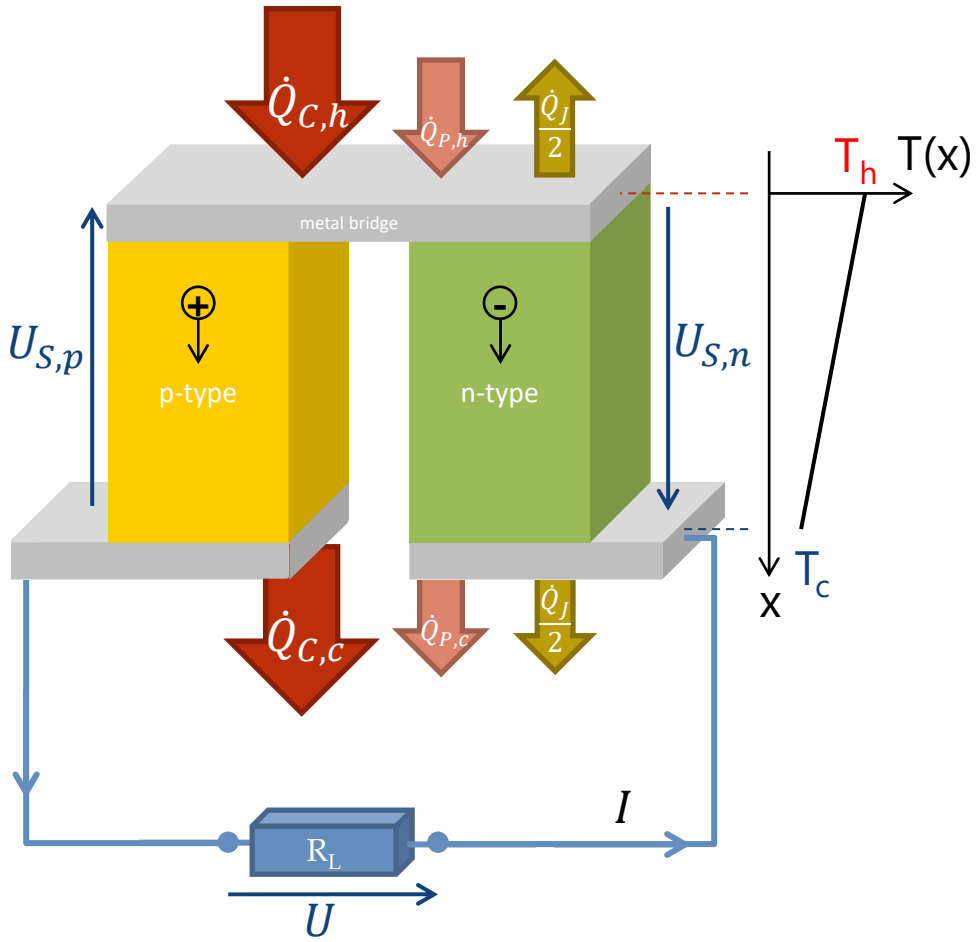

Figure 2.3: Illustration of one thermocouple to show the physical effects which occur in a TEG; assumptions: steady-state, heat flows only in $\mathbf{e}_x$ direction.

In total, there are five effects in thermoelectric legs which occur when a temperature gradient is applied over the legs. At first, they will be described in general with a local dependency and then simplified for engineering use.

Already without an electrical connection, due to the temperature difference on both sides, there will be a **thermal conduction**. For this, the **Fourier's Law** gives the following equation:

$$\dot{\boldsymbol{q}} = -\lambda \boldsymbol{\nabla} T \ , \tag{2.8}$$

which here becomes with the given assumptions:

$$\dot{Q}_{\mathrm{C,h/c}} = \frac{\lambda_{\mathrm{p/n}}}{d} A \, \Delta T \ , \tag{2.9}$$

where $\dot{Q}_{\mathrm{C}}$ is the rate of heat flow by the conduction (indices h and c stand for hot and cold side in Figure 2.3), $\lambda_{\mathrm{p/n}}$ is the sum of the heat conductivities of p-type and n-type material, d the length of the thermoelectric leg and A the cross-sectional area. The applied temperature difference leads to an **electromotive force** (EMF), the **Seebeck effect**, which is the second physical effect, see Equation (2.10) and with the given assumptions Equation (2.11).

$$\boldsymbol{E}_{\mathrm{emf}} = -\alpha \boldsymbol{\nabla} T \ , \tag{2.10}$$

$$U_{\mathrm{S}} = \ U_{\mathrm{S,\,p}} + U_{\mathrm{S,\,n}} = \left(\alpha_{\mathrm{p}} - \alpha_{\mathrm{n}}\right) \Delta T = \alpha \Delta T \ , \tag{2.11}$$

with $\boldsymbol{E}_{\mathrm{emf}}$ as the EMF and U_s as the Seebeck voltage (indices p and n stand for the p-type and n-type material). If an electrical resistor (R_{L}) is connected to the thermocouple, a further heat flow arises due to the electric current flow. It is the **internal Joule heating**, presented by **Joule's First Law**:

$$\frac{\mathrm{d}P_{\mathrm{J}}}{\mathrm{d}V} = \boldsymbol{J} \cdot \boldsymbol{E} \ , \tag{2.12}$$

and so it follows here:

$$\dot{Q}_{\mathrm{J}} = I^2 \rho_{\mathrm{p/n}} \frac{d}{A} \ , \tag{2.13}$$

where P_{J} is the resistive power loss, V is the volume, $\boldsymbol{J}$ is the current density, $\dot{Q}_{\mathrm{J}}$ the rate of heat flow by resistive power loss and $\rho_{\mathrm{p/n}}$ is the sum of the electrical resistivities of p-type and n-type material. The common agreement is that half of the Joule heating is added to the cold side and the other half to the hot side, because the heat rises all-around the leg, see [LiBe2007] and [Ju++2008]. The current flow through the junction of the thermoelectric material also leads to a further rate of heat flow, due to the already mentioned **Peltier effect**:

$$\dot{Q}_{\mathrm{P,h/c}} = \pi I = \left(\pi_{\mathrm{p}} - \pi_{\mathrm{n}}\right) I \ , \tag{2.14}$$

where $\dot{Q}_P$ is the Peltier heat (indices h and c stand for the hot and the cold side) and π is the Peltier coefficient (indices p and n stand for the p-type and n-type material). With the Thomson relation ($\pi = \alpha T$ or $\tau = T\frac{d\alpha}{dT}$, where $\tau = (\tau_\mathrm{p} - \tau_\mathrm{n})$ is the Thomson coefficient) it follows:

$$\dot{Q}_{\mathrm{P,h/c}} = \alpha\, T_{\mathrm{h/c}}\, I = \left(\alpha_\mathrm{p} - \alpha_\mathrm{n}\right) I T_{\mathrm{h/c}}\,. \tag{2.15}$$

The last effect in a thermoelectric generator is the **Thomson effect**. It describes the heat flow, which occurs when a current flows through the thermoelectric material, which is under a temperature gradient:

$$\dot{\boldsymbol{q}} = -\tau \boldsymbol{J}\, \boldsymbol{\nabla} T\,, \tag{2.16}$$

$$\dot{Q}_\mathrm{T} = -\tau I \frac{\mathrm{d}T}{\mathrm{d}x} = -IT\frac{\mathrm{d}\alpha}{\mathrm{d}x}\,, \tag{2.17}$$

where $\dot{Q}_\mathrm{T}$ is the rate of heat flow due to the Thomson effect. The Thomson heat flow overlays with the internal Joule heating and is often neglected (also in the following) due to the significantly smaller order of magnitude, [LiBe2007] and [MoKn2014].

These are the five effects occurring when a temperature gradient is applied over a thermocouple and a load resistance is connected. Consequently, there are **three governing equations** for the system. One considers the heat flow on the hot side, one on the cold side and the other the current flow:

$$\dot{Q}_\mathrm{h} = \dot{Q}_{\mathrm{C,h}} + \dot{Q}_{\mathrm{P,h}} - \frac{\dot{Q}_\mathrm{J}}{2} = \frac{\lambda_{\mathrm{p/n}}}{d} A\, \Delta T + \alpha\, I T_\mathrm{h} - \frac{1}{2}\left(I^2 \rho_{\mathrm{p/n}} \frac{d}{A}\right), \tag{2.18}$$

$$\dot{Q}_\mathrm{c} = \dot{Q}_{\mathrm{C,c}} + \dot{Q}_{\mathrm{P,c}} + \frac{\dot{Q}_\mathrm{J}}{2} = \frac{\lambda_{\mathrm{p/n}}}{d} A\, \Delta T + \alpha\, I T_\mathrm{c} + \frac{1}{2}\left(I^2 \rho_{\mathrm{p/n}} \frac{d}{A}\right), \tag{2.19}$$

$$I = \frac{U_\mathrm{S}}{R_\mathrm{L} + R_\mathrm{i}} = \frac{\alpha \Delta T}{R_\mathrm{L} + R_\mathrm{i}}\,, \tag{2.20}$$

with R_i as the inner resistance of the TEG. Thus, the produced electrical power is:

$$P_\mathrm{el} = R_\mathrm{L} I^2\,. \tag{2.21}$$

The maximum possible power ($P_{\mathrm{el,\,max}}$) is calculated according to Equation (2.22). Normally, TEGs are devices which deliver low voltage and high current. A rule of thumb is that the power output is nearly proportional to the area of the thermoelectric leg and inversely proportional to the length.

$$P_{\mathrm{el,\,max}} = \frac{U_\mathrm{S}^2}{4R_\mathrm{i}}\,, \text{ with } R_\mathrm{i} = R_\mathrm{L}. \tag{2.22}$$

The three material parameters, Seebeck coefficient α, electrical resistivity ρ and thermal conductivity λ are the key parameters of thermoelectric devices, cf. Equation (2.18), (2.19) and (2.20). That is why a dimensionless parameter for the assessment of thermoelectric material was introduced, the so-called figure of merit ZT, see Chapter 2.2 in [Gold2010]:

$$ZT = \frac{\alpha^2}{\lambda\rho}\, T\,. \tag{2.23}$$

It is desirable to have a very high figure of merit and consequently, a high Seebeck coefficient and with different signs for the thermoelectric legs as well as a small thermal conductivity and a small electrical resistivity. The efficiency of a TEG can be calculated as shown in Equation (2.24) or with ZT as shown in Equation (2.25).

$$\eta_{\mathrm{TEG}} = \frac{P_{\mathrm{el}}}{\dot{Q}_{\mathrm{h}}}, \tag{2.24}$$

$$\eta_{\mathrm{TEG}} = \frac{T_{\mathrm{h}} - T_{\mathrm{c}}}{T_{\mathrm{h}}} \cdot \frac{\sqrt{1+ZT}-1}{\sqrt{1+ZT}+\frac{T_{\mathrm{c}}}{T_{\mathrm{h}}}}. \tag{2.25}$$

The maximum electrical power is achieved for $R_{\mathrm{L}} = R_{\mathrm{i}}$ and the maximum efficiency is achieved if the relation between load and inner resistance is given by Equation (2.26), see Figure 2.4:

$$\frac{R_L}{R_i} = \sqrt{1 + ZT}\,. \tag{2.26}$$

Figure 2.4 shows a schematic of the current voltage, current power and current efficiency curve of a thermoelectric device.

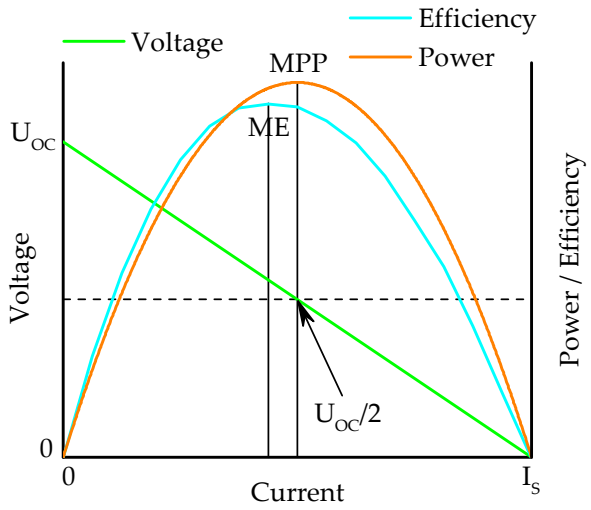

Figure 2.4: Current voltage, current power as well as current efficiency curve of a thermoelectric device. The maximum power point (MPP), the maximum efficiency point (ME) and the open-circuit voltage (U_{OC}) as well as the short-circuit current (I_S) are labeled.

Until now, only one thermocouple has been considered as this is sufficient to explain the basic physical effects. A real thermoelectric generator consists of a high number of such thermocouples, which are, in the most common cases, connected electrically in series and thermally in parallel. The thermoelements in such a module are connected with good electrical conductors, for example copper stripes. The device is enclosed by ceramic plates, which electrically isolate the module and have a good heat transfer. The schematic structure is shown in Figure 2.5. For the thermoelectric device's respective generator, the above mentioned equations remain the same, but with a scaling

factor N. This is the number of thermocouples in one thermoelectric device. So, the Seebeck voltage for the complete device is given by Equation (2.27), which is derived from Equation (2.11):

$$U_S = N \cdot \alpha \Delta T \ . \tag{2.27}$$

The equations for the heat flows on the cold and hot side are given in Equation (2.28), based on Equation (2.18) and (2.19):

$$\dot{Q}_{h/c} = N \cdot \frac{\lambda_{p/n}}{d} A \, \Delta T + N \cdot \alpha I T_{h/c} \pm \frac{1}{2}(N \cdot I^2 \rho_{p/n} \frac{d}{A}) \ . \tag{2.28}$$

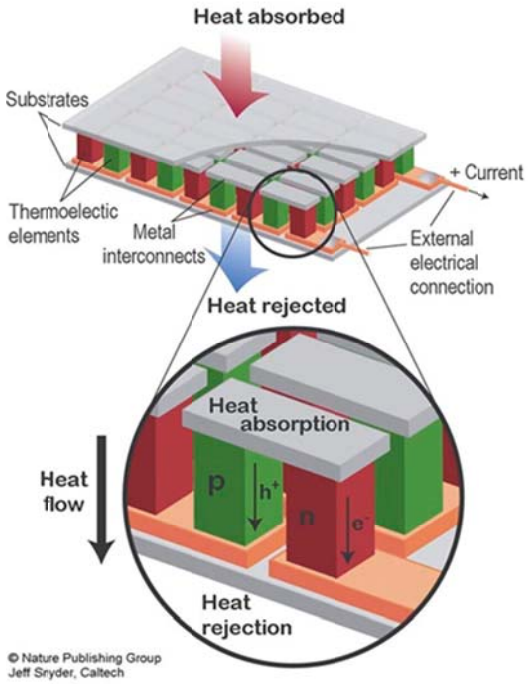

Figure 2.5: Thermoelectric device, visible are the thermocouples, the metal bridge as well as the ceramic plates, [SnTo2008].

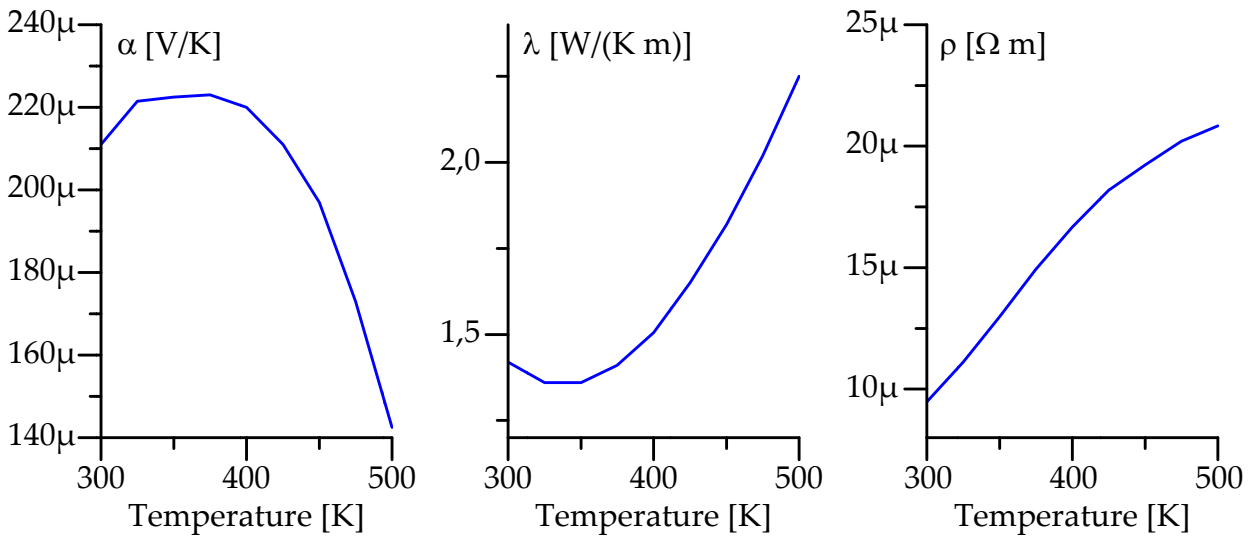

Figure 2.6: Material properties (Seebeck coefficient α, thermal conductivity λ and electrical resistivity ρ) of bismuth telluride, [Fe++2014], material properties based on [Ther2016].

At the beginning of this subchapter, it is assumed that there are temperature-independent parameters, but this is only valid for small temperature differences. The temperature dependency of the Seebeck coefficient $\alpha(T)$, the thermal conductivity $\lambda(T)$ and electrical resistivity $\rho(T)$ is shown in Figure 2.6 for Bi_2Te_3, [Fe++2014].

Many researchers choose a mean value for the temperature to solve the thermoelectric equations. This is sufficient for small temperature ranges, but not for bigger ones, cf. Figure 2.6. To get a more accurate solution of a thermoelectric system mainly for a bigger temperature range, it is advisable to split a thermoelectric leg in many infinitesimal segments. Thus, the above mentioned equations can be used, as for each segment the assumption of a small temperature difference is valid. A more detailed description of this approach will be explained in Chapter 3.3.

2.4.2 Thermoelectric Materials

As already mentioned in the previous section, the quality of a thermoelectric material is generally defined by its figure of merit. A good thermoelectric material has to have a high Seebeck coefficient to produce a high voltage, needs a low thermal conductivity to reduce the heat losses over the leg and has to have a high electrical conductivity to reduce ohmic losses. However, there are also critical voices seeing indeed the figure of merit as an appropriate performance parameter, but this can also mislead in some applications, cf. [Nard2011]. As TEGs are used under different temperature conditions, there are well suited thermoelectric materials for certain temperature ranges. Figure 2.7 gives an overview of different thermoelectric materials and their figure of merit as a function of the temperature and the advantages and disadvantages are compared in Figure 2.8, [Kö++2016]. Actually, purchasable TEGs are mainly based on bismuth telluride, but the main research is focused on lead tellurides, silicides, half-heuslers and skutterudites and of course on the nanoscale size [SnTo2008]. In addition to the goal of a higher value of ZT, there are also other objectives like the reduction of costs (raw material price and production price) and the use of eco-friendly materials. The research work in the area of developing new thermoelectric material is very intensive. This is especially supported by the various societies, the German Thermoelectric Society (DTG), the European Thermoelectric Society (ETS) and the International Thermoelectric Society (ITS), which also organize annual conferences such as the European Conference on Thermoelectrics (ECT) and the International Conference on Thermoelectrics (ICT). There is also a large consortium of about 250 members, companies and research institutions, working on new thermoelectric materials in the EUREKA cluster Metallurgy Europe. If a thermoelectric EHS is designed, the temperature operation conditions have to be observed and accordingly, the thermoelectric material has to be chosen.

Bismuth telluride (Bi_2Te_3): Bismuth telluride is the favorite material for the low temperature sector (between 0°C and 200°C), as can be seen in Figure 2.7. In this range, it has the greatest figure

of merit for p and n-type material. At the moment, it is the thermoelectric material with the widest spread. The accepted average value for ZT is between 0.8 and 1.1 [SnTo2008].

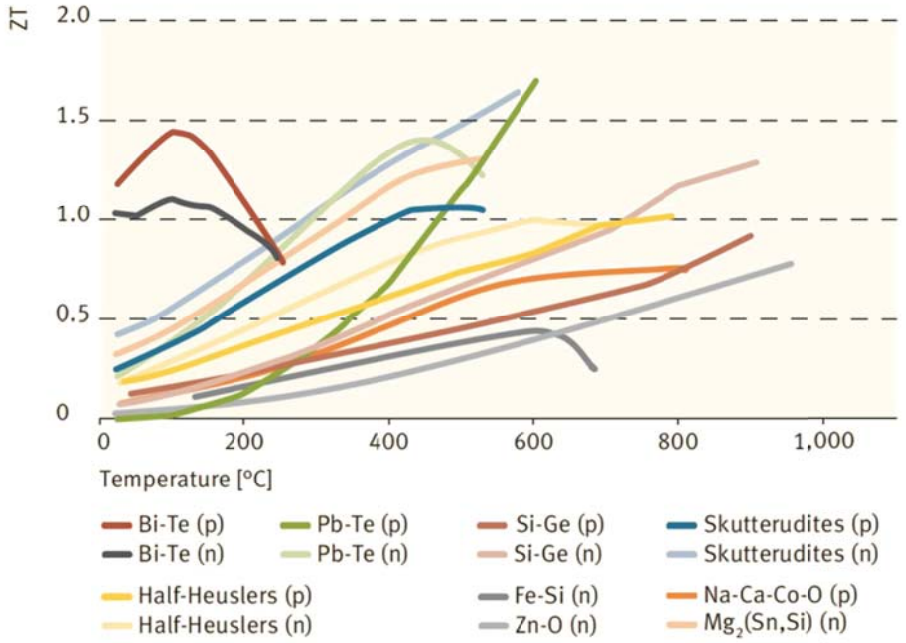

Figure 2.7: Overview of different thermoelectric materials and their figure of merit as a function of the temperature [Kö++2016].

Materials	*Bi_2Te_3*	*PbTe*	*SiGe*	*$MnSi_{1.73}$*	*Mg_2-SiSn*	*$CoSb_3$*	*Oxides*	*Half-Heuslers*
	Commercial and space modules			*Research modules*		*Prototypes*		
Figure of merit (ZT)	*>1.0*	*>1.0*	*<1.0*	*≥ 1.0*	*≥ 1.0*	*> 1.0*	*< 1.0*	*≥ 1.0*
Operational temperature	*< 300 °C*	*< 500 °C*	*< 900 °C*	*< 550 °C*	*< 550 °C*	*< 520 °C*	*< 700 °C*	*< 550 °C*
Long-term stability	■	■	■	■	■	■	■	■
Mechanical stability	■	■	■	■	■	■	■	■
Thermal stability		■	■	■	■	■	■	■
Chemical stability	■	■	■	■	■	■	■	■
Toxicity	■	■	■	■	■	■	■	■
Environmental aspects	■	■	■	■	■	■	■	■
Raw material availability	■	■	■	■	■	■	■	■
Large-scale manufacture	■	■	■	■	■	■	■	■

■ *Positive assessment* ■ *Negative assessment* ■ *Contradictory data*

Figure 2.8: Comparison of different thermoelectric materials [Kö++2016].

Lead telluride (PbTe): For power generation in a mid-temperature range (between 200°C and 600°C), lead telluride is the preferred thermoelectric material. The peak ZT is about 0.8 and with suitable admixtures, a ZT over one can be reached [SnTo2008].

Silicon-germanium (Si-Ge): Silicon-germanium is a high temperature material for usage in a temperature range over 600°C. The ZT value is not so high, but the material resists the high temperatures [SnTo2008].

Skutterudite: Skutterudites are the mineral $CoAs_3$ and other compounds in the same family. They have a crystal structure with a unit cell, which contains an empty space. In this void, an impurity atom can be placed and so the lattice conductivity can be reduced to a very low level. The operating conditions are between 300°C and 550°C, Chapter 9.4 in [Gold2010] and [TrSu2006].

Half-Heusler alloys: The Heusler alloy is a ferromagnetic metal alloy. In a half-Heusler alloy, some places in the cubic lattice are unoccupied, Chapter 9.6 in [Gold2010]. It has many advantages, see Figure 2.8, but the ZT value is still not so high.

Nanostructured materials: The improvement of the thermoelectric properties of the bulk materials is currently a research focus for many material scientists and physicists, and that is why nanostructured materials (nanocomposites) are also tested [SnTo2008]. With the inclusion of nanocomposites in existing thermoelectric bulk materials, the material scientists try to increase the figure of merit by reducing the thermal conductivity and increasing the electrical conductivity [AlRa2013].

2.4.3 Fabrication

There are numerous possible ways to fabricate thermoelectric devices. The most common methods to produce the thermoelectric elements are zone refining, Bridgman method, and press and sintering [MaBu1995]. Wafers are sliced from ingots and then, the thermoelectric legs are ripped out from the wafers. A goal of the producer of thermoelectric devices is the reduction of the size of the thermoelectric material. Besides saving raw material, a smaller and lighter device is also beneficial. However, a heat transport problem is going hand in hand with the material reduction or more specifically with the reduction of the module dimensions, see Chapter 10.2 in [Gold2010]. If the cross-sectional area of the ceramic plates is reduced, it is more difficult to transfer the heat from the source to the sink without an extreme temperature difference. The solution would be to increase the space between the thermoelectric legs, but then the heat losses due to convection, conduction and radiation will be increased. Thus, there will be an optimal size for the space between the thermoelectric legs, Chapter 10.2 in [Gold2010].

The second problem with the miniaturization of the thermoelectric module is the rising of the electrical contact resistance, which goes hand in hand with the reduction of the length of the legs. Nowadays, it is still extremely difficult to measure the electrical contact resistance. Usual accepted values are between $0.84 \cdot 10^{-10}$ and $8.4 \cdot 10^{-10}\,\Omega m^2$, cf. Chapter 10.3 in [Gold2010]. The contact materials used (metallic contact between legs and ceramic insulation plates) have to match electrically, physically and chemically with the thermoelectric material for a good thermoelectric device, compare for example the coefficient of thermal expansion [Kö++2016]. The ceramic plates are necessary for good thermal conductivity and the electrical insulation of the thermoelectric legs with the surrounding. Sometimes the ceramic plates have slitting on the face to destress the

module due to the thermal cycling. The most common method to connect the copper conductors with the ceramic plates is to print and burn a circuit pattern. Then, the copper conductors are soldered to this circuit pattern [MaBu1995]. Finished thermoelectric devices can be the normal flat one, but also segmented or cascaded. Figure 2.9 shows the composition of a segmented and a cascaded generator. The usage of different thermoelectric material is visible for the segmented generator (cf. different colors), which is of interest for high temperature differences, as every material has a temperature range where it works the best. It is also obvious that even in flat thermoelectric generators, the p and n-doped legs do not need to have the same dimensions.

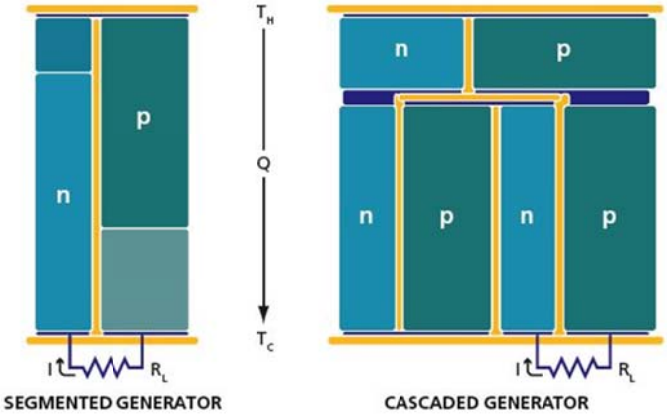

Figure 2.9: Schematic diagram comparing segmented and cascaded thermoelectric generators [Snyd2004].

2.4.4 *Fields of Application*

The fields of application for thermoelectric generator systems are very widespread. Thereby, it is possible to divide them into two main application groups: terrestrial and space applications, where the terrestrial applications can again be divided, see below. Already in Chapter 2.2, some space applications for thermoelectric energy harvesting systems are mentioned. The power generated by such systems can amount to several hundred watts. The core of these systems is a RTG or MMRTG. The advantage of this nuclear power source is the compact size, self-supply, reliability, long lifetime and operational flexibility. The thermal coupling is based on conduction or radiation. In total, the United States of America has launched over 41 RTGs; 38 of these are still active in outer space or on other planets. A detailed overview can be found in Table 1 in [Benn1995]. For terrestrial applications there can be differentiated between high and low temperature conversion. High temperature conversion is mostly linked with RTG or fossil-fueled TEGs. Here, the temperature is not waste heat, but is specifically generated for the TEG system. Application fields for RTG on Earth include weather stations, navigational aids, subsea operations and military or governmental applications. In the case of fossil-fueled TEGs, mostly propane, butane or natural gas is used as fuel. The application field for such systems is mainly the communication industry with radio, television, microwaves and telephone [Hall1995]. The low temperature conversion

plays an important role for waste heat, thus heat sources, which are freely available. Here, the efficiency is not so important and TEG-based EHS are very interesting. Some examples will be presented in Chapter 6. Natural low temperature heat sources include geothermal energy, ocean thermal energy, peat deposits and of course thermal solar energy [RoMa1995].

2.4.5 *Commercially Available Thermoelectric Generators*

Nowadays, there are some companies who sell thermoelectric generators. Most commercially available TEGs consist of bismuth telluride. Some popular TEG sellers, who usually also sell accessories like heat pipes or heat sinks and small gadgets are:

- European Thermodynamics Ltd., Leicestershire, United Kingdom: http://www.europeanthermodynamics.com/,
- Hi-Z Technology, Inc., San Diego, United States of America: http://www.hi-z.com/,
- Marlow Industries, Inc., Dallas, United States of America: http://www.marlow.com/,
- Quick-Ohm Küpper & Co. GmbH, Wuppertal, Germany: http://www.quick-ohm.de/,
- Tellurex, Traverse City, United States of America: http://tellurex.com/ and
- Thermalforce, Berlin, Germany: http://www.thermalforce.de/.

Sellers especially for the low temperature sector are:

- Micropelt, Freiburg, Germany: http://www.micropelt.com/index.php and
- Otego, Karlsruhe, Germany: http://www.otego.de/de/,

while Otego is still in the development phase of its products and they use an organic semiconductor as thermoelectric material.

High temperature TEGs, based on calcium manganese or lead tin telluride, are marketed by:

- TECTEG MFR., Aurora, Canada: http://thermoelectric-generator.com/ and
- Thermonamic, Nanchang, P.R. China: http://www.thermonamic.com/.

There are also companies who sell big thermoelectric power generation systems, which can generate from a few hundred watts up to 25 kilowatts (cf. E1 from Alphabet Energy):

- Alphabet Energy, Inc., Hayward, United States of America: https://www.alphabetenergy.com/,
- Thermonamic, Nanchang, P.R. China: http://www.thermonamic.com/ and
- Telgen, Moscow, Russia: http://www.telgen.ru/.

These systems clearly consist of more than only the thermoelectric devices. They need a fuel system, a burner, the thermoelectric converter, a heat sink, the housing and the electronics. The most common fuels are propane, butane and natural gas. The systems are economically useful, especially when it comes to reliability, a long interval between service, low maintenance and a long

life [McNa1995]. As thermoelectric generators already deliver these properties, the other components also have to fit these so as not to ruin any significant advantage.

Figure 2.10 shows an overview of different thermoelectric devices. From left to right, there are a TEG of Hi-Z Technology, a TEG of European Thermodynamics and a TEC of Thermonamic. The standard size for TEGs is normally 40 x 40 mm, but other sizes are also possible.

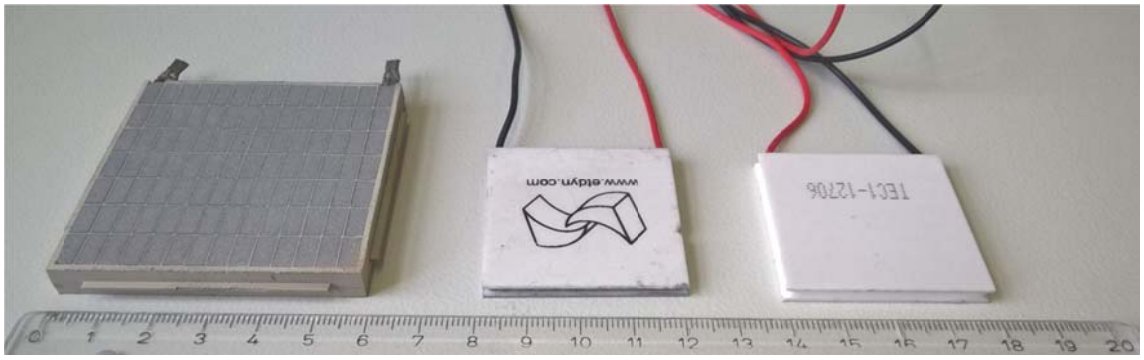

Figure 2.10: An overview of different thermoelectric devices, a TEG of Hi-Z Technology, a TEG of European Thermodynamics and a TEC of Thermonamic are pictured (from left to right).

2.4.6 Sources of Failure

To build up a thermoelectric EHS, many things have to be considered. There are a lot of sources of failure which can largely be avoided if they are known. In principle the failure sources can be divided into two categories, the external influences (environmental influences) and the installation errors. An overview of the different sources of failures and their assignment is shown in Table 2-3.

Table 2-3: Different sources of failures for thermoelectric EHSs divided into environmental influences and installation errors [MaBu1995].

environmental influences	moisture	high temperature	thermal cycling	mechanical stress
installation errors	mounting	handling	heat sink	current drain

The single sources of failure are described in the following, [MaBu1995] and [Sche2007]:

- **Moisture:** If an electrical current flows through a thermoelectric module and it is exposed to high moisture, galvanic corrosion at the thermoelements, conductor stripes or solder can occur. This reduces the efficiency of the thermoelectric device.
- **High temperature:** High temperature can destroy thermoelectric material. This leads to thermal diffusion of metal ions or solder in the legs and thus reduces the efficiency. Moreover, the thermoelectric material can decompose.

- **Thermal cycling:** Rapid thermal cycling causes thermal stress on the device. The device expands and contracts. To guarantee a long life time, it is necessary to reduce the amount of thermal cycling and to lengthen the heating phase and the cooling phase.
- **Mechanical stress:** Mechanical stress, which occurs during a shock or vibration, poses no problem as long as the device has been attached properly. Otherwise, there may be massive movements of the plates against each other due to the thermal expansion. This shear forces can destroy the device. To prevent such a situation, springs can be used to fix it.
- **Mounting:** It is important to know that the thermoelectric device will bend due to the thermally different stress on both sides. One side contracts, whereas the other side stays constant or expands. This results in a bending of the device. That is why a soldering of one side to the heat sink or heat source is not advantageous. The device requires the ability to deform.
- **Handling:** The pressure load on the thermoelectric device should be evenly distributed. Otherwise, the ceramic plates can crack or break and this increases the risk of short circuits between the thermolegs. Moreover, a strong torque on the connection cables causes a release of the cables.
- **Heat Sinking:** If the heat sink is not capable of dissipating enough heat, the solder connections can melt and when they are completely disjoined, the device will be out of order. Therefore, it is very important that the heat sink match with the heat to be dissipated.
- **Current drain:** A pulsed current drain (pulse width modulation (PWM)) is to be avoided and a continuous current drain should be ensured.

Figure 2.11 shows some common failure images: molten solder joints of the lead wires due to high temperatures (a), cracks in the ceramic plate due to an incorrect pressure load (b), broken corners caused by too firmly tightened screw connections which gives the device no possibility to expand during thermal stress (c) and molted matrix material caused by too high temperatures (d). To avoid such failures, a suggestion of a model-based multi-physics development process is given in Chapter 4.

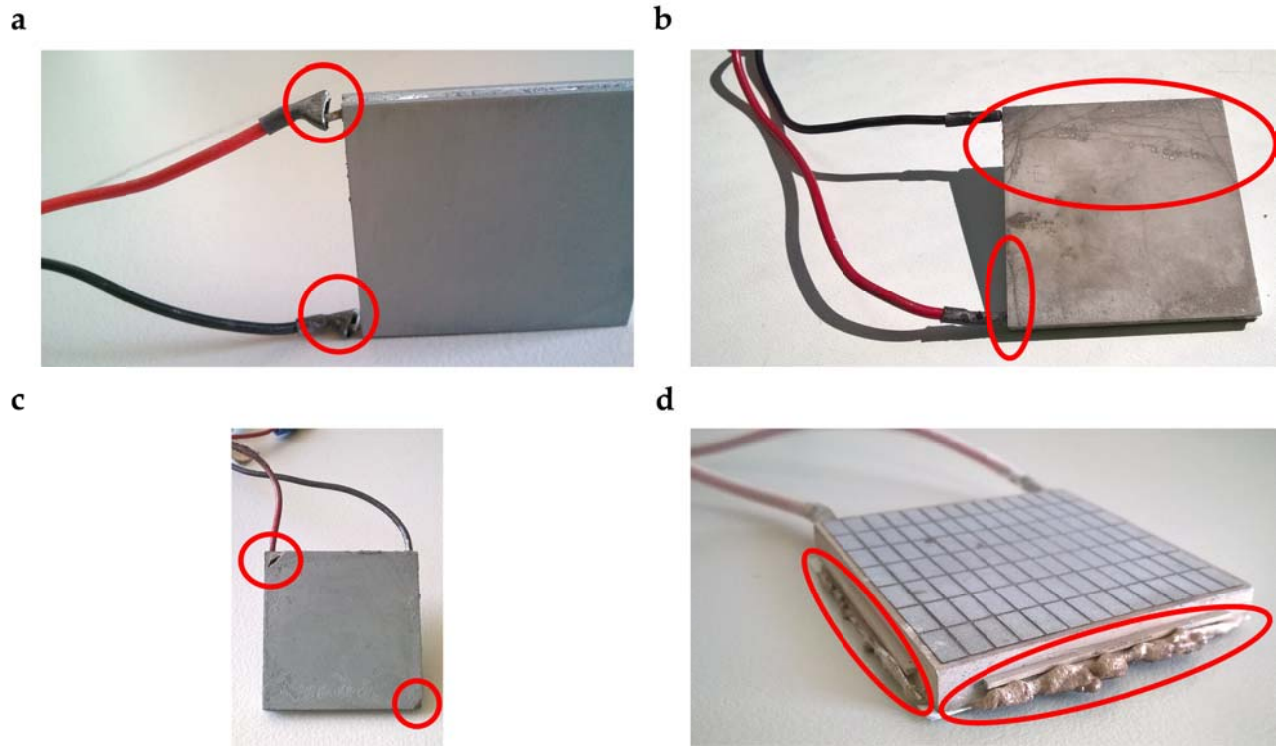

Figure 2.11: Some failure images of damaged TEGs; a: molten solder joints of the lead wires due to high temperatures; b: cracks in the ceramic plate due to an incorrect pressure load; c: broken corners caused by too firmly tightened screw connections which gives the device no possibility to expand during thermal stress; d: molted matrix material caused by too high temperatures

3 Multiphysics Simulation

For a model-based development of thermoelectric energy harvesting systems, a multiphysics simulation is necessary. Therefore, this chapter describes the development of a Modelica library, called `EHSTEG` *library, which fulfills this purpose. The V-model approach is applied to develop the library and hence, the principles of this approach will be presented first. This will be followed by a short description of the open modeling language Modelica and the simulation environment Dymola, which are used here. After that, the core model of thermoelectric legs based on a one-dimensional spatial resolution is presented, followed by the expansion of this model to an overall Modelica library for complete thermoelectric devices (*`ThermoelectricGenerator` *library). Afterwards, the independent* `HeatPipe` *library is described, which is useful for heat transfer in thermoelectric EHSs. Then further necessary system components, like for example different cooling methods, are established. Finally, this all flows into one library, called* `EHSTEG` *library, which is a library for the purpose of a model-based development of complete thermoelectric energy harvesting systems. To conclude this chapter, a few modeling instructions are given.*

3.1 V-model Approach

To do a multiphysics simulation of thermoelectric EHSs, a library will be developed in this chapter. This should provide end-users with an easily manageable tool to configure such systems. Therefore, a software development approach, the V-model, is used, see [BrDr1995]. Figure 3.1 shows the different stages of the V-model, in which from left to right, the time axis of the development process is shown and top-down the decomposition of the process. Although it is a model for the software development process, it applies for the building of a thermoelectric EHS library as well [MeLi2000]. At first, a design phase with increasing decomposition is passed through. Afterwards, the test phase starts bottom-up with the smallest components and ends with the complete system test.

The design phase starts with a requirements analysis, e.g. the recuperation of waste heat into electrical energy, and a preliminary rough design of possible systems, e.g. the use of a thermoelectric EHS. This will be followed by a more detailed design, e.g. component classes which are required for a thermoelectric EHS (heat source, heat transfer, thermoelectric device, cooling option, electrics, and so on) and finally ends up with a component design. The modeling and implementation of finally found and necessary components is done in Chapters 3.3 to 3.5, whereas the independent `ThermoelectricGenerator` library is presented in Chapter 3.3 and the independent `HeatPipe` library in Chapter 3.4. The further components which are needed for the model-based development of thermoelectric EHSs are depicted in Chapter 3.5. The structure of the

finally developed `EHSTEG` library, which involves the usage of the `ThermoelectricGenerator` and the `HeatPipe` library, reflects the V-model approach and is shown in Chapter 3.6.

After the design phase and the implementation—which will be done here in Modelica, compare the following subchapter—the testing phase starts. Here, different tests validate the designs done before. First, the single components are tested, then a cluster of components (integration test) and after that complete thermoelectric EHSs (system test), which ends with the acceptance test. Of course, the verification and validation of design elements can lead to an adjustment of these, which can therefore become an iterative process. Information on the test phase—meaning the verification and validation of previously developed components—is also shown in the following subchapters, whereas complete modeled thermoelectric EHSs will be shown in the application Chapter 6.

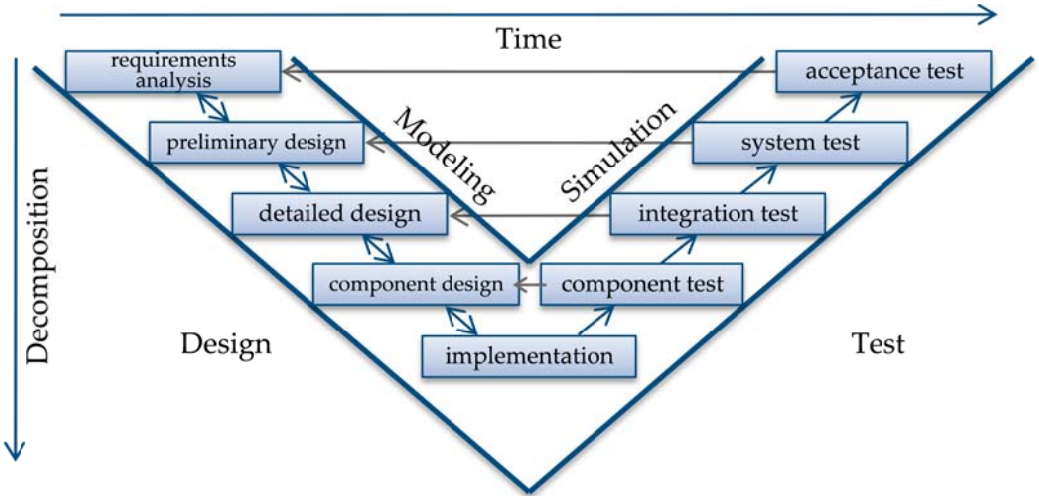

Figure 3.1: V-model, a system development process.

3.2 Modelica/Dymola

Modelica is an open and free modeling language, which is component-oriented and allows a structure-preserving way of modeling complex physical systems by direct use of ordinary and differential-algebraic equations. The components are reusable, which is supported by graphical model diagrams on distinct hierarchical levels. A lot of Modelica libraries are available, e.g. mechanical, electrical, hydraulic, pneumatic, fluid, control, thermal and more. So, the range of applications is very versatile. That is the reason, why Modelica has been used in industry since 2000 for example by Audi, BMW, Daimler, Ford, Toyota, VW, ABB and Siemens [Mode2016]. The language was initiated by Hilding Elmqvist in 1996 and is continually developed by the non-profit Modelica Association, which also develops the free Modelica Standard Library [Otte2013]. A commercial simulation environment for Modelica is Dymola from Dassault Systèmes.

The great advantage compared to other simulation tools is the possibility of a multiphysics and component-oriented simulation. The usage of different physical domains in one model is possible

and thus, is advantageous for the development of thermoelectric EHS as they consist of thermal, thermoelectrical, fluid and electrical effects as well as control aspects. In contrast to other works where only the TEGs themselves are modeled, e.g. in Matlab/Simulink [TsLi2010], in SPICE [Ch++2011] and [LaLu2011], by transferring thermal into electrical behavior, or in finite-element method simulation tools such as COMSOL [Eb++2009], or ANSYS [AnLo2005] and [Zi++2010], the multiphysics simulation concept presented here can model the complete thermoelectric EHS. So, the use case here is a very typical one for the modeling language Modelica.

3.3 Model of a Thermoelectric Device

3.3.1 Component Design

The core idea is the development of a generic model for thermoelectric devices which can be used for thermoelectric power generation. The model should be very flexible, so that different materials as well as different geometric dimensions are adjustable. It is often assumed that the material parameters, the Seebeck coefficient α, the thermal conductivity λ and the electrical resistivity ρ are temperature-independent. In real systems, this is only valid for small temperature differences, see material curves in Figure 2.6. Thus, a calculation with averaged parameters serves only as a reference and that is why a better modeling approach has to start with a generic segmentation of the thermoelectric legs which was also done by some other researchers, like in [Juni2010], Chapter 2.2.3 or in [Li++2010] and [Fa++2014]. Now, with the segmentation of a thermoelectric leg, average material properties for one segment as well as a small temperature difference over one segment is given and this justifies the usage of temperature-independent material properties for this section in this temperature range.

The detailed model of a thermoelectric device, especially for the thermoelectric legs applied in this work, is reproduced in [Fe++2014]. F. Felgner has developed the thermoelectric core model on which the later presented `ThermoelectricGenerator` library of this work is based, and this core model will be presented in this section. Figure 3.2 illustrates the model structure in Modelica/Dymola on the right hand side and the corresponding physical structure on the left hand side. The core component of the model of a thermoelectric device is one segment of a thermoelectric leg, cf. Figure 3.2(a) and Figure 3.2(d). Building on that, Figure 3.2(b) and Figure 3.2(e) show the thermoelectric leg assembled by many segments and finally, Figure 3.2(c) shows a complete thermoelectric device with N leg pairs. Figure 3.2(f) is the matching Modelica model of the device. In the following, the steps to come from a single segment of a thermoelectric leg to a complete thermoelectric device are explained, where the equations presented in Chapter 2.4.1 are the basis for this.

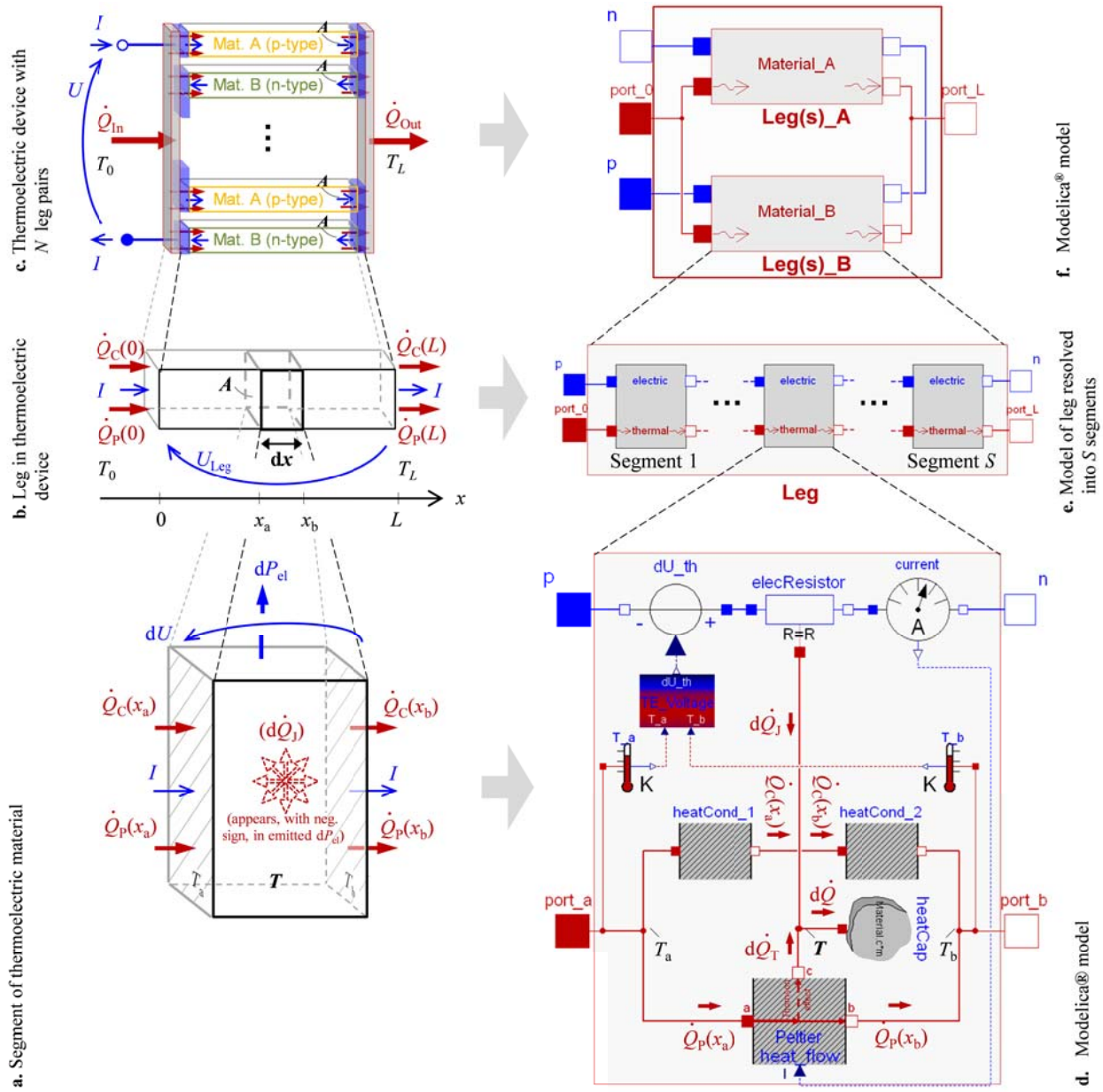

Figure 3.2: Modelica core model of a thermoelectric device on the right hand side and the corresponding physical structure on the left, taken from [Fe++2014]: (a) segment of a thermoelectric leg, (d) corresponding Modelica model; (b) one thermoelectric leg of the device, (e) model of one leg resolved into *S* segments; (c) thermoelectric device with *N* leg pairs, (f) corresponding Modelica model.

In [Fe++2014], the electrical behavior of one physical segment (Figure 3.2(a)) is given by Equation (3.1):

$$\mathrm{d}U = \mathrm{d}U_{\mathrm{th}} - \mathrm{d}U_{\mathrm{R}} = \alpha\left(-\frac{\partial T}{\partial x}\right)\mathrm{d}x - \mathrm{d}R \cdot I\,, \tag{3.1}$$

where $\mathrm{d}U_{\mathrm{th}}$ is the thermal voltage due to the EMF, the Seebeck voltage, and $\mathrm{d}U_{\mathrm{R}}$ is the voltage drop due to the material resistance $\mathrm{d}R$. The thermal behavior for the segment results from an energy balance and is shown in Equation (3.2), [Fe++2014], compare also Equation (2.18) and (2.19).

$$c\rho\frac{\partial T}{\partial t}A\mathrm{d}x = \mathrm{d}\dot{Q}_\mathrm{c} - \mathrm{d}\dot{Q}_\mathrm{T} + \mathrm{d}\dot{Q}_\mathrm{J} = -\frac{\partial}{\partial x}\left(-\lambda\frac{\partial T}{\partial x}\right)A\mathrm{d}x - IT\frac{\partial \alpha}{\partial x}\mathrm{d}x + I^2\frac{r}{A}\mathrm{d}x\,, \qquad (3.2)$$

where the left hand side is the derivative of the internal energy (ρ stands here for the density), c is the specific heat capacity and the right hand side is the heat absorption due to conduction, the heat absorption due to the Thomson effect and the Joule heat production. The series connection of multiple segments represents finally a one-dimensional discretized thermoelectric leg, cf. Figure 3.2(b) and Figure 3.2(e). For more modeling details see [Fe++2014].

In the end, the assumptions made lead to a thermally transient, electrically static and electronically static thermoelectric material behavior.

To come now to the complete device as shown in Figure 3.2(c), a further parameter N has to be introduced as shown in Chaper 2.4.1. A thermoelectric device normally consists of a multiplicity of thermoelectric couples and one couple again consists of a p-doped leg ($\alpha > 0$) and an n-doped leg ($\alpha < 0$), which are thermally in parallel and electrically in series. N is here the number of couples, which is normally about 100, and with an additional discretization S of every leg, there would be $2N \cdot S$ sates to calculate. As the legs are thermally in parallel and have the same current, all p-doped legs (of material A) can be merged to one A-leg and the same can be done for the n-doped legs (of material B) to one B-leg. To achieve the correct results now, several parameters have to be multiplied by N, cf. (2.27) and (2.28). So finally, there are only $2 \cdot S$ states to calculate, see Figure 3.2(f).

3.3.2 Validation

In line with the V-model approach, the thermoelectric device component is now tested and validated (component test). The model is tested with real measurements, cf. [Fe++2014]. For that purpose, a static and a dynamic validation was done.

To validate the steady-state behavior, the previously developed model of Chapter 3.3.1 (transient distributed-properties model, $\mathrm{TrDP}_{\alpha\mathrm{Int}}$) and a simple model consisting of one segment per leg and using an average temperature (static averaged-properties model, StAP)—both named like in [Fe++2014]—are compared with data given by manufacturer datasheets (Thermalforce). Besides geometrical information used as model parameters, the datasheets for different TEGs give data for the load voltage and current. The different types vary in the number of thermocouples and in the geometrical size of the thermoelectric legs. This information has validity for a temperature difference of 100 K, where the hot side is at 423.15 K. Table 3-1 shows the correctness of load voltage (load resistance is equal to internal resistance of TEG) for both models. The steady-state deviation of the StAP model turns out to be negligible if the considered TEG operates between 300 and 400 K, cf. [Fe++2014]. The results for the internal resistance show major differences of up to 60%. As described in the V-model approach, there now has to be an iteration step to refine the

component. It can be assumed that the differences in the internal resistance is due to the neglected contact resistances between the thermocouples (up to 287), which leads to the improvement described below of this thermoelectric device model. If the value of the internal resistor is corrected, the static validation for the load current (Table 3-2) shows the correctness of the models.

Table 3-1: Steady-state validation of TrDP$_{\alpha Int}$ and StAP models for load voltage (TEGs from Thermalforce) [Fe++2014].

Type	Datasheet	TrDP$_{\alpha Int}$		StAP	
	U_L (V)	U_L (V)	Error (%)	U_L (V)	Error (%)
127-200-9	2.808	2.782	-0.93	2.800	-0.28
199-200-5	4.320	4.362	+0.97	4.391	+1.64
254-200-7	5.508	5.568	+1.09	5.608	+1.82
287-150-16	6.534	6.29	-3.73	6.336	-3.03

Table 3-2: Steady-state validation of TrDP$_{\alpha Int}$ and StAP models for load current (TEGs from Thermalforce) [Fe++2014].

Type	Datasheet	TrDP$_{\alpha Int}$		StAP	
	I_L (A)	I_L (A)	Error (%)	I_L (A)	Error (%)
127-200-9	0.596	0.591	-0.84	0.594	-0.34
199-200-5	1.726	1.743	+0.98	1.755	+1.68
254-200-7	0.542	0.548	+1.11	0.552	+1.85
287-150-16	0.480	0.462	-3.75	0.465	-3.12

The test setup for the dynamic validation is done with a step response scenario: an initially cooled TEG is instantaneously placed on the hot surface of a copper block. A TEG 199-200-5 of Thermalforce with a load resistance of 2.7 Ω (internal plus resistance between the contacts) is used. A temperature-controlled heating plate acts as heat source. A measurement PC logs the voltage over the resistance. The arithmetic average of three series of measurements is compared with the simulation result. The Modelica model is shown in Figure 3.3 as well as the test setup in the inset of Figure 3.3.

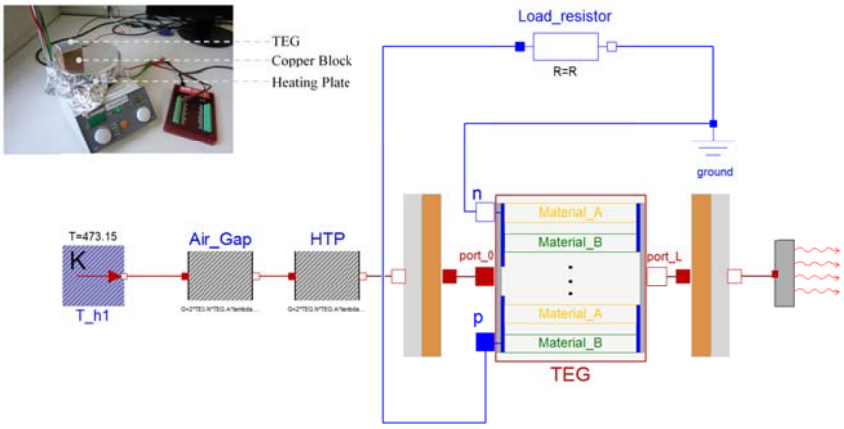

Figure 3.3: Modelica model of the experimental setup for dynamic validation, inset: test setup [Fe++2014].

A comparison with the different TEG models is shown in Figure 3.4. The results of the simulation models are in good accordance with the measurements. Figure 3.4 does not show the step response of the pure TE material but the dynamic behavior for the complete TEG (including ceramics). Because of the inert behavior of the peripheral components, the dynamics of the TEG have little effect.

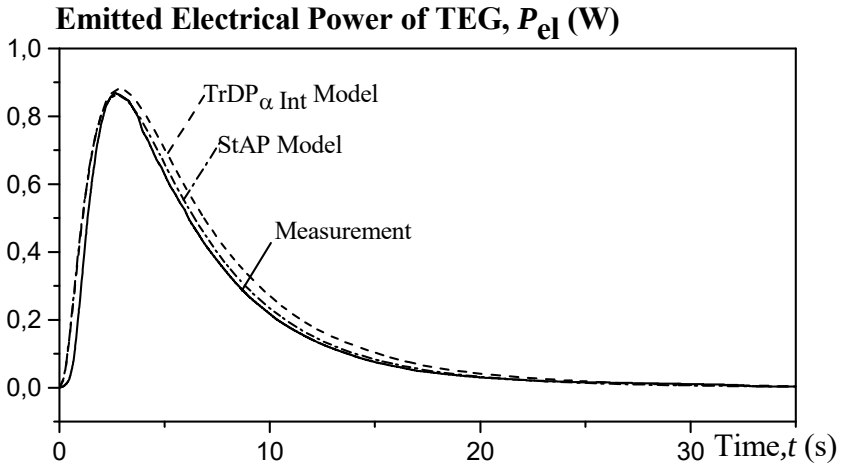

Figure 3.4: Dynamic validation: Comparison of the arithmetic average of three series of measurements with the two different TEG models [Fe++2014].

3.3.3 `ThermoelectricGenerator` Library

The aforementioned model of the thermoelectric legs provided by [Fe++2014] is the core of the developed modeling library `ThermoelectricGenerator`, which is developed for the dynamic simulation of TEGs in one-dimensional spatial resolution and is presented in [NeEF2014]. The library is usable by end users without deeper knowledge through a graphical user interface (GUI), see Figure 3.5. In addition to the core model, the library also considers the leg connectors and the packaging of thermoelectric devices. So, the previously described model, which is correct for thermoelectric legs and their serial connection, is now expanded to a model for real thermoelectric devices. Figure 3.5 shows the top dialog box, which is the main parameter list for a thermoelectric device. There, the geometric parameters can be set. In the first underlying dialog box (red frame), the thermoelectric material properties as well as the leg connector properties can be set. This represents the model from F. Felgner. The second underlying dialog box (blue frame) adjusts the packaging properties.

In the library, it is assumed that each side of the thermoelectric device has a uniform temperature resulting in a one-dimensional modeling. As already mentioned, the dynamics of the TEG is modeled thermally transient, electrically static (no electrical capacities are considered), and electronically static (charge displacement without delay). An overview of the library structure and the top-level diagram of a thermoelectric device model are shown in Figure 3.6. The top-level model of a complete thermoelectric device (`TEG_Module`) uses further models from four sub-

packages. It reflects the concept of component-oriented modeling, whereas the model of connected thermoelectric legs (CTEL) is in the center, surrounded by ceramic plates. The library contains several more or less detailed models of CTELs in the sub-package `inner_TEG`. All CTEL models are derived from one base class (`CTEL_base`). This base class defines the connectors of the components.

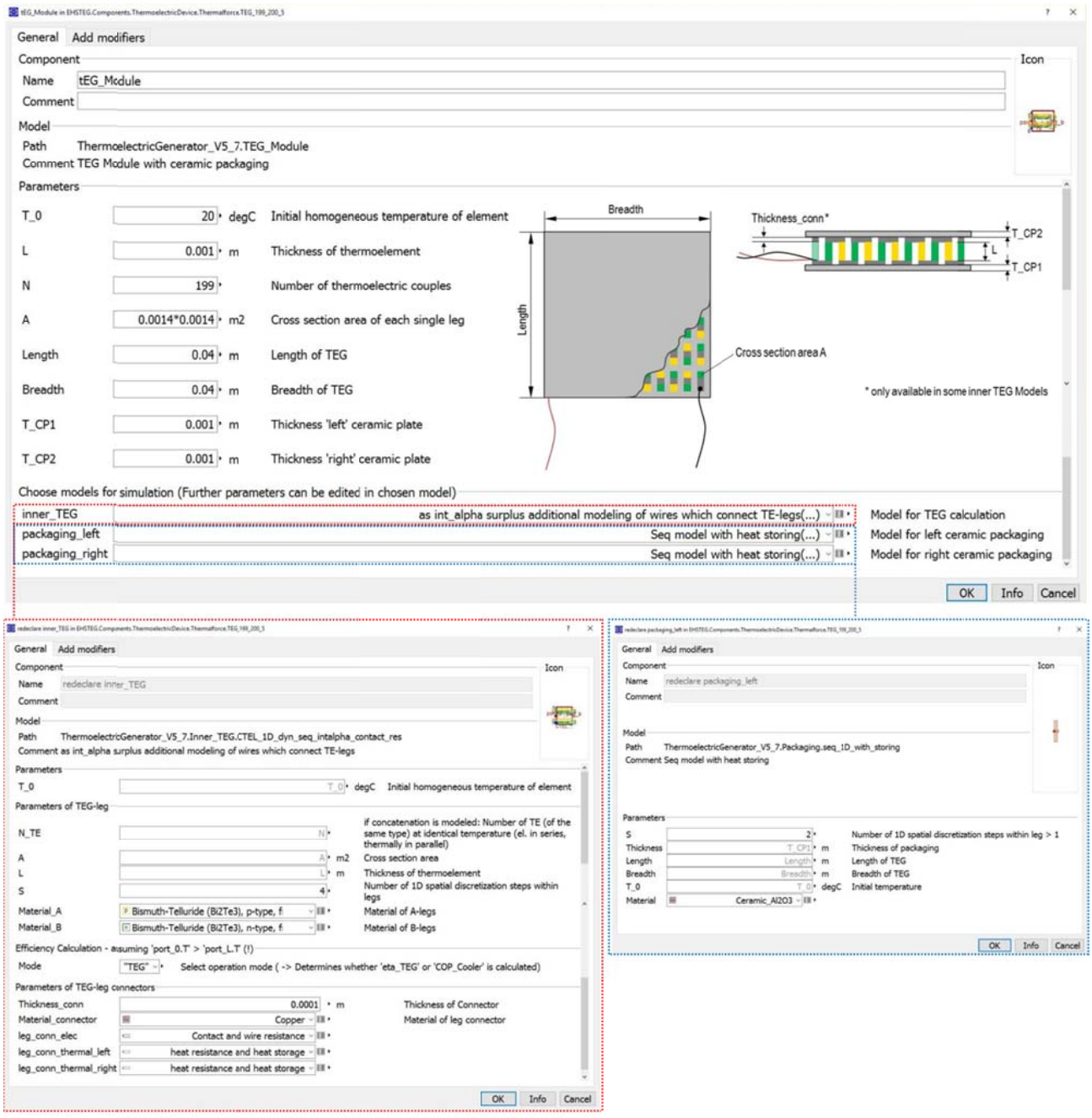

Figure 3.5: GUI of a thermoelectric device in the `ThermoelectricGenerator` library. The top dialog box is the main box, where the geometric parameters can be set. The red dialog box sets the thermoelectric material properties as well as the leg connector properties and the blue dialog box adjusts the packaging properties.

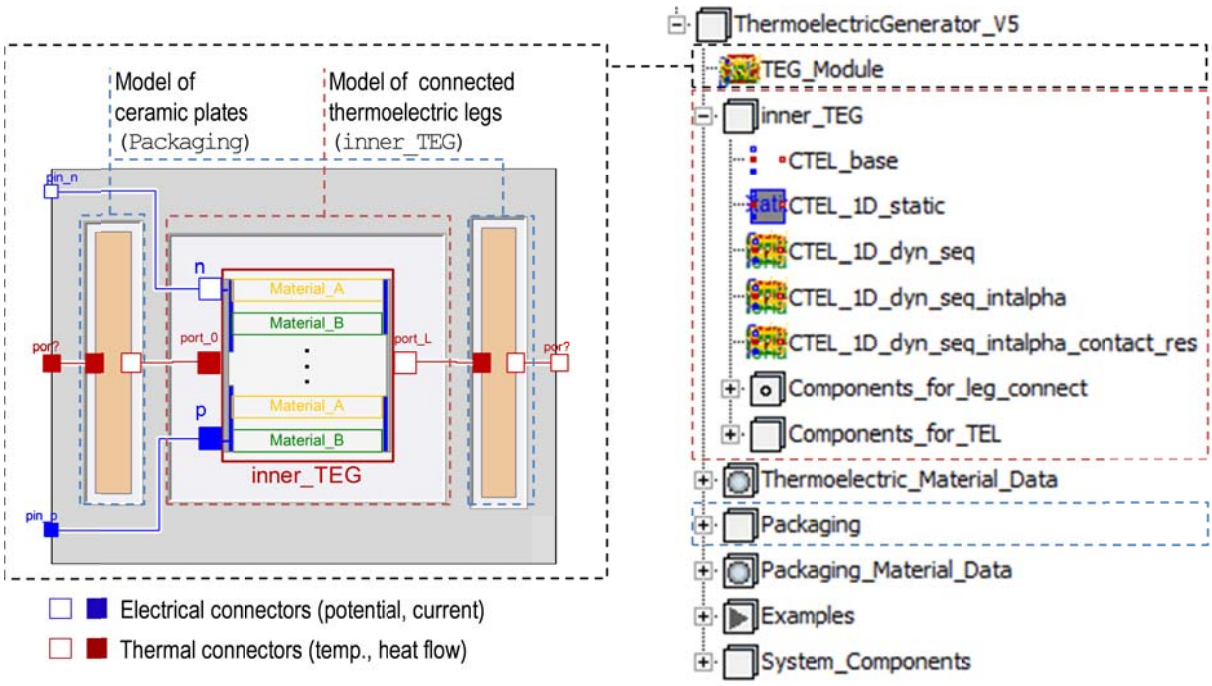

Figure 3.6: Top-level diagram of a thermoelectric device (left) and library structure (right) [NeEF2014].

By means of this modeling concept, the user of the library can easily select the appropriate CTEL model used by the `TEG_Module`. The simple model `CTEL_1D_static` corresponds to the aforementioned StAP model, the `CTEL_1D_dyn_seq` to the TrDP model and the `CTEL_1D_dyn_seq_intalpha` to the $TrDP_{\alpha Int}$ model; for more information about the differences see [Fe++2014]. The `CTEL_1D_dyn_seq_intalpha_contact_res` is the new model based on the $TrDP_{\alpha Int}$ model, which includes the electrical and thermal effects of the bonds connecting the thermoelectric legs (TELs). The electrical behavior is described by the line resistance, determined by material and geometrical parameters, and the contact resistance. The value for the contact resistance is based on Chapter 10.3 of [Gold2010] and is a changeable parameter in the model. The model for the heat transfer of the surrounding ceramic plates is changeable. There is the option to use a model for an ideal heat transfer without any storage and thermal resistance, as well as a model following the one-dimensional heat equation involving thermal conduction and a heat capacity. For the calculation, material and geometric parameters of the TEG are used.

The parameters of the CTEL models are adjustable via the GUI presented in Figure 3.5. The corresponding thermoelectric material data is loaded from data records provided in the sub-package `Thermoelectric_Material_Data`. Data for p and n-doped Bi_2Te_3 and PbTe are currently available. These data records contain temperature-dependent material parameters like the specific heat capacity and Seebeck coefficient which are considered by the CTEL models. If required and if material data is available, new materials can easily be added to the library. The package `Packaging` contains several models of the surrounding ceramic plates. Some of these models use the material data given in `Packaging_Material_Data`.

Finally, an open source Modelica library for the modeling of thermoelectric devices, including the leg connectors and the packaging of thermoelectric devices, was built up in a multi-physics manner and is named `ThermoelectricGenerator` library.

3.4 Model of a Heat Pipe – `HeatPipe` library

3.4.1 Component Design

A main challenge to build up a thermoelectric EHS is a good heat transfer to and from the TEG. The temperature difference over the device should be very high and so it is important to transfer as much heat as possible to the hot TEG side and to dissipate the waste heat from the cold TEG side. As heat pipes have a 1000-fold better thermal conductivity than copper [Onot2008], they are very suited to this purpose. This is the reason why a `HeatPipe` library has been developed in this context.

Heat pipes belong to the category of heat exchangers and are heat transfer devices containing a working fluid. As they are closed systems, they do not need maintenance—just as TEGs. The first heat pipe was presented by Gaugler in 1942 [Gaug1944]. Today, they are mainly used in spacecraft applications and computer systems for the thermal management of the components. The basic operating mode of a heat pipe is comparable with a thermodynamic cycle, whereas the main physical effects responsible for the heat transfer are thermal conduction and phase transition. The basic structure of a heat pipe is shown in Figure 3.7a.

A heat pipe is normally an evacuated pipe with a wick structure inside, soaked with a working fluid. The wick structure is arranged such that a vapor space is in the middle. At the hot surface of the heat pipe, the working fluid absorbs the heat and evaporates. Then, the vapor streams to the cold surface of the heat pipe and releases the latent heat, where it condenses. Due to the capillary action, the condensed working fluid flows back to the hot surface, where the cycle starts anew [Onot2008]. There is no pump necessary meaning a heat pipe is a passive heat transfer device and the return takes place through the capillary structure. The process corresponds to a thermodynamic cycle. Theoretically, the heat pipe can be separated into three zones, the evaporation, the adiabatic and the condensation zone, cf. Figure 3.7. In general, different combinations of wall material, wick material and working fluid are possible.

For modeling a heat pipe for thermoelectric EHSs in Modelica/Dymola, three different modeling approaches are studied, namely the single resistance approach, the resistance network approach and the physical approach, as described below.

The **single resistance approach** is a very simple modeling approach. A single thermal resistance represents the heat pipe's behavior. The value of the thermal resistance is normally given by the datasheet of the heat pipe.

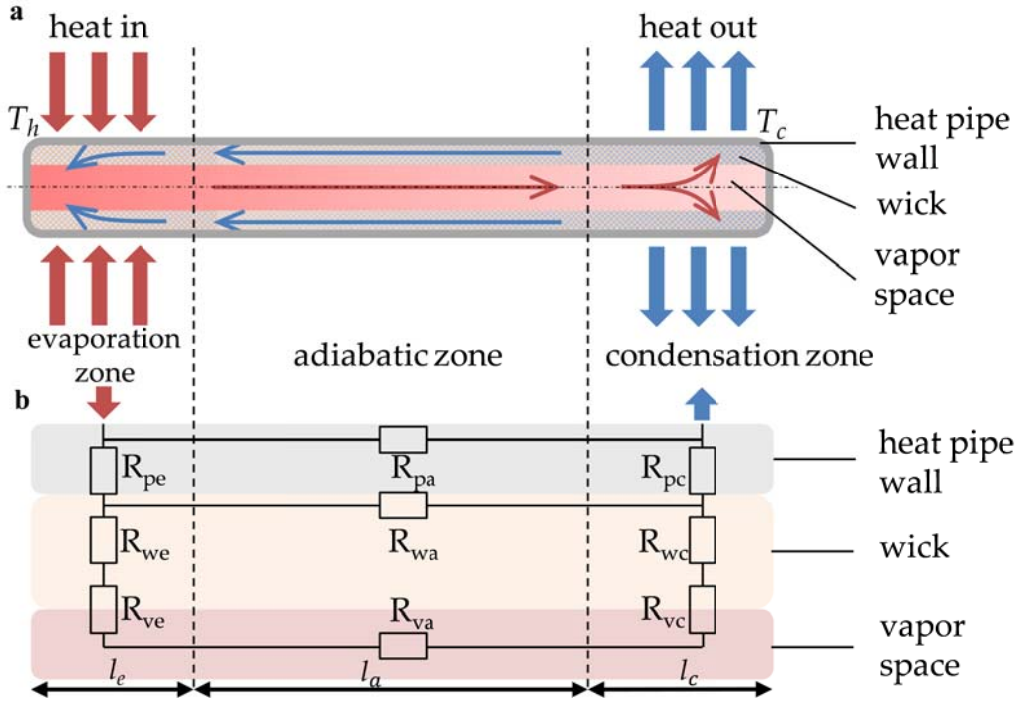

Figure 3.7: a) Basic structure and working principle of a heat pipe, b) Thermal equivalent network of a heat pipe [NeFr2017b].

A more detailed modeling approach is the use of a **thermal equivalent network** of a heat pipe as shown in Figure 3.7b. The equations to calculate the thermal resistances are primarily the ones for radial and axial resistances. Only the equivalent resistance R_{va} for the axial heat transfer in the core is different. `ThermalResistor` components of the Thermal Library of the Modelica Standard Libraries [Mode2016] can be used to build up the network. In this approach, material, medium and geometrical properties are included. The single components are modified according to the following Equations (3.3) to (3.6). The radial thermal resistances are given in Equation (3.3), the axial resistances by Equation (3.4):

$$R_{jk} = \frac{\ln(r_o/r_i)}{2\pi L_k \lambda_j}, \tag{3.3}$$

$$R_{jk} = \frac{L_k}{\pi \lambda_j \left(r_o^2 - r_i^2\right)}, \tag{3.4}$$

where R_{jk} is the thermal resistance, r_o and r_i the outer and inner radii of the considered section, L_k the length and λ_j the thermal conductivity, whereby $j \in \{p='pipe', v='vapor', w='wick'\}$ and $k \in \{a='adiabatic', c='condensation', e='evaporation'\}$. R_{ve} and R_{vc} are the thermal resistances of the vapor-liquid surfaces at the evaporation and the condensation zone. R_{va} is the thermal resistance for the axial heat transfer of the vapor in the vapor space. It is calculated from Equation (3.5), according to Chapter 16.1 in [Shab2010].

$$R_{va} = \frac{8\mu_v L_{eff} T_v}{\pi \rho_v^2 r_v^4 \Delta h_v^2}, \tag{3.5}$$

with μ_v as the dynamic viscosity of the vapor, L_{eff} as the effective length of the heat pipe, see Equation (3.6), T_v as the temperature of the vapor, ρ_v the density of the vapor, r_v the radius of the vapor space and Δh_v as the latent heat of vaporization.

$$L_{eff} = l_a + 0.5 \cdot (l_e + l_c) , \tag{3.6}$$

with l_k as the length of the adiabatic (a), evaporation (e) or condensation (c) zone.

For the single resistance approach and the resistance network approach, the required heat flow through the heat pipe is then obtained by the following equation:

$$\dot{Q} = \frac{\Delta T}{R_{th}} , \tag{3.7}$$

where $\dot{Q}$ is the heat flow rate transported through the heat pipe, ΔT the temperature difference between evaporation and condensation zone and R_{th} the thermal resistance either given by the single resistance or the resistance network.

The third approach is the **physical approach** for a steady state. Here, the physical equations for heat transfer and fluid flow theory are summarized to model the heat pipe behavior. The following equations are from [Mich2004], Chapter 2 of [ReMK2014] and [Step2006] and are valid for the assumption of a laminar flow in the vapor space under steady state conditions. A more detailed description of the physics, also considering turbulent flows and different limitations to heat transport in a heat pipe can be found in Chapter 2 of [ReMK2014] and [Step2006]. As the working fluid flows in a closed system, for correct operation, the following condition has to be met:

$$0 = \Delta p_c + \Delta p_v + \Delta p_l , \tag{3.8}$$

where Δp_c is the capillary pressure difference, Δp_v the vapor pressure difference and Δp_l the liquid pressure difference. The capillary pressure difference is calculated by:

$$\Delta p_c = \frac{2\sigma}{R_{eff,\,min}} \cos \vartheta , \tag{3.9}$$

with σ as the surface tension of the working fluid, ϑ as the wetting angle and $R_{eff,\,min}$ [Kabe2006] is calculated by Equation (3.10), with the groove width w and the diameter of the wire d,

$$R_{eff,\,min} = \frac{w+d}{2} . \tag{3.10}$$

The liquid pressure difference Δp_l is calculated by two summands, one reflects the hydrostatic pressure $\Delta p_{l,\,h}$ and the other the flow pressure loss $\Delta p_{l,\,s}$, which is identified with the help of Darcy's Law.

$$\Delta p_l = \Delta p_{l,\,h} + \Delta p_{l,\,s} , \tag{3.11}$$

$$\Delta p_{l,\,h} = -\rho_l g h = -\rho_l g \cdot (\pm l \sin \varphi) , \tag{3.12}$$

$$\Delta p_{\mathrm{l,\,s}} = -\frac{\nu_{\mathrm{l}}}{K A_{\mathrm{l}} \Delta h_{\mathrm{v}}} \cdot \dot{Q}\, L_{\mathrm{eff}} \,. \tag{3.13}$$

Here, ρ_{l} is the density of the liquid, g the gravity constant, h the height, l the length of the heat pipe and φ the angle between heat pipe and horizontal. ν_{l} is the kinematic viscosity of the working fluid, K the permeability of the wick structure, see Equation (3.14), and Δh_{v} the evaporation enthalpy. The negative sign in Equation (3.12) is valid if the evaporator side is below the condenser side; otherwise the positive sign has to be used.

$$K = \frac{d^2 \epsilon^2}{122\,(1-\epsilon)^2} \,, \tag{3.14}$$

with ϵ as the porosity of the wick structure. The last missing summand of Equation (3.8), Δp_{v}, is calculated by:

$$\Delta p_{\mathrm{v}} = \Sigma_{\mathrm{k}} \Delta p_{\mathrm{v,\,k}} \,. \tag{3.15}$$

$$\Delta p_{\mathrm{v,\,k}} = -\frac{32 \mu_{\mathrm{v}}}{A_{\mathrm{v,\,a}} \Delta h_{\mathrm{v}} d_{\mathrm{v}}^2} \cdot \dot{Q} \cdot l_{\mathrm{k}} \,, \tag{3.16}$$

with $A_{\mathrm{v,\,a}}$ as the vapor cross-sectional area, d_{v} as the hydraulic diameter of $A_{\mathrm{v,\,a}}$ and $k \in \{a = \text{'adiabatic'}, c = \text{'condensation'}, e = \text{'evaporation'}\}$. Equations (3.8) to (3.16) are the main physical equations for the steady-state behavior of a heat pipe and contain the physical, material and geometrical properties as well as the properties of the medium and are implemented in a Modelica model. However, it is not always possible or easy to gain access to all needed parameters.

3.4.2 Validation

To validate the different developed heat pipe models according to the V-model, a test bed is built (heat pipe from [Conr2015]), see Figure 3.8 and measurements are recorded. To guarantee an almost adiabatic heat transfer in the heat pipe, glass wool is used to coat the pipe, see Figure 3.8b. The direct validation of the heat flow is not possible without too much effort and therefore only individual temperature states are validated as indications. The result of the comparison of measured data with the simulation data for steady-state scenarios is given in Table 3-3. All modeling approaches of the heat pipe, described previously, conform very well to the measurement data. The error fluctuates in the range of ± 4.2 %. Surprisingly, the simplest approach is the most accurate one for the steady-state scenario. The adjusted parameters are shown in Appendix **A.1**.

The result of a dynamic scenario is presented in Figure 3.9. However, only the single resistance and the resistance network approach are considered, as the physical approach is only valid for steady-state conditions. Moreover, the simulation result for a solid copper rod is also shown in the diagram. Here, one can see that the heat transfer performance of a heat pipe is significantly better than the performance of a comparable pure copper rod. In the inset diagram, it is apparent that

both approaches only slightly differ from measurement. It is notable that again, the simple resistance model shows the best conformity with measurements.

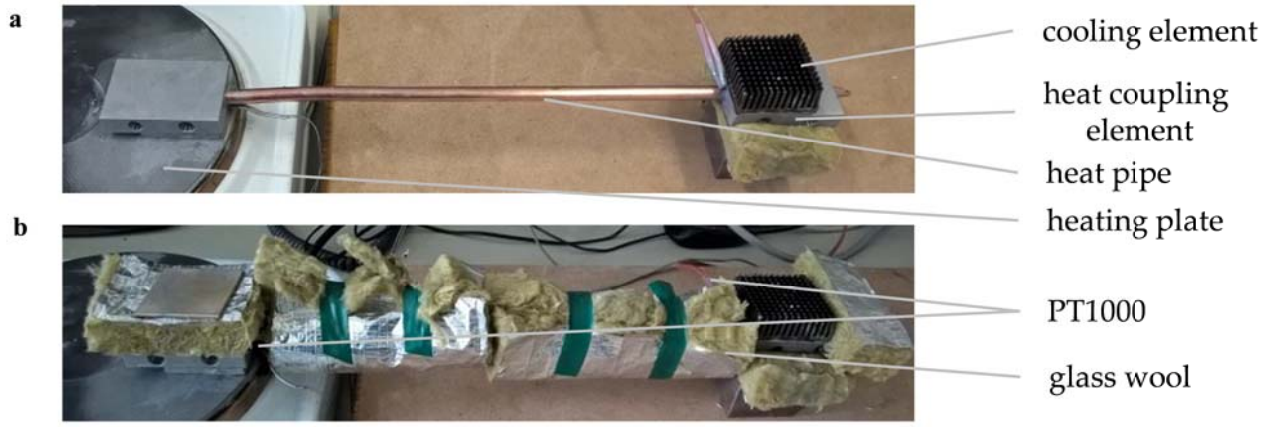

Figure 3.8: a) test bed showing the heat source (heating plate), the heat coupling elements on both sides with the heat pipe between them, the cooling element as well as the two temperature sensors (PT1000); b) test bed as in a), though completely coated with glass wool [NeFr2017b].

Table 3-3: Comparison of measurement data with the simulation results for a steady-state scenario. The measured hot side temperature is given as input to the simulation model. Approach 1 corresponds to the single resistance approach, Approach 2 to the resistance network approach and the physical approach is represented by Approach 3.

hot side temp.	real cold side temp.	Approach 1		Approach 2		Approach 3	
		simulation	**error**	simulation	**error**	simulation	**error**
140°C	132.9°C	135.5°C	**2%**	138.5°C	**4.2%**	130.6°C	**-1.7%**
130°C	125.6°C	125.9°C	**0.2%**	128.6°C	**2.4%**	127.7°C	**1.7%**
120°C	115.8°C	116.3°C	**0.4%**	118.9°C	**2.7%**	113.3°C	**-2.2%**

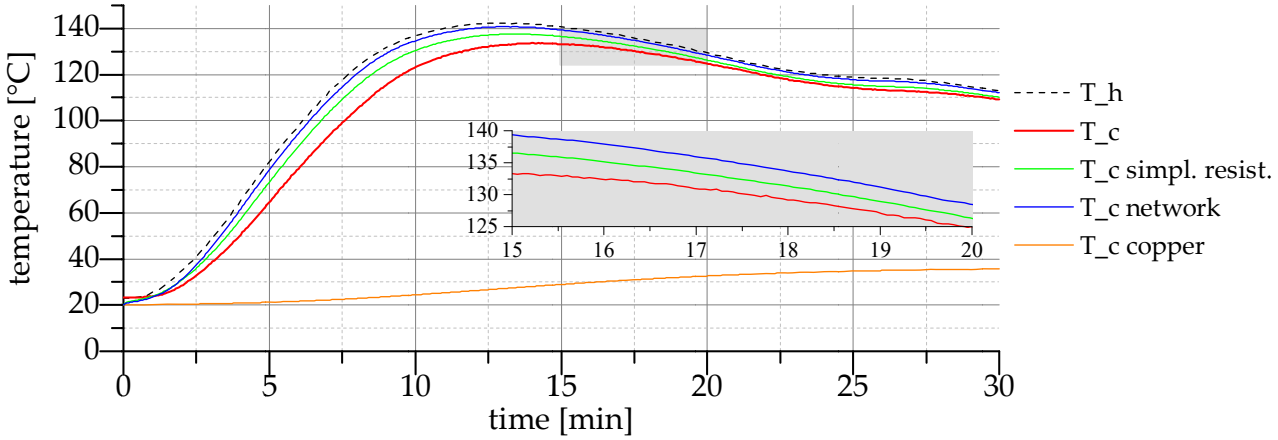

Figure 3.9: Comparison of real measurement with the simulation result of approach 1 (simple resistance) and approach 2 (resistance network) as well as a solid copper rod [NeFr2017b].

All three models have shown very good accuracy. They consider partially physical, material and geometrical properties as well as the properties of the medium. Interestingly, the simplest approach is the most accurate one and is thus appropriate for energy harvesting applications where only the temperature difference and the heat transfer are of interest. As soon as more information about the heat pipe itself is required, more complex models have to be used.

The `HeatPipe` library was also presented by the author in [NeFr2017b] and the structure of the library is shown in Appendix **A.2**.

3.5 Further System Components

3.5.1 Heat Source

For a complete EHS, further components are necessary such as heat sources—an exemplary system arrangement of an EHS is shown in Figure 3.13. Two main components are developed as heat sources. One is a heat source with direct contact to a surface (thermal conduction), e.g. in the case of a heating plate, and the other component heats a medium (convection), e.g. in the case of an exhaust gas pipe. For the heat source models, one can resort to the Modelica Standard library, particularly the thermal and the fluid libraries. Here, the key module is in each case a Modelica `CombiTable1Ds` which is more or less a look-up table for the temperature profile as a function of the time. The intermediary values are interpolated. These temperature profiles normally come from real measurements which will be described in more detail in Chapter 4. The heat source components are either connectable by a thermal port (heat source component with direct surface contact) or by a fluid port (heat source component with medium) with the other components. As these are standard Modelica ports, user-defined heat source components can also be used under the condition that they support these port types. In the case of a moving fluid, a pump or knowledge about the flow velocity of the heated medium is necessary.

3.5.2 Heat transfer

For the heat transfer from a heat source to the TEGs, the two above mentioned possibilities—thermal conduction and/or convection—have to be considered, whereby ultimately a thermal conduction always brings the heat to the hot TEG sides in the cases studied here. Thus, in thermoelectric EHSs, different heat transfers have to be modeled. The simplest is the heat transfer in the form of thermal conduction from a mainly simple geometric surface to another, e.g. the heat transfer from a heating plate through a plane copper plate and from there to a thermoelectric device. Here, conductor and capacitor models from the Modelica Thermal Library can be used. Normally, there are two conductor elements and between them a capacitor model. Based on this approach, there is a model for a copper plate and an aluminum half shell. In addition to that, the aluminum half shell also considers the convection to the ambient air and hence, also includes a

convection component. The model of an aluminum half shell will later be used for the EHS at a thermostat, cf. Chapter 6.1. Usually, there is also the need to use heat transfer paste between different components, but nevertheless there can be very small air gaps between different contact surfaces. Due to the very low thickness of the heat transfer paste and the air gap, these models only consist of a thermal conductor and have no heat capacity inside. In all mentioned components, the material parameters are already adjusted, but the geometrical parameters have to be set up by the end-user and adapted to the specific case. Nevertheless, the material parameters can also easily be changed.

The second form of heat transfer beneath thermal conduction is the transfer through convection. The modeling of the medium flow can be done with `DynamicPipe` components from the standard Fluid Library. For the `EHSTEG` library, the component `PipeSection` is developed which consists of two pipe elements whereas one will be indirectly attached with the thermoelectric device and the other represents the convection to the ambient air of the exposed pipe. To get the heat out of the medium, e.g. heat pipes or heat sinks (in a reverse manner) can be used or to get the heat from the pipe surface, e.g. aluminum half-shells can be used.

3.5.3 Cooling Elements

Component Design

To achieve a high electrical power output of TEG-based EHSs, it is not sufficient to only transfer the heat to the hot TEG side. Also, it is necessary to dissipate the heat from the cold TEG side to maintain a high temperature difference over the thermoelectric device. Therefore, both cooling possibilities, namely active and passive cooling methods, are modeled.

The passive cooling elements are the typically known heat sinks. They are heat exchangers and transfer the heat from a hot component to a medium, which is very often the surrounding air. The functionality is based on an extreme increase of the surface size, which thus delivers a better way to dissipate the heat to the medium. This surface enlargement is done by a large number of fins and a good thermally conductive material. To model such a cooling element, it is necessary to know the material and the geometrical parameters as well as the number of the fins. Based on the geometrical parameters and the number of fins, an equivalent surface area and an equivalent thickness is calculated in the model and then finally used in a combination of conductor, capacitor and convection components of the Modelica Standard Library.

Active cooling elements can be divided again into forced air or liquid cooled elements. Forced air cooling elements or CPU cooling elements are very similar to the passive heat sinks except for the fact that an additional fan is available. Thus, the heat dissipated to the surrounding air will be carried away faster and so, a bigger amount of heat can be dissipated by the cooling element. To

set up the speed of the fan and the additional power consumption, look-up tables based on the datasheet and as a function of the adjusted duty cycle are integrated. Figure 3.10 shows the Modelica model of a forced air cooling element with the parameterization for the CPU cooler 'Scythe Katana 4' [Scyt2015]. The green rectangle is the cost port, which will be explained later.

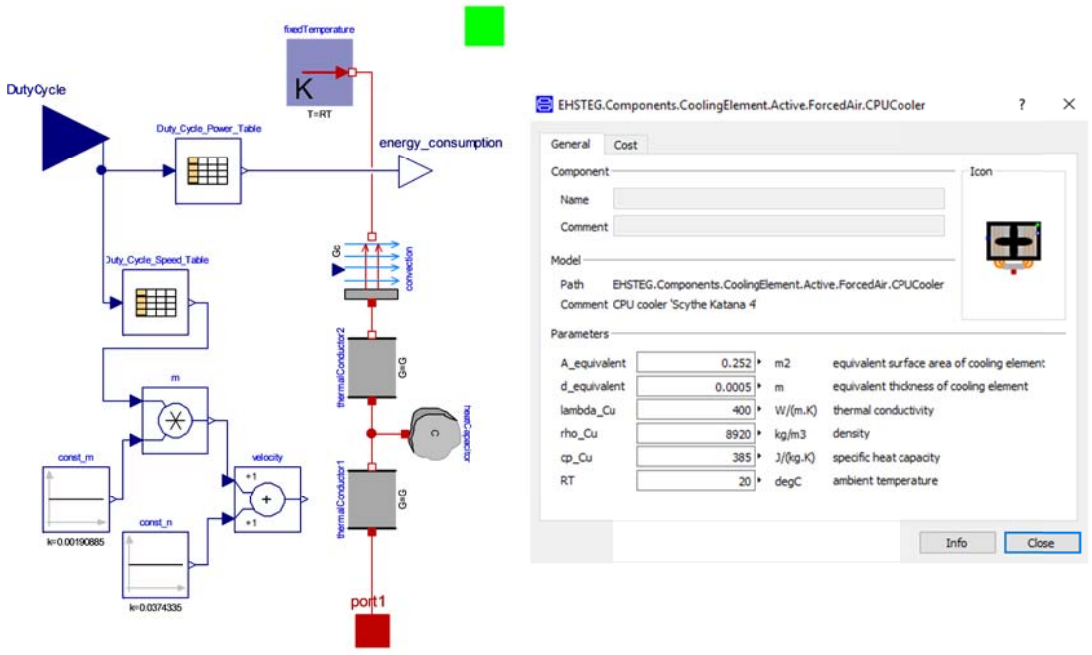

Figure 3.10: Modelica model of a forced air cooling element with parameterization for CPU cooler 'Scythe Katana 4'

The second form of active cooling is with liquid cooled elements. A working fluid, water or a special cooling medium, e.g. ethylene glycol can be used to cool down the cold TEG side. In the EHSTEG library liquid cooled elements are also modeled, but only with water as a cooling medium and as simple as possible. The water model from the Modelica Standard Media Library is used and so, the working fluid can easily be changed to other media, if their properties are known. In total, there are four models related to liquid cooling. These are the cooling element itself which will be directly attached on the TEGs cold side, a distributor model to split up or join different medium flows, an ideal cooling unit as well as a more detailed cooling unit. In the simulation model, like in the real component, the cooling unit consists of a pump and a tank. In the ideal model, the cycle is open and it is assumed that the cooling medium is always cooled down to room temperature, whereas in the other model the cycle is closed and the tank has an interface to the ambient air and thus really cooled down the working fluid. In the latter case, it is possible that the cooling unit is not powerful enough to cool down the medium back to ambient temperature and so the temperature of the working fluid will increase slightly over the usage time. The cooling element itself is modeled with a dynamic pipe containing wall heat transfer from the Modelica Fluid Library.

Validation

In this section, the forced air cooling element model will be validated. Figure 3.11 shows a comparison between measured data and simulation results of the forced air cooling element. For this purpose, a heating plate serves as heat source. On it, a thermoelectric generator and a copper plate, and on the top the cooling element, which are all connected by heat transfer paste. In the upper diagram of Figure 3.11 the temperature of the heating plate is maintained at around 195°C and in the lower diagram at about 170°C; temperature of heating plate corresponds to T_{hot}. The blue line shows the measured temperature at the copper plate and the blue dashed line the simulated temperature at the copper plate. Over time, there is a change in the duty cycle, which is marked with gray vertical lines and the concrete values of the duty cycle are written in gray letters. The simulation shows very good accuracy.

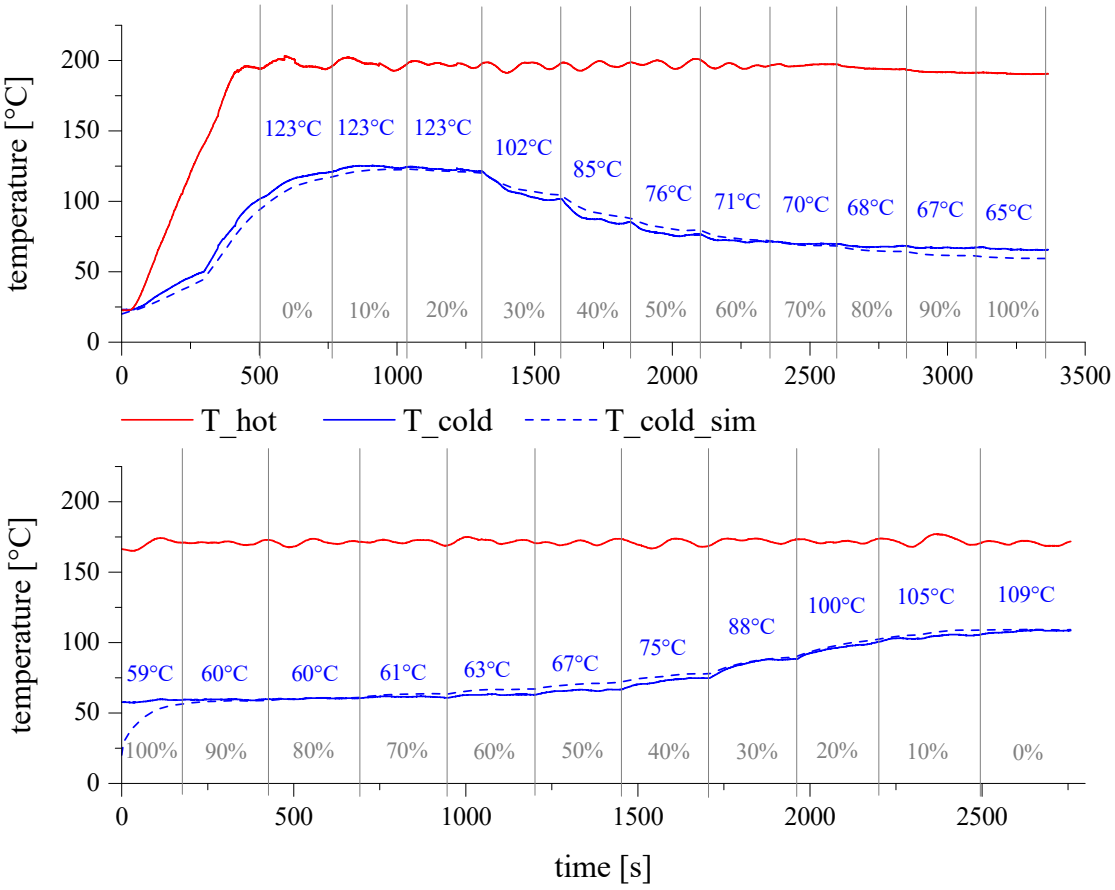

Figure 3.11: In both diagrams, simulation results are compared with measurement data; above: heating plate has a temperature of 195°C and the duty cycle of the fan varies from 0 to 100%; below: heating plate has a temperature of 170°C and the duty cycle varies from 100 to 0%.

3.5.4 Electrics

In this component class, the necessary electrical components for a thermoelectric EHS are modeled. The electrics itself can be very complicated, e.g. there are many different publications about the

developing of a maximum power point tracker (MPPT), which can be used especially for thermoelectric applications, see [MoSK2012], [MoKK2015], [Ph++2013], [Ma++2014]. In most cases and also in this work, the electrical components are store-bought and so a detailed modeling is not necessary, rather a consideration at the highest level of abstraction is enough. That is why the MPPT model here consists of a simple adjustable load resistor and a voltage and current measurement. The quantity of the load resistor is equal to the inner resistance of the TEG-based system. Therefore, in the equation sector of the main model, the overall inner resistance has to be calculated and has then to be given to the MPPT model as parameter. As each thermoelectric device model calculates its inner resistance directly, this will be no problem. An efficiency factor is also integrated in the MPPT model to get more realistic results.

Beneath the MPPT model there are also some other components, like for example an ideal commuting switch, which is mainly based on the Modelica Standard Library and is useful for the modeling of controlled thermoelectric EHSs.

3.5.5 Controlling

In Chapter 5 different control concepts for thermoelectric EHSs will be presented. Therefore, a controlled CPU cooling element model is developed. The basis of the `CPUCoolerControlled` model is the previously described model of a forced air cooling element, which has the duty cycle as input. In contrast, the input variable for the controlled model is the hot TEG side temperature and a look-up table is deposited in the model to adjust the duty cycle of the cooling element as a function of the hot side temperature. The purpose is to have the best ratio between energy input and thus cooling efficiency to increase the energy yield of the TEG due to a higher temperature difference over the device. To receive a suitable lookup table, the planned EHS has to be modeled with the concrete cooling element and thermoelectric device and then the `Optimization` Library, developed by the German Aerospace Center (DLR), has to be used.

3.6 Energy Harvesting Library - `EHSTEG`

All the aforementioned Modelica components and models finally end up in three libraries for Modelica, namely the `ThermoelectricGenerator`, the `HeatPipe` and the `EHSTEG` library. Thereby, the `EHSTEG` library serves the purpose of a model-based development of thermoelectric EHSs, whereas it needs both of the other libraries to work properly.

The structure of the `EHSTEG` library is shown in Figure 3.12. The two main packages are `Components` and `Examples`. The `Components` package is subdivided into the five system components described in Chapter 3.5, a `Cost` package, a `Miscellaneous` package and a `ThermoelectricDevice` package, where thermoelectric devices of four companies are already parameterized: two TEGs of Thermalforce.de, a Peltier element and a TEG of European

Thermodynamics Ltd., a TEG of Hi-Z Technology, Inc. and a Peltier element of Hebei I.T. (Shanghai) Co., Ltd. It is important to note that the same material data for Bi_2Te_3 is used in each case, but in reality every company has its own material composition and so the material data are slightly different. In the `Examples` package, different examples are presented as well as the simulation models of the real application examples from Chapter 6.

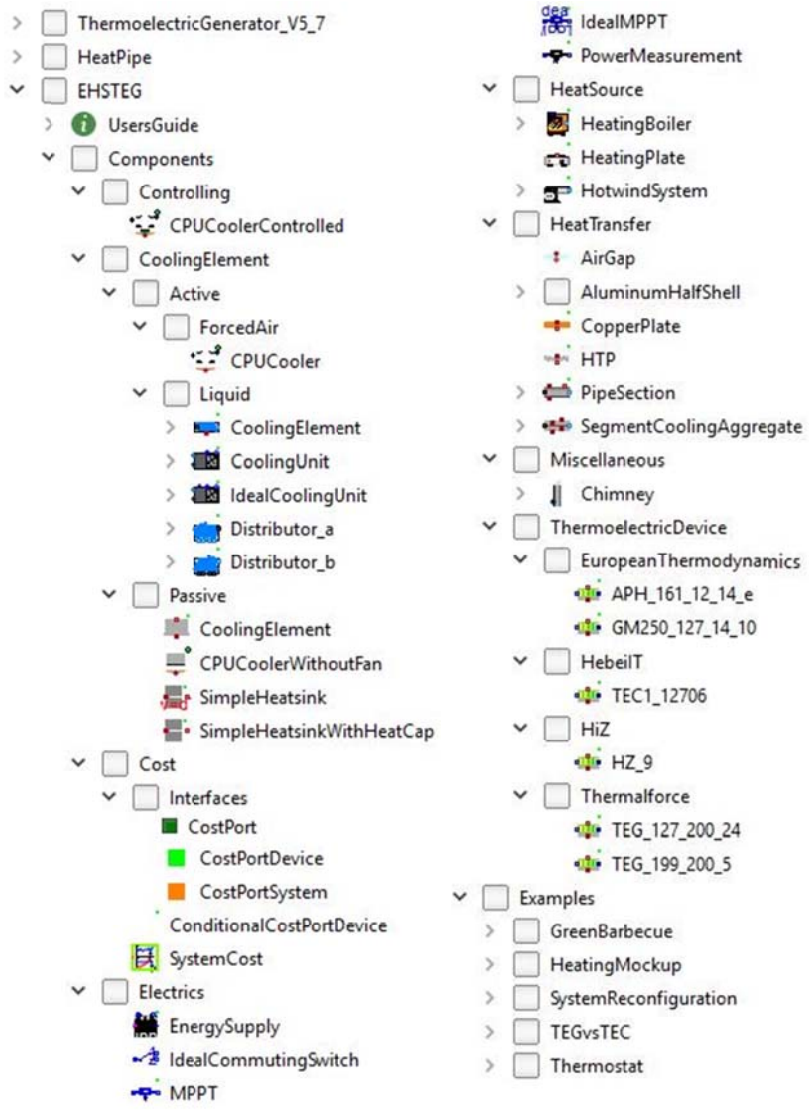

Figure 3.12: Structure of the `EHSTEG` library

An imaginary example of a thermoelectric EHS is shown in Figure 3.13. To give as large as possible an overview of the different heat transfer and cooling variants, many of the components are presented in this one model. The first pipe section shows an aluminum half-shell and a passive cooling element, the second section a heat pipe for heat transfer to the TEG as well as a forced air cooling element, the third section a copper plate and a liquid cooled system and the fourth section a segment cooling aggregate and a controlled forced air cooling element. A complete real system will be modeled and described during the development process in Chapter 4.2.

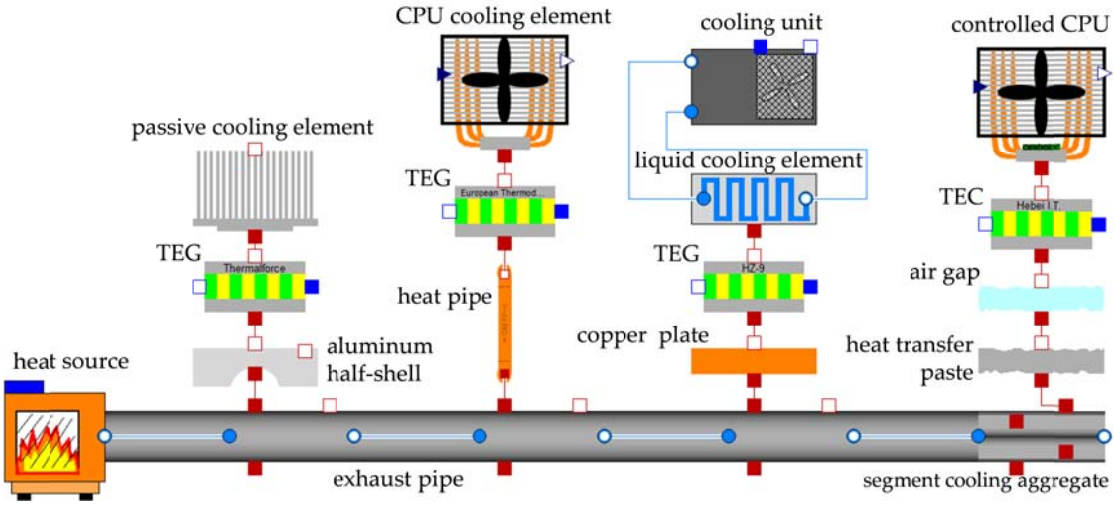

Figure 3.13: An imaginary example of a thermoelectric EHS to give an overview of different heat transfer and cooling methods.

Besides the simulation of the thermal and electrical behavior of such thermoelectric EHSs, also the costs are taken into account in the `EHSTEG` library. For this purpose, the costs—investment cost and cost per year—are integrated in the components and can be activated and then connected with a main component where the costs are automatically summarized, cf. [FeEF2012].

With the `EHSTEG` library developed here, thermoelectric EHSs can be modeled and simulated as well as designed and controlled, which was the first objective of this contribution as presented in Chapter 1.2. This library provides an end-user with an easy tool to configure and build-up these systems in the simulation environment of Modelica/Dymola. It is possible to plan and test different possible variants of a thermoelectric EHS before putting it into practice. Moreover, a rough overview of the expected costs is given. In addition to that, already existing systems can be tested and improvements can be made based on the simulation model.

The idea of model-in-the-loop (MIL) simulation at one of the first stages and hardware-in-the-loop (HIL) simulation at a later date are also realizable with the `EHSTEG` library during the development process. These concepts are modified in this context, as MIL and HIL simulations are usually used in the case of embedded systems. The understanding of both of these methods in this context is described in the following.

MIL simulation means the simulation of the EHS in a very early stage of development. Beside the EHS simulation, the environment also has to be modeled, e.g. the heating circuit of a building. In the MIL simulation, the planned EHS can be tested with a simulation model of the environment on effectiveness and reasonableness. In the end, MIL is a cost-efficient possibility to test EHSs before buying hardware components or modifying existing constructions. A MIL simulation will for example be done in Chapter 6.1 with the thermostat example.

HIL simulation is a method to test EHSs during their development and operation. The completely developed EHS will be tested with a so-called plant simulation. This plant simulation represents the environment as well as possible and is connected with the real EHS. The HIL simulation has to run in real time, which is possible in Dymola and the input values for the EHS are delivered by the simulation model. To close the loop, the behavior of the output values has to return to the model. With this concept, the mode of operation of a real EHS can be tested before it will be attached to a real system.

3.7 Modeling Instructions

From Chapter 3.3 to Chapter 3.5 the single components were modeled and validated. The next step in the context of the V-model approach is to test the integration of these components in a bigger system (integration and system test). Thereby, it happens sometimes that the simulation model does not fit very well to the real setup. This can have different reasons. First, the parameters of the components should be carefully checked. Many parameters can be directly derived from the respective datasheets or may be requested from the company. For example the geometrical parameters are often mentioned in the datasheets or the power consumption of the fan in relation to the duty cycle. Nevertheless, there are usually further parameters which are not given in advance. These parameters have to be measured by the user himself. First and foremost, the measurement of the planned heat source is very important, as this is the basis of the model-based development of thermoelectric EHSs. For the other model components, dummy values can first be used, or the real parameters if the final used components are already known. If only the heat source is known, this means that only a rough estimation of the thermoelectric EHS can be done first and with further clarity about the other components, the simulation results will become more accurate. Another important point is to use the heat transfer paste model and/or the air gap model to get more realistic results as this comes closer to the real heat transfer with all their losses. In this work, it has been found that the air gap model with an air gap thickness of 0.02 mm should always be used when using the heat transfer paste model. If the two models are used in combination, realistic simulation results are obtained which also cover the measured values. Otherwise, the simulated heat transfer is too positive and so, the simulated electrical output power is too high.

4 Development Process

In this chapter, the second objective of this work—the elaboration of a development process to support the setup of a thermoelectric EHS—is done. First, an overview and a scheme of the development process are given. This scheme is a guide to get the optimal thermoelectric EHS for a concrete application, as there are three main challenges to solve: to guarantee an optimized thermal connection of the TEGs, to find a good design for the EHS and to find an optimized electrical connection. The development process is then illustrated by means of an example. After explaining all of the steps of the presented scheme in a short way for the example, the main steps are explained in more detail in the following subchapters, which are the 'Selection of Thermoelectric Device', the 'Thermal Design', the 'Mechanical Design' and the 'Electrical Design'.

4.1 Overview

This chapter presents a development process for thermoelectric EHS and was also presented in [NeFr2016b]. To realize thermoelectric EHSs, different challenges have to be solved where the three main challenges are: to guarantee an optimized thermal connection of the TEGs, to find a good design for the EHS, and to find an adequate electrical connection. Therefore, a development process is presented here. The process is divided into different steps and supports the developer in finding an optimized thermoelectric EHS for a given heat source and given objectives (technical and economical). During the process, several steps are supported by simulation models. Based on the developed `EHSTEG` library in Modelica/Dymola in Chapter 3, thermal, thermoelectrical, electrical, and control components can be modeled, integrated into different variants, and verified step by step before the system is physically built and finally validated. The process is illustrated by the example of the green barbecue through all the steps. The green barbecue is presented in more detail in Chapter 6.2.

A scheme of the suggested model-based multiphysics development process is shown in Figure 4.1. It is divided into different steps and provides support to the developer of a thermoelectric EHS. The model-based steps are in the shaded area. There are ten steps in total, six of which may be done in or rather supported by a simulation. In the following, each step is described. In practice, this development process is realized in an iterative fashion.

Selection of Heat Source

First of all, the available heat sources in an existing process and possible locations to extract waste heat without disturbing the original process have to be found. This step may typically be done with measurements.

Objectives

When the appropriate location to attach and realize an EHS is found, the objectives have to be specified. These objectives could be the preferable voltage level, the desirable performance yield, as well as the investment costs. Depending on these three criteria, further decisions in the development process are influenced, e.g. whether an MPPT is needed or how many TEGs have to be installed.

These first steps can also be switched in the development process. So the objectives can first be determined and then a suitable heat source and a suitable position have to be found.

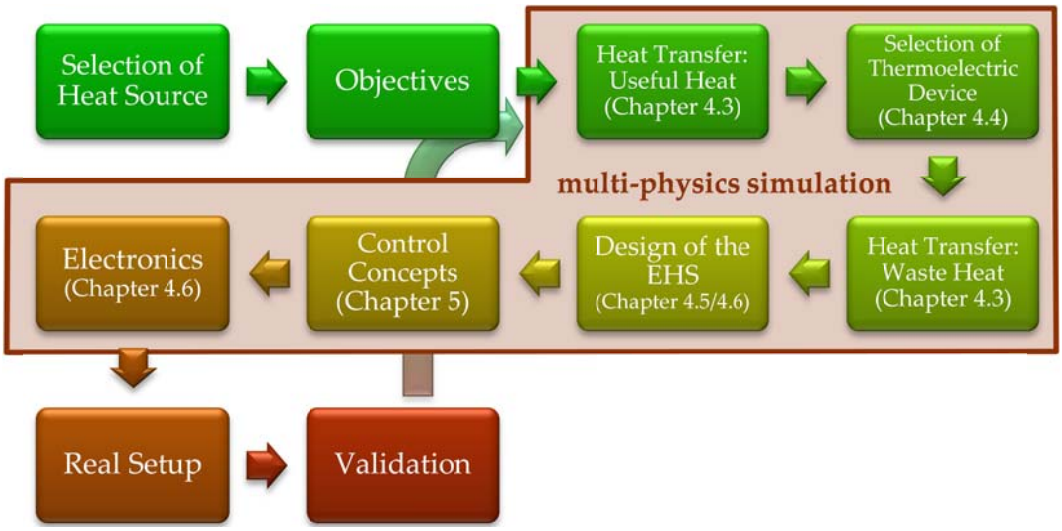

Figure 4.1: Model-based development process for thermoelectric energy harvesting systems [NeFr2016b].

The following six steps can be realized within the multiphysics simulation:

Heat Transfer: Useful Heat

One of the main challenges in realizing an EHS is getting the waste heat to the TEG hot side. There are different possibilities to realize good heat transfer, e.g. use of good thermally conductive materials or installation of heat pipes, cf. Chapter 16.1 in [Shab2010]. Heat pipe models consisting of a quantity of thermal resistors or containing the fluid mechanics, phase changes, and different types of heat transfer can be used with the `HeatPipe` library, developed in Chapter 3.4. As the thermal design is a very important aspect, more information about it will follow in Chapter 4.3.

Selection of Thermoelectric Device

As the possible TEG hot-side temperatures are known, the developer can now choose a suitable kind of TEG. The main focus here is on the behavior of the thermoelectric material in an available

temperature range (i.e., comparing the figure of merit of different materials). For this step, the model of a thermoelectric device from the `ThermoelectricGenerator` library, developed in Chapter 3.3 can be used. The replacement of expensive TEGs by cheaper Peltier elements is also possible in some cases, as will be explained in Chapter 4.4.

Heat Transfer: Waste Heat

To dissipate the heat on the TEG cold side, there are different options. Both passive cooling with heat sinks and active cooling elements are conceivable. Moreover, air- and liquid-cooled options exist. All of these cooling methods have already been modeled in the `EHSTEG` library. To use them, the developer only has to set up parameters such as the number and dimensions of fins, the relationship between the duty cycle and revolutions per minute of the fan, and the properties of the cooling pump medium.

Design of the EHS

Having defined the optimized thermal connection of the TEGs and chosen the TEGs themselves, the next challenge is to find the design of the EHS according to the given objectives of performance yield and investment costs. This contains the assignment of the used number of TEGs as well as their arrangement. Furthermore, one has to determine how the TEGs should be connected, i.e., all in series, in parallel, or a mixture of both structures. Each kind of connection has its own advantages and disadvantages. For example, in an all-series connection the voltage level of the EHS is higher, thus perhaps requiring fewer electrical components, e.g. only a step-down instead of a buck–boost converter. At the same time, such an EHS is more prone to failure, e.g. the complete EHS will produce no electrical power if only one TEG fails. As a result, it may be beneficial to model and simulate various configurations. The mechanical design will be examined carefully in Chapter 4.5 and the electrical circuitry in Chapter 4.6.

Control Concepts

After the design of the EHS is chosen, there are still optimization possibilities in operation mode. For one, the cooling elements for both forced-air cooling elements and liquid-cooled systems may be controlled via their duty cycle. Moreover, the configuration of the TEG array structure can be changed during operation (cf. [NeFF2014]). The control concepts will be described in an extra chapter, cf. Chapter 5.

Electronics

The last challenge is to find an optimal electrical connection. One important component of this is the electrical storage, since the energy recovered by the TEG-based EHS fluctuates greatly. If the system contains a battery, a charge regulator and an MPPT are necessary or advantageous, see Chapter 4.6.

The last two steps are done following the simulation:

Real Setup

The optimal EHS found by way of the multiphysics simulation in the previous steps may now be realized. Attention should be paid to the details, for example, protective circuits, which are not modeled in the system, but are necessary in a real setup.

Validation

The measurement data from the real setup can now be compared with the simulation results and with the objectives defined at the beginning. The setup as well as the simulation model can be adapted if necessary, thus leading to an iterative design.

4.2 Exemplary Development Process

In [NeFr2015], an EHS on a fireplace called Green Barbecue was presented as shown in Figure 4.2a. The Green Barbecue recovers electrical energy from the heat of the fire using TEGs. To develop this thermoelectric EHS with the challenges of good thermal and electrical connections as well as an optimized design, the scheme presented here (Figure 4.1) was followed and a multiphysics simulation model used (Figure 4.2b). In the following, each step of the scheme is presented for the green barbecue.

The objectives of this thermoelectric EHS are to charge a mobile device, to supply an amplifier to play music, or to use the energy produced in an automotive 12 V socket receptacle. (**Objectives**)

The design process began with the selection of the heat source by way of temperature measurements at various positions around the barbecue housing during a burning process. The measurements delivered the result that the hottest place is near the grate. However, the temperatures there are too hot for currently available thermoelectric materials, and furthermore, this site has insufficient space for cooling elements. For this reason, a slightly higher position was chosen for the assembly. (**Selection of Heat Source**)

Having found a position to attach the EHS, the multiphysics simulation model helped to construct the system itself (Figure 4.2b). Using the simulation, different variants of the heat transfer to and from the TEGs were tested. First, direct heat transfer, by attaching the TEGs directly to the steel wall of the fireplace, was considered in the simulation. This, however, was found not to be a practical solution in reality due to the deformation of the steel wall during the burning process that caused the flat connection between the TEGs and wall to be lost. As a result, another design iteration and simulation iteration step was performed, whereby the heat transfer to the TEGs was realized with copper insets in the housing walls. Since they are thicker than the original steel wall,

no deformation under thermal stress is observed and good heat transfer ensured. (**Heat Transfer: Useful Heat**)

The selection of the thermoelectric device and design of the EHS steps were also done in Modelica. While currently available TEGs all employ Bi_2Te_3, it is very easy to integrate other materials into the TEG model. (**Selection of Thermoelectric Device**)

For the TEG cold side, a liquid-cooled system can be excluded for portability reasons, and a simulation showed that a forced air CPU-cooling element had advantages over a free convection cooling element. (**Heat Transfer: Waste Heat**)

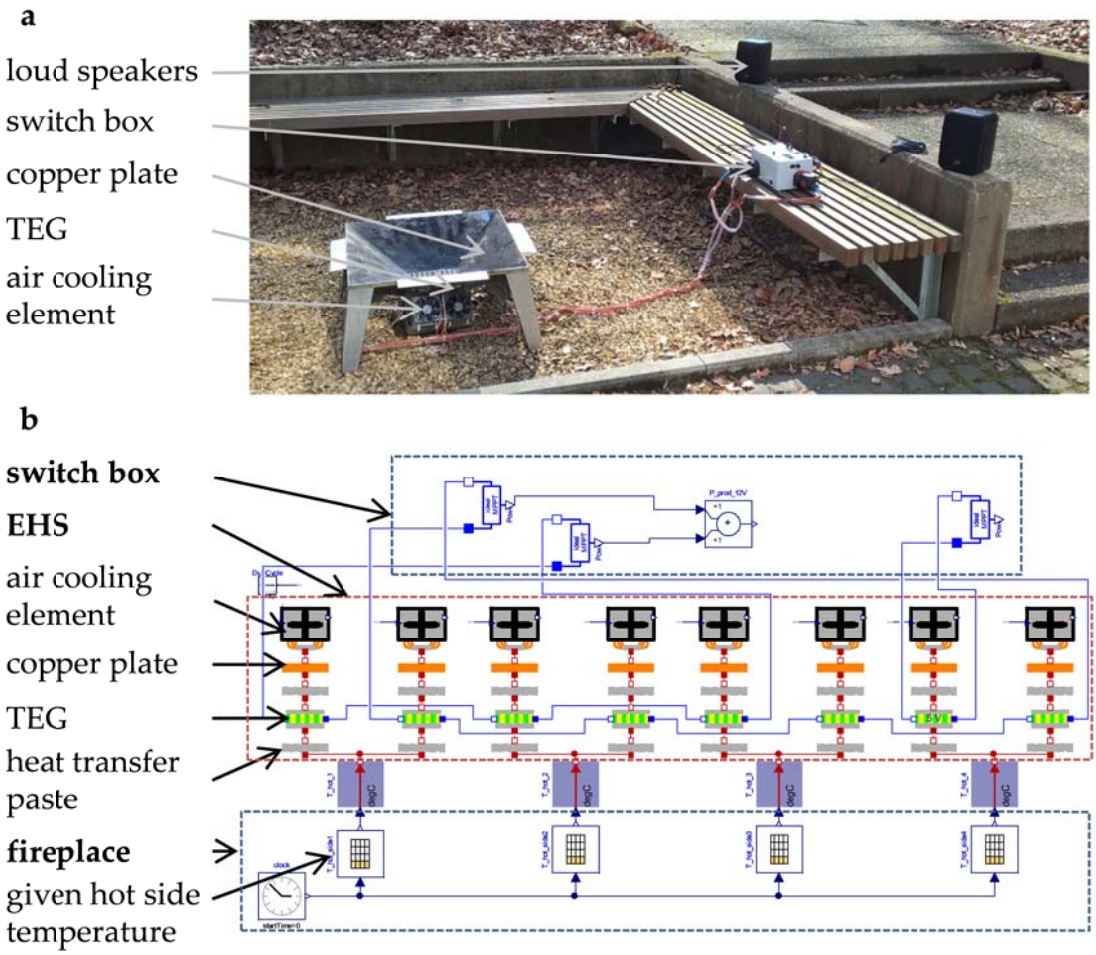

Figure 4.2: a) Picture of the green barbecue; also visible is the switch box and the connected loud speakers; b) multiphysics simulation model in Modelica/Dymola of the green barbecue [NeFr2015].

For the design of the EHS, the best solution in this case was an assembly of eight TEGs. Two TEGs are installed per side. Considering the electrical circuitry, one TEG sources the mobile device power supply and the other seven the remaining applications, cf. [NeFr2015]. In the second version of the green barbecue, which is described in [NeFr2017a] and Chapter 6.2, the electrical connection differs slightly. (**Design of the EHS**)

The control strategy for the cooling elements was also developed within the simulation model. The CPU-cooling element can be controlled depending on the hot-side temperature, thereby striking a balance between the power consumption of the cooling element and the power produced by the TEGs, cf. [NeFF2014] and Chapter 5. (**Control Concepts**)

For an optimized electrical power output, an MPPT is connected to the TEGs. (**Electronics**)

Finally, the system has to be built up in reality and the previously made objectives must be compared with the real values and possible improvements are to be carried out. (**Real Setup** and **Validation**)

After this quick and short introduction into the complete development process, the main import steps, which can be grouped into five main themes—thermal design, selection of thermoelectric device, mechanical design, electrical design and control concepts—are described in more detail in the following subchapters; the control concept in the following chapter. In addition to this, also the possible sources of failure, which were presented in Chapter 2.4.6, have to be considered and to be avoided in the installation of an EHS.

4.3 Thermal Design

As mentioned at the beginning of this chapter, one of the three main challenges is to guarantee an optimized thermal connection of the TEGs which includes both sides of the device. Thus, a good heat transfer to the hot side of the TEG is necessary as well as a good heat transfer from the cold side of the TEG to the heat sink.

For the heat transfer from a heat source, different variants are possible based on thermal conduction, thermal convection and in rare cases thermal radiation. At the end it is nearly always thermal conduction which brings the heat to the hot and from the cold TEG side. But there are also exceptions, e.g. in [Eb++2016], where only thermal radiation transfers the heat to the TEGs. As a uniform temperature distribution over the thermoelectric device is advantageous, the TEGs are covered, for example, by thin copper plates or other thermally conductive plates. To bring the heat from the heat source to the conductive plates, different variants can be used. For example heat pipes can be installed, as they have a better thermal conductivity than pure copper, which brings additionally the advantage of a local separation between the original process and the EHS [Li++2017]. Of course, also a direct connection of the TEG/conductive plate block to a hot surface is possible, as it will be done for the green barbecue (Chapter 6.2). If the heat source is a flowing medium and the surface temperature of e.g. a pipe is too low and the process itself will not be disturbed, the heat can be extracted from the flowing hot medium, as it will be done in the case of the heating mockup (Chapter 6.3).

To dissipate the heat on the TEG cold side, heat sinks have to be used. These can be passive heat sinks or active cooling elements, air or liquid-cooled. In general, the cooling efficiency of liquid-cooled elements is higher compared to forced air or passive cooled systems, as the fluid is capable to transport more heat than air. Nevertheless, the disadvantages are predominant in the use case for EHSs: On the one hand, a liquid system needs a pump to circulate the cooling medium as well as a fan to cool it down and this usually consumes more electrical power than a simple fan. Moreover, liquid systems are more complex as they need beneath a pump also a tank and a compensating reservoir. So, they have bigger dimensions than forced air or passively cooled systems and this is very uncomfortable for small EHSs at very often hard-to reach places with little space. In addition to that, the use of a working fluid needs a very accurate handling of the system, because any leakage must be avoided. That is why in the EHSs developed here, see Chapter 6, only passive or forced air cooling elements are used.

It is definitely necessary to use heat transfer paste between the different components to avoid air gaps between the contact surfaces, as they reduce the heat transfer significantly.

Furthermore, it is very useful if the thermal resistances match, as presented in [Snyd2008] and [Stev2001]. According to [Snyd2008], it is possible to increase the electrical power output of a thermoelectric EHS by conducting more heat through the device under the assumption that the temperature difference over the thermoelectric stays constant; which is normally not given for most real heat sources. A thermal equivalent circuit of a thermoelectric EHS is shown in Figure 4.3 to illustrate this assumption. ΔT_{supply} is the temperature difference between heat source and cold source, Θ_{TE} is the thermal resistance of the thermoelectric device and Θ_{Hx} is the combined thermal resistance of the hot and cold side heat exchangers in series. The thermal resistance can be represented as:

$$\Delta T = \dot{Q} \cdot \Theta \,. \tag{4.1}$$

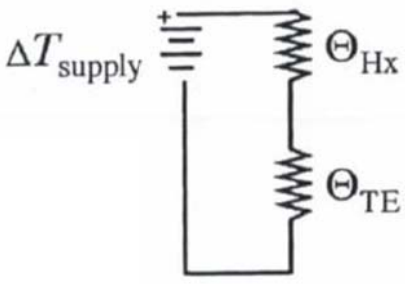

Figure 4.3: Thermal equivalent circuit of a thermoelectric EHS [Snyd2008].

If the thermal equivalent circuit is compared with an electrical circuit, the temperature difference can be seen as a voltage source, the thermal resistances as electrical resistances and thus, the heat flow rate through the heat exchangers and the thermoelectric device as electrical current. This fact

implies that the temperature drop over the heat exchangers influences the heat flow through the thermoelectric and finally the electrical power output of the EHS. This means that if the temperature difference were completely over the thermoelectric device, there would be no electrical power production. The reason lies in the fact that then the temperature drop over the heat exchanger would be zero and thus, there would be no heat flow either through the heat exchangers or through the TEG. If the temperature difference over the heat exchangers increases, a heat flux arises and this increases the power output. However, the temperature difference over the TEG will decrease ($\Delta T_{\mathrm{TE}} = \Delta T_{\mathrm{supply}} - \Delta T_{\mathrm{Hx}}$) and this will reduce the efficiency.

Consequently, in [Snyd2008] and [Stev2001], it was shown that for a maximum power output, the thermal resistance of the heat source and sink have to match with the thermal resistance of the TEG ($\Theta_{\mathrm{Hx}} = \Theta_{\mathrm{TE}}$). In [Snyd2008], it is finally shown that under matched conditions, the temperature drop over the TEG is exactly half of the total temperature difference ($\Delta T_{\mathrm{TE}} = \frac{\Delta T_{\mathrm{supply}}}{2}$).

As a conclusion, it can be summarized that if one is free of any limitation, e.g. in space or in the purchasable thermoelectric devices and cooling components or heat exchangers, the thermal resistance of the TEG should match to the resistance of heat source and sink. However, in most cases, restrictions prevail and so it is necessary to try as much as possible to come close to this optimal ratio.

4.4 Selection of Thermoelectric Device

One important step of the presented development process is the selection of the thermoelectric device. As presented in Chapter 2.4.2, there are different thermoelectric materials and for different application temperatures, there are specific thermoelectric materials with the highest figure of merit. Moreover, a normal user must be comfortable with the thermoelectric materials, which are available on the market. This currently reduces the selection significantly.

Another possibility is to use a Peltier element (TEC) instead of a TEG for temperatures below 100°C [NeFr2016a]. Whereas the former is normally known for cooling applications or heat pump uses, it can also be used as a generator. The efficiency of thermoelectric materials for the low temperature sector (between 0°C and 200°C) is actually not very high, but the costs for TEGs are. As TECs and TEGs consist of the same thermoelectric material for this temperature sector (Bi_2Te_3), the upcoming question is in which temperature range and under which conditions expensive TEGs can be replaced by cheap TECs. Therefore, the similarities and differences between TECs and TEGs will be presented first.

Figure 4.4 shows a TEG and a TEC side by side. At first glance, they look very similar. Both have the same dimensions, encircling ceramic plates and a red and black wire. The thermoelectric base material used is also identical. In both cases it is Bi_2Te_3, which is the standard material for TECs

and the most common material for TEGs, especially if they are constructed for usage in a temperature range between 0°C and 250°C. At the moment, Bi_2Te_3 is the optimal thermoelectric material for this range with a ZT value of about 0.7 for room temperature. However, each manufacturer has a different doping of its thermoelectric base material and unfortunately there is rarely more detailed information about it. The number of thermocouples is not visible in Figure 4.4, but given in the datasheets of the selected TEC [Hebe2016] and TEG [Euro2016]. In these examples, in both cases they consist of 127 thermocouples, which are connected electrically in series.

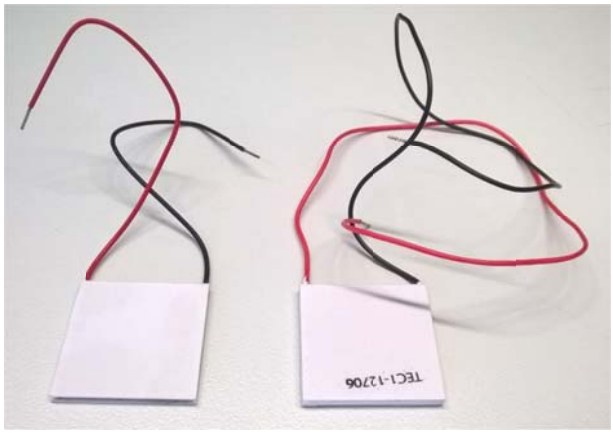

Figure 4.4: A picture of a TEG (left) and a TEC (right) side by side [NeFr2016a].

Figure 4.5 shows the visible differences. In Figure 4.5a, the side view of both devices is shown in comparison, below the TEG and above the TEC. It is obvious, that the thermocouples of the TEC are surrounded by a filling material and the couples of the TEG not. However, there are also TEGs which are surrounded by a filling material. Furthermore, the thickness of both devices is different. The TEC is a little bit thicker than the TEG, whereas the dimensions of the ceramic plates are in both cases identical. Figure 4.5b illustrates the inner life of the devices and it is apparent that the thermoelectric legs have different dimensions. Moreover, there are also some more invisible differences. In total, there are five points where the two devices can differ from each other in general [TECT2014].

1. **Ceramic Plates:** The ceramic plates of TEGs are exposed to higher temperatures and consequently, this means a higher stress. Especially the thermal cycling provides a high stress for the ceramic material. That is the reason why some TEGs have slitting on the face to destress the module.
2. **Soldering:** As TECs are constructed for applications around room temperature, a standard solder is used whose melting point is 138°C. In the case of Bi_2Te_3-TEGs, the soldering has to withstand temperatures above 200°C.

3. **Wires:** The connection cables of TEGs are attached on the cold side of the device to protect them from the heat. This means that in the case of a TEG, there is a predefined hot and cold side. Moreover, the wires are stiffer, as the insulating material is very often Teflon, which endures higher temperatures and so they are harder to bend. Additionally, the wires are thinner, because TEGs carry less current than TECs; TEGs between 1 and 2 A and TECs between 4 and 6 A, see Figure 4.4. Therefore, the wires of TECs are thicker and as a result of the lower temperature, polyvinyl chloride (PVC) is used as an insulating material.
4. **Dimensions of Thermoelectric Legs:** In Figure 4.5b, the inner life of both thermoelectric devices is presented and it is visible that the thermoelectric legs have different dimensions. The TEG has larger elements, whereas the TEC has smaller but higher elements. The larger element size in TEGs means a larger heat flow through the device and thus a higher power output.
5. **Lapping:** A further difference between TEGs and TECs is the accuracy of the thickness. In TECs, the thickness is not very exact, whereas in TEGs the thickness of different devices has to be very uniform. Normally, in EHSs many TEGs are connected in series to generate a higher power output and so it is very important that a uniform contact of all TEGs is ensured. Otherwise, there would be an under-heated TEG, which drastically reduces the power output of the complete system [Chen2014a].

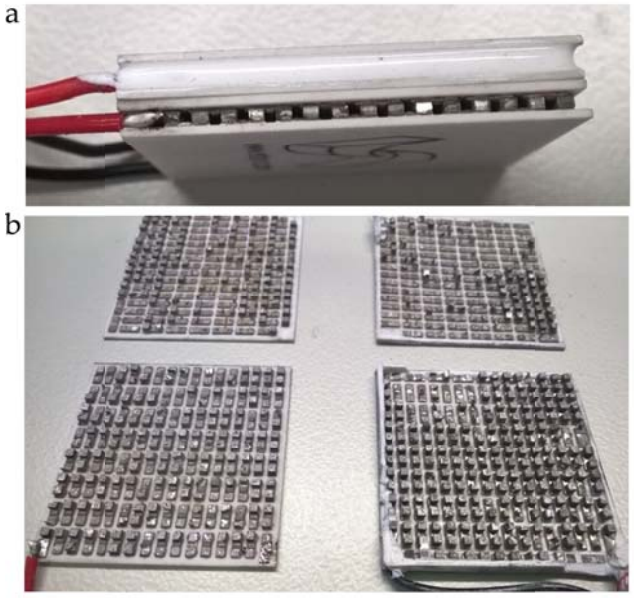

Figure 4.5: a: Side view in comparison, below the TEG and above the TEC; b: Inner life of both thermoelectric devices, on the left a TEG and on the right a TEC [NeFr2016a].

As the similarities and the differences between TEGs and TECs are now familiar, the upcoming question is whether or not it is reasonable to replace a TEG with a TEC in an EHS. Therefore, two thermoelectric devices, a TEG at the price of 35.85€ [Euro2016] and a TEC at the price of 2.37€ [Hebe2016], are selected. Table 4-1 shows a comparison between both devices with the given data

from the datasheets. The gray columns highlight the similarities. The general differences of these specific examples, as described before, are compared in Table 4-2.

An experimental set-up is planned to measure firstly the open circuit voltage and in a next test procedure the generated electrical power. Figure 4.6 shows the set-up. A heating plate serves as the heat source and a CPU-cooling element as the heat sink. Figure 4.7 presents a close-up view. The TEG is visible (later replaced by the TEC), which is enclosed by two copper plates to guarantee a uniform heat distribution on the device surfaces. Moreover, one channel is cut into each copper plate to position a PT1000 temperature sensor inside. With it, it is possible to measure the hot and the cold temperature on both sides of a thermoelectric device. The data acquisition is done with LabJack U6®, which is directly connected to a PC, running LabVIEW 2015®. To measure the electrical power produced, and as the internal resistances of both devices are almost identical, a load resistance with a value of 2.9 Ω is connected to the thermoelectric device as can be seen in Figure 4.6.

Table 4-1: Comparison of the selected TEC (TEC1-12706, [Hebe2016]) and TEG (GM250-127-14-10, [Euro2016]). The data are from the datasheets with the exception of the ceramic material for the TEG (it is a plausible assumption). The gray areas are matches of the two devices (except the thickness). The index L stands for the load values and R_i for the inner resistances [NeFr2016a].

Device	Dim.	T_{hot}	$\Delta T_{max}/T_{cold}$	I_{max}/I_L	U_{max}/U_L	R_i	Q_{max}/Q	No. couples	Thermoelec. material	Ceramic material	Solder material
TEC1-12706	40x40x3.9 mm	50°C	75°C (ΔT_{max})	6.4 A (I_{max})	16.4 V (U_{max})	2.3 Ω	57 W (Q_{max})	127	Bi_2Te_3	Al_2O_3	BiSn (138 °C)
GM250-127-14-10	40x40x3.4 mm	250°C	30°C (T_{cold})	2 A (I_L)	4.96 V (U_L)	2.49 Ω	~198 W (Q)	127	Bi_2Te_3	*Al_2O_3*	N.N.

Table 4-2: Differences of these specific examples of a TEC and a TEG in relation to the five points described before [NeFr2016a].

	TEC1-12706	GM250-127-14-10
1. Ceramic Plates	Al_2O_3	very probably also Al_2O_3
2. Soldering	BiSn (melting point at 138°C)	A different solder as it withstands higher temperatures than 138°C
3. Wires	Diameter of the wires is identical, but the TEG wires are attached at the cold side and they are stiffer.	
4. Thermoelectric Legs	smaller, higher legs (1.4 x 1.4 x 1.7 mm)	larger and lower legs (1.5 x 1.5 x 1.1 mm)
5. Lapping	No information as only one device per type is examined.	

Figure 4.6: Experimental set-up to measure in a first round the open circuit voltage of a thermoelectric device and in the next step the generated electrical power. A heating plate serves as heat source and a CPU-cooling element as heat sink [NeFr2016a].

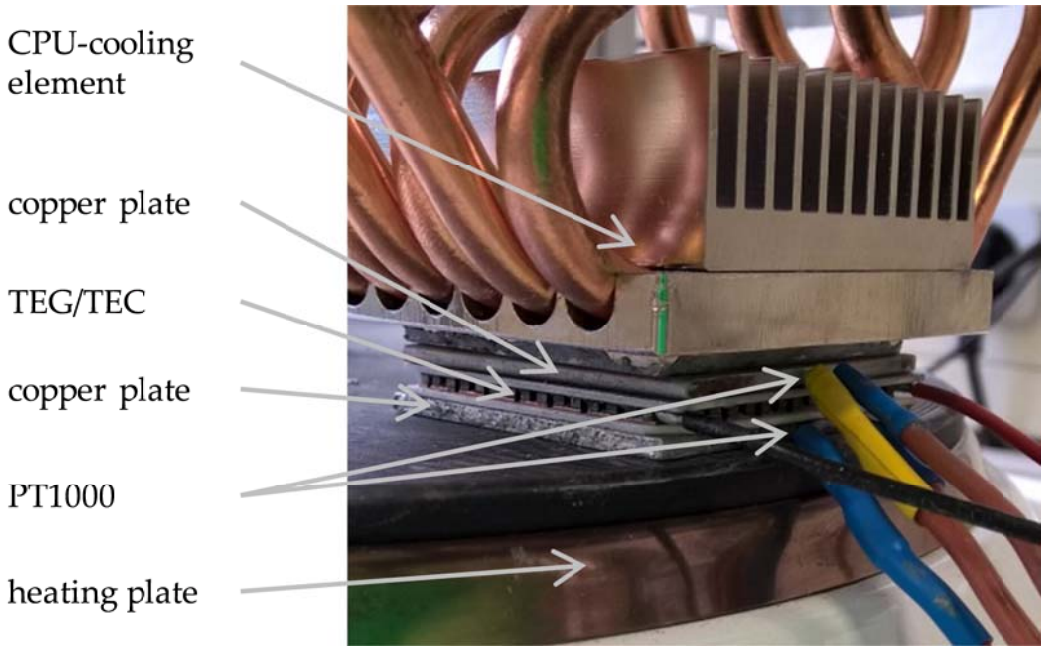

Figure 4.7: Close-up view of the experimental set-up. The TEG is visible as well as the copper plates which enclose the TEG, and the cables of the PT1000 temperature sensors for measuring the hot and cold TEG/TEC side temperature [NeFr2016a].

The test procedure is identical in both scenarios. The heating plate is switched on, the temperature increases and after a certain time, the heating plate is switched off. In the case of the TEC, the heating plate is switched off, when a hot side temperature of 135°C is reached.

In addition, a simulation is done with Modelica/Dymola. The measured temperatures are given to the models of a TEC and a TEG and the open circuit voltages as well as the produced electrical power with a connected load of 2.9 Ω are simulated. For the modeling, the `ThermoelectricGenerator` library is used, cf. Chapter 3.3.3.

The results of the measurements and the simulation are shown in Figure 4.8 and Figure 4.9. Figure 4.8 shows the measured open circuit voltage (U_{OC}), the simulated open circuit voltage ($U_{OC,sim}$) and the hot side temperature (T_{hot}) of each device plotted against the temperature difference. It is visible that the measured open circuit voltage of the TEC is higher than of the TEG for the same temperature difference applied and at almost the same temperature levels (compare hot side temperature curves). Moreover, the simulation shows the same effect, higher open-circuit voltage of the TEC, and is almost identical with the real data, except the end of the lines.

In the case of the TEG, the switch-off temperature is 235°C. It depends on the maximum operation temperature for each device. The TEC/TEG is destroyed for temperatures over 140°C/250°C.

In Figure 4.9, the produced electrical power of the TEG and TEC as well as the simulated electrical power of both is compared. To measure the produced power, a constant load resistance (2.9 Ω) is connected to the thermoelectric device and the load voltage is tapped. It is obvious that the produced electrical energy for both devices is approximately identical. For smaller temperature differences, the TEC seems to be even more powerful, compare inset in Figure 4.9, but this can probably also be due to measurement uncertainties. Here, only a constant load resistance is connected to guarantee similar conditions for both devices. In an optimal EHS, the use of an MPPT is recommended to increase the electrical power output. In addition, it is apparent in Figure 4.8 and Figure 4.9 that no real hysteresis phenomena occur. The small hysteresis may be due to non-identical internal conditions or hysteresis effects in the sensors.

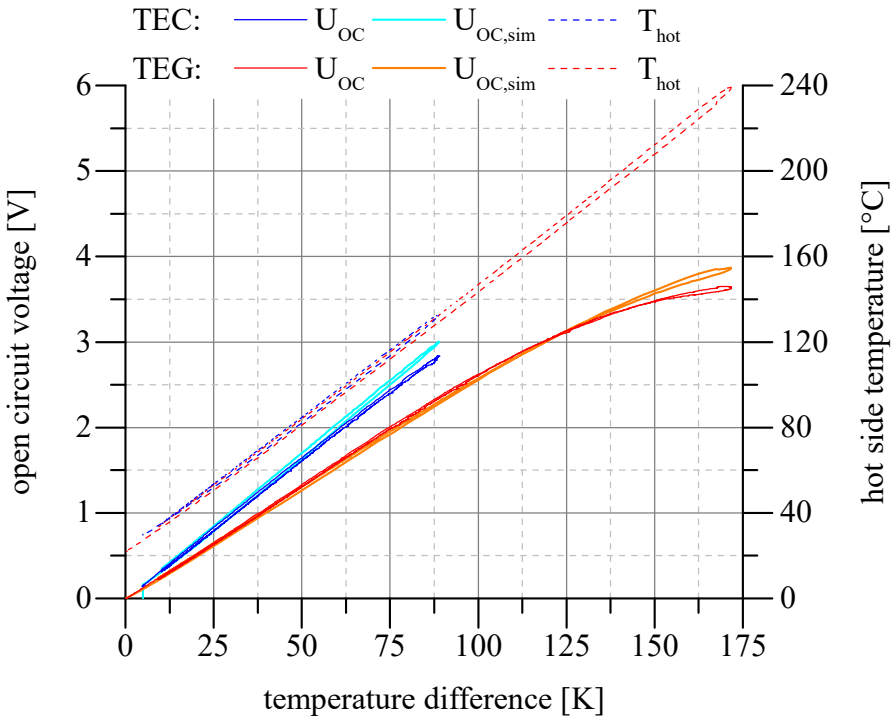

Figure 4.8: Comparison of the measured and simulated open circuit voltage between TEG and TEC, plot against the temperature difference [NeFr2016a].

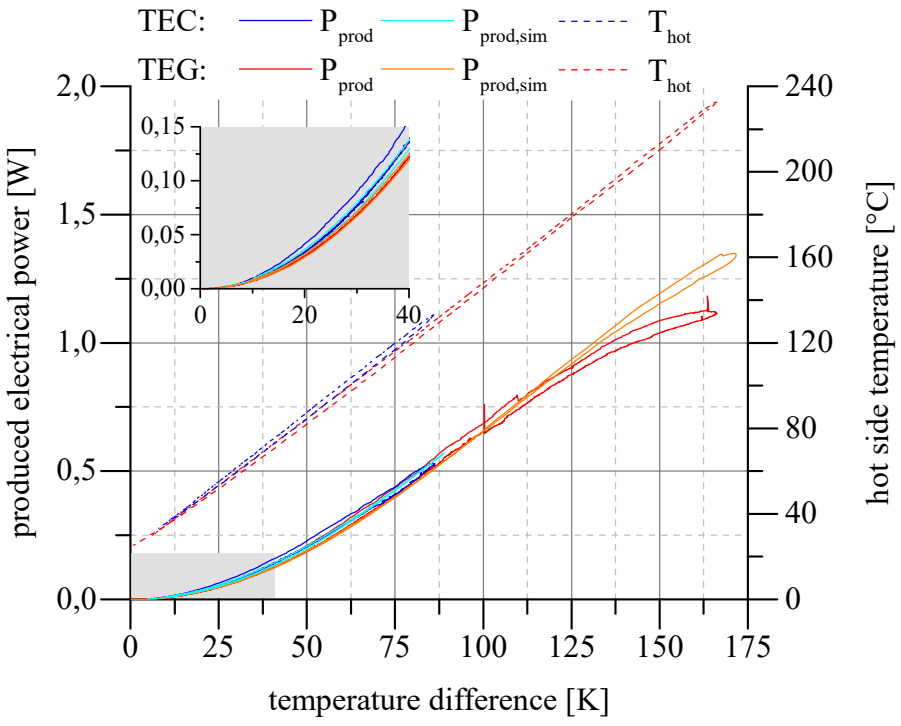

Figure 4.9: Comparison of the measured and simulated produced electrical power between TEG and TEC, plot against the temperature difference. The inset shows an enlargement for the low temperature differences [NeFr2016a].

An application example is the self-supplying electrical thermostat, which is installed at our Chair using TECs instead of TEGs, cf. Figure 4.10, and which will be described in more detail in Chapter 6.1.

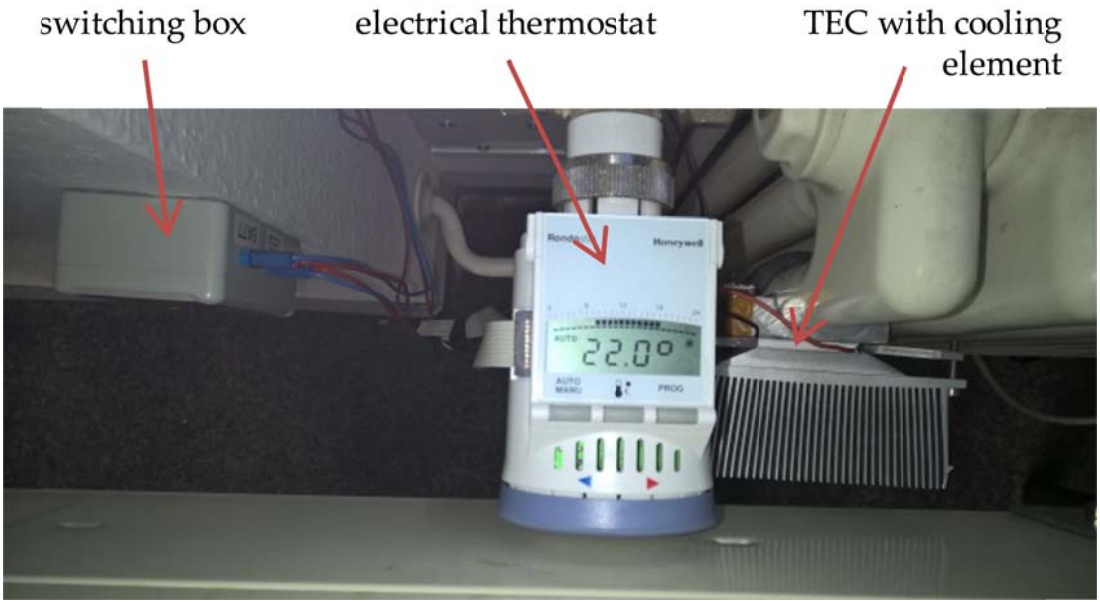

Figure 4.10: Self-supplying electrical thermostat using a TEC instead of a TEG. In the middle is the electrical thermostat, on the right the attached TEC with the cooling element and on the left the switching box with MPPT and accumulator [NeFr2016a].

The thermoelectric device is located between an aluminum half-shell, which is directly attached on a heating tube, and a passive cooling element. The temperature difference over the device is about 3 K and the EHS produces about 3.5 mW. This electrical energy is stored in an accumulator and is enough to supply the electrical thermostat. The costs of the hardware and the electronics stay equal, but with the usage of the TEC instead of the TEG, a cost savings of 33.48€ is achieved.

Finally, it can be said that for the power generation in the temperature range between 0 and 100°C—according to the two elements that were examined here—a TEC can be used just as well as a TEG. This result is very decisive for the development of economically worthwhile thermoelectric EHSs. By the fact that a TEC is 15 or more times cheaper than a TEG, small thermoelectric EHSs can find a wider field of application. Either the costs can be reduced or, for the same investment, more TECs can be installed and thus more electrical energy can be produced.

4.5 Mechanical Design

The second challenge in building a thermoelectric EHS is to find a good design for the system. This contains mainly the assignment of the used number of TEGs as well as their arrangement. The number of the TEGs is often dependent on the objectives, either on the preferable voltage level and the anticipated performance yield or on the available investment costs. Furthermore, the located positions to extract waste heat without disturbing the original process are also a limiting factor. To test different number of TEGs, different positions and calculate the investment costs for each case, the `EHSTEG` library can be used. For this purpose, the user has to model the process of the waste heat and has to inform oneself about possible connection points for TEGs. Then, the applicable

TEGs have to be modeled as well as the applicable cooling components. Moreover, one has to think about further components, e.g. heat transfer components. For example in the case of an exhaust gas pipe, there is the option to collect the heat from the outside wall of the pipe, e.g. with an aluminum half-shell as in the case of the thermostat, see Figure 4.11a (cf. Chapter 6.1). Another option is to extract the heat from the flowing medium, e.g. with a segment cooling aggregate as in the case of the heating mockup, see Figure 4.11b (cf. Chapter 6.3).

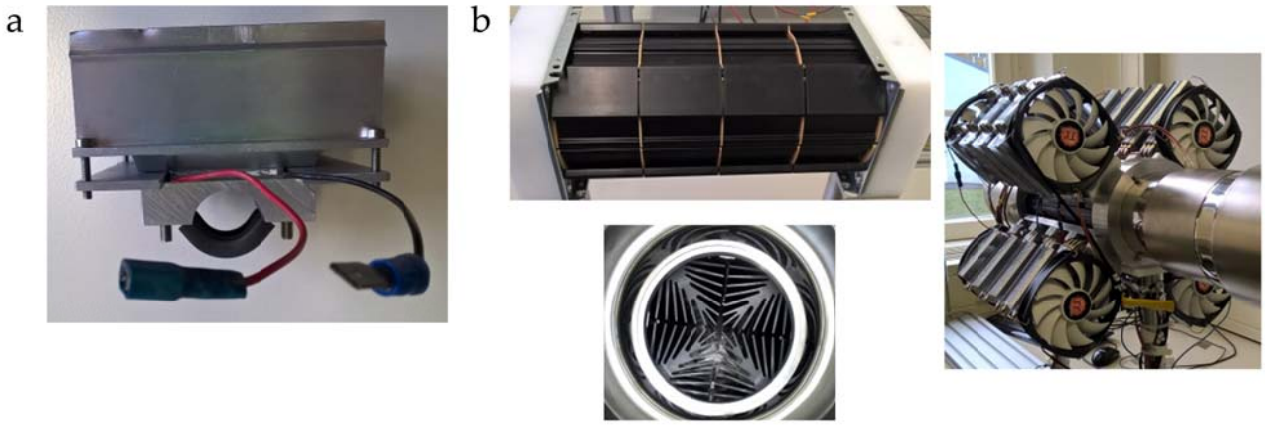

Figure 4.11: a: aluminum half-shell to attach a TEG at a heating tube, also visible is the attachment of the cooling element; b: segment cooling aggregate to extract heat from a flowing medium, also visible is the attachment of the active air cooling elements.

Now, with this different simulation models, different scenarios can be played through until a final and satisfying system design is found, which fits the previously made requirements. Additionally to the theoretical respectively simulative found solutions, there are also some things that must be observed in the real installation, e.g. how to fix the chosen cooling elements in the system. Two solutions can also be seen in Figure 4.11. Furthermore, the installation of sensors has to be considered. If the hot and the cold TEG side have to be measured, e.g. small channels can be cut into the thermal conductive plate, where the temperature sensors can be inserted.

4.6 Electrical Design

The last challenge is an optimal electrical connection of the components, which can be divided into two connection tasks, the internal and the external connection.

Very often, a thermoelectric EHS consists of a multiplicity of TEGs and so there are different circuitry options for the internal connection. If we consider for example an EHS with eight TEGs, all eight can be connected in parallel (8p) or in series (8s). Furthermore, a mixture can be taken of both of them, e.g. two TEGs in parallel and then the four parallel blocks in series, respectively (2p4s). Figure 4.12 shows the three aforementioned circuitry examples and Table 4-3 the corresponding simulation results for the voltage level, the power production and the inner

resistance of the TEG system (load resistance is equal to inner resistance) for a fictitious EHS example, where the hot side temperature of all TEGs is 150°C and the cold side temperature 50°C. In [Chen2012] and [Chen2014b], different TEG array circuits are investigated.

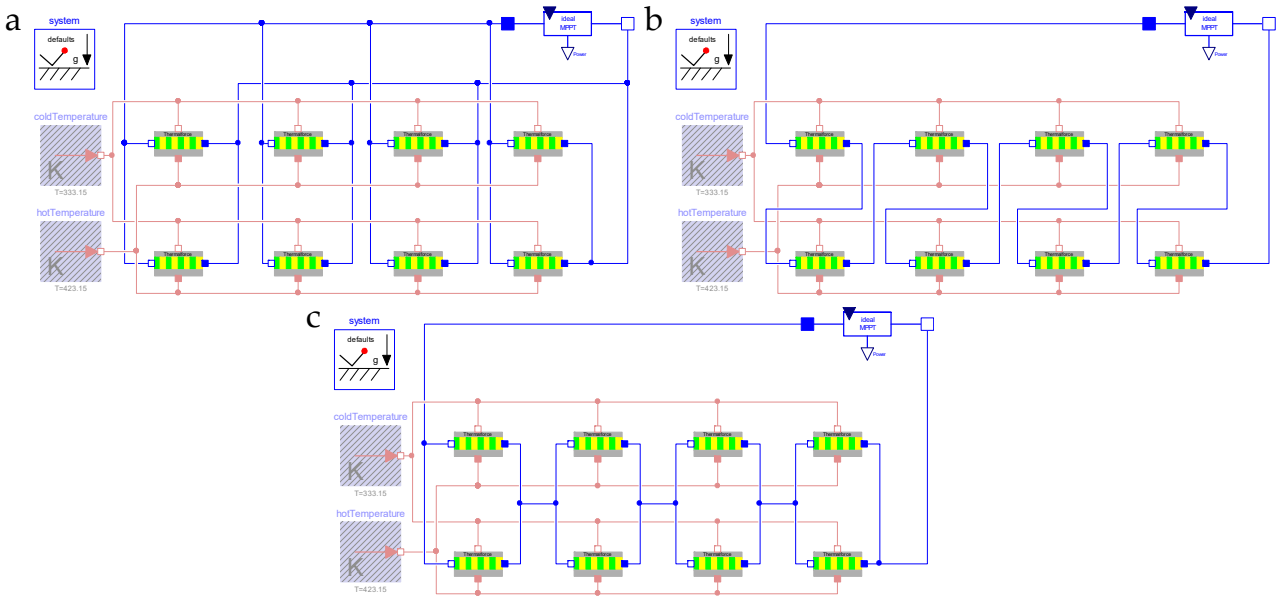

Figure 4.12: Different circuitry options for the internal connection of thermoelectric EHS; a: eight TEGs in parallel (8p); b: eight TEGs in series (8s); c: two TEGs in parallel and four parallel blocks in series (2p4s).

In Table 4-3, it is obvious that the power production, for an adapted load resistance is identical in all three cases. However, the voltage output of the system fluctuates enormously. Now, the preferred circuitry option depends on the given circumstances. If the preferable voltage level is e.g. a 12 V line, in the case of 8p, a step-up converter is necessary and in the case of the both others a step-down converter. The results given are for a steady-state scenario, but if there is a dynamic behavior like in almost every real process, the voltage of the 2p4s circuitry will also alternate and so in this case, there is the need to use a buck-boost converter as the output voltage can also be under 12 V. As buck-boost converters are normally more expensive, in the case of a desired 12 V output line, the 8p circuitry with a step-up converter or the 8s circuitry with a step-down converter are privileged. However, the failure rate increases with an 8s connection, as one defective TEG will cause a crash of the complete EHS.

The previously made conclusions are of course very comprehensible and simple to make, but if there are also different and fluctuating temperature levels for different TEGs (now, they are not all exposed to the same temperature level), it will become more difficult to find an optimal circuitry without simulation. Especially, as under-heated TEGs will act as resistances and not as voltage sources as expected, a simulation of the system is necessary to find an optimal circuitry. Besides the determination of the circuitry matrix in a static manner, a dynamic circuitry matrix is also possible, which can also be used for controlling purposes. That is why the dynamic circuitry is

explained in the next chapter. A recommendation is to connect TEGs with the same temperature levels in parallel and then these parallel blocks in series with each other. Between these blocks, switches can be integrated to have a partial dynamic circuitry matrix

Table 4-3: Simulation results (power, voltage and inner resistance) for different circuitry options in a steady-state, fictitious EHS.

Circuitry	Power [W]	Voltage [V]	Resistance [Ω]
8p	45.1927	4.07974	0.368296
8s	45.1927	32.6379	23.5709
2p4s	45.1927	16.319	5.89273

The second point of the electrical design considers the external connection. One important component of this is the electrical storage, since the energy recovered by the TEG-based EHS fluctuates greatly. If the system contains a battery, a charge regulator and/or an MPPT is advantageous. As was already shown by many authors for other systems, e.g. photovoltaic systems, also for thermoelectric EHSs it is absolutely recommended to use an MPPT to increase the power output of the system, [Ga++2012], [Ph++2013].

5 Control Concepts

In this chapter, different possible control concepts for thermoelectric EHSs are introduced. They are necessary to improve the electrical power output of such systems. Therefore, an exemplary system is described and modeled primarily, at which the different control concepts are then applied. Afterwards, different options to control the cooling elements will be presented. Thereby, the control of forced air and liquid cooling elements are elaborated upon. Then, the concept of system reconfiguration in offline and online mode is taken into account, which will be done for single TEGs according to the work of M. Chen as well as for pairs of TEGs, which seems more reasonable for more obvious system layouts. Also a brief outlook for arrays of TEGs will be given. Then, the developed control concepts are summarized in control laws and finally presented in a model-based system assessment for the exemplary system of oil-fired heating.

5.1 System Description and Modeling

To show different control concepts, an exemplary EHS will be presented on which the different control concepts are then applied. First, the construction of a possible real EHS and the transfer of these real conditions to the model level will be described. After having a working simulation model, different control concepts are compared for an optimal control design to increase the power output for various heating scenarios. These control ideas have also been published in [NeFF2014] and [NeFF2015]. For this purpose, pairs of TEGs (pTEGs) are installed on an exhaust pipe alongside the exhaust gas stream. However, with the exhaust gas losing heat in a downstream direction, the final pTEG may lower the overall EHS performance due to their electrical resistance. With the help of the simulation model presented here, it is possible to remove detrimental pTEGs from the EHS. This removal may happen either statically, i.e. in the design phase, or dynamically, i.e. by finding the ideal instant of time to disconnect and to revive them during operation, cf. Chapter 5.3. Moreover, an assessment of two different cooling options is made; forced air and liquid cooling and for each cooling method, an individual control strategy is defined to maximize the power output of the EHS, see Chapter 5.2. Finally, based on the system reconfiguration and cooling control, different control laws are derived in Chapter 5.4, followed by a model-based system assessment in Chapter 5.5 for the example given.

Here, the considered EHS is a system consisting of eight TEGs and is built on the exhaust pipe of an oil-fired heating system. Eight TEGs are installed in pairs, with both TEGs of each pair subject to identical temperature conditions. In the end, there are four pTEGs operating under different temperature conditions. Figure 5.1 shows an example of such a system. It shows the first possible cooling principle, cooling by liquid, in which one cooling unit supplies two pTEGs; later, this fact will be of importance. The liquid cooling units only have one state and consume 12.2 W with a

maximal cooling capability of 400 W. The reason for this lies in the condition of using simple disposable cooling elements, due to the objective of modifying existing heating systems in a very simple and economic way. Considering that one liquid cooling unit is responsible for four TEGs, one TEG consumes 3.05 W of electrical power for cooling purposes. Electrically, the TEGs of one pTEG are connected in parallel, while the four pTEGs are connected in series. For different control concepts, there are electrical bypasses between the pTEGs to disconnect or connect specific pTEGs.

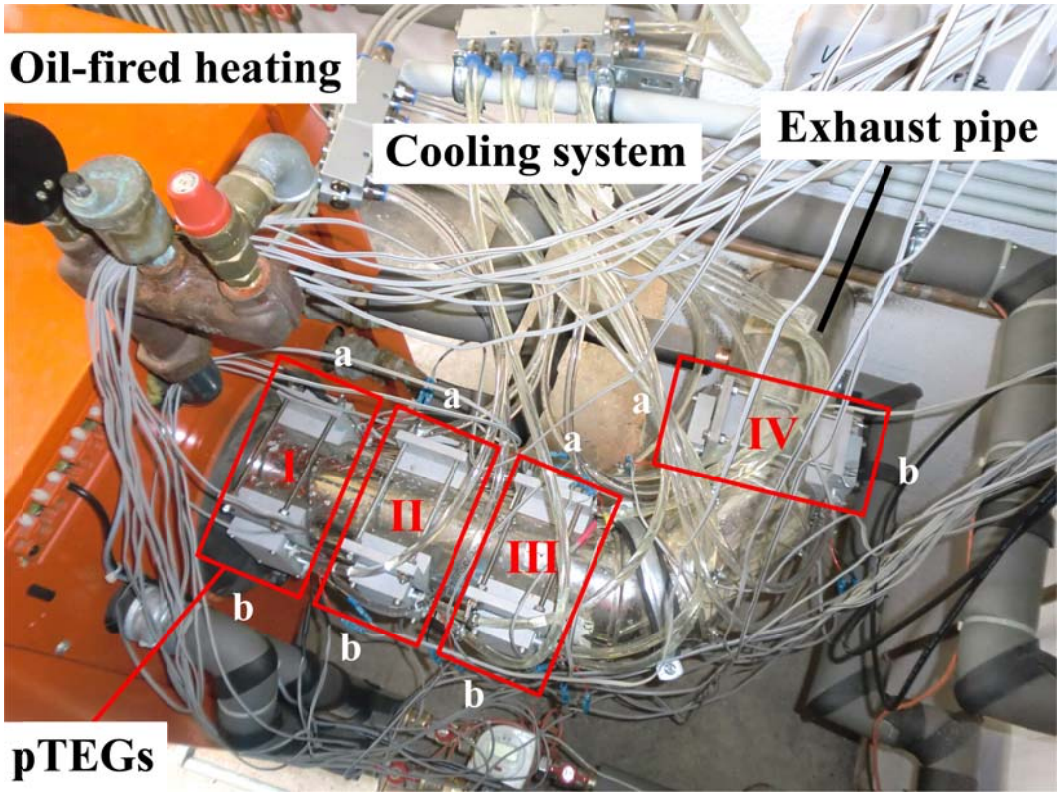

Figure 5.1: Test bench on an exhaust pipe of an oil-fired heating system consisting of four pTEGs (marked with roman numerals), each includes two TEGs (marked with 'a' and 'b') and a liquid cooled system [NeFF2014] and [NeFF2015].

For the modeling of this system, the `EHSTEG` library is used, see Chapter 3.6. Here, TEG 199-200-5 from Thermalforce is installed and the graphical user interface of the TEG model has to be fed with data from the TEG datasheet [Ther2015]. For the modeling of the liquid cooling system, water is used as a cooling medium for modeling simplification. Measurement data of the real oil-fired heating deliver the necessary information to model the heating component and to simulate real behavior of the exhaust gas. For maximum power output of the EHS, a MPPT is necessary to adapt the internal resistance of the system to the load. For that reason, the ideal MPPT model component is used, which gets the values of the internal resistances of the TEGs from the TEG-components itself and thus calculates the optimal load resistance for the circuit. The energy consumption and generation of the components is integrated inside each model and the component `PowerSupply` serves as a battery for the liquid cooling system. In addition to it, the main system directly

calculates the complete produced electrical energy by pTEGs (gross energy) and the real gained energy (= gross energy minus energy consumption of the cooling components; equates to the net energy).

Figure 5.2 shows the complete system model in Dymola and highlights the different components. To illustrate all possible cooling options, the first two pTEGs are water cooled and the last two pTEGs are air cooled (only for illustration, later there is either a pure water cooling or a pure air cooling). The electrical wiring and in particular the bypasses for the eventual control of the system are visible, whereas for a better overview, the other connection lines like fluid and thermal connections are hidden.

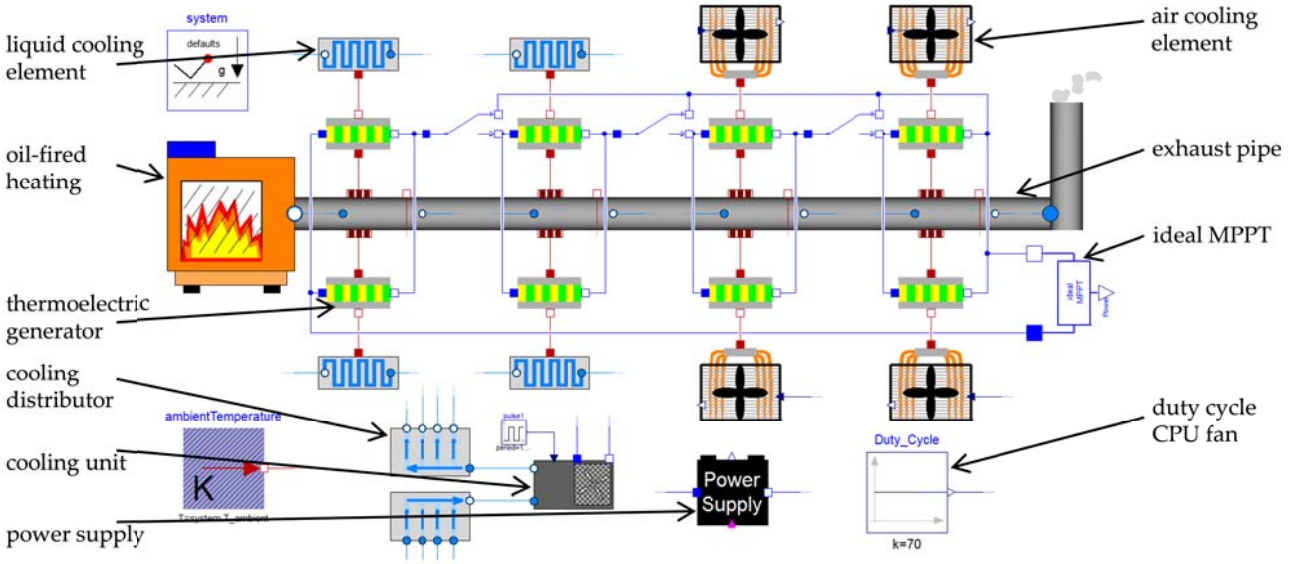

Figure 5.2: Model of the EHS in Modelica/Dymola showing the different components and in particular the different cooling options. The electrical wiring is represented by the navy blue lines [NeFF2014] and [NeFF2015].

In general, the temperature of the heating exhaust gas fluctuates between 120°C and 200°C [Pasc2015], [Gerw2015] and [Nowo2003]. Figure 5.3 shows a real measurement curve (black) of an oil-fired heater under full-load operation over a period of 2,100 s. One can see that the final temperature is about 205°C for this special heating scenario. So it is obvious that this heater is an older one and not really efficient. Moreover, Figure 5.3 shows two further measurement curves for an on/off behavior (50% on and 50% off as well as 20% on and 80% off) of the heating and one fictitious ideal steady state curve for full-load operation based on the upper bound of the real measured exhaust gas temperature curve. In the following, the three colored curves in Figure 5.3 serve as simulation inputs and are representative for three different heating loads. In the end, two different heating modes, full-load operation and on/off behavior are considered, whereby the latter one is split up in two scenarios with a ratio of 50/50 and 20/80. The full-load operation mode can be

considered as an on/off ratio of 100/0. The curves have been recorded in the `Oil-FiredHeating` component.

All results in the following subchapters are simulation results of the modeled TEGs and cooling elements. In this example, it is an ideal EHS, which means that the heat of the working fluid will be transferred without loss to the hot side of the TEGs; equally from the cold TEG side to the cooling elements. In reality, of course there have to be further components to transfer the heat of the fluid to the TEGs which cause heat losses, thus reducing the hot side temperature and finally reducing the electrical energy output, cf. heating mockup in Chapter 6.3. However, the temperature curves of the exhaust gas are measurements from a real oil-fired heater and so, the results developed here can be transferred to real applications. The power output may be lower, but the control concepts are working just as well.

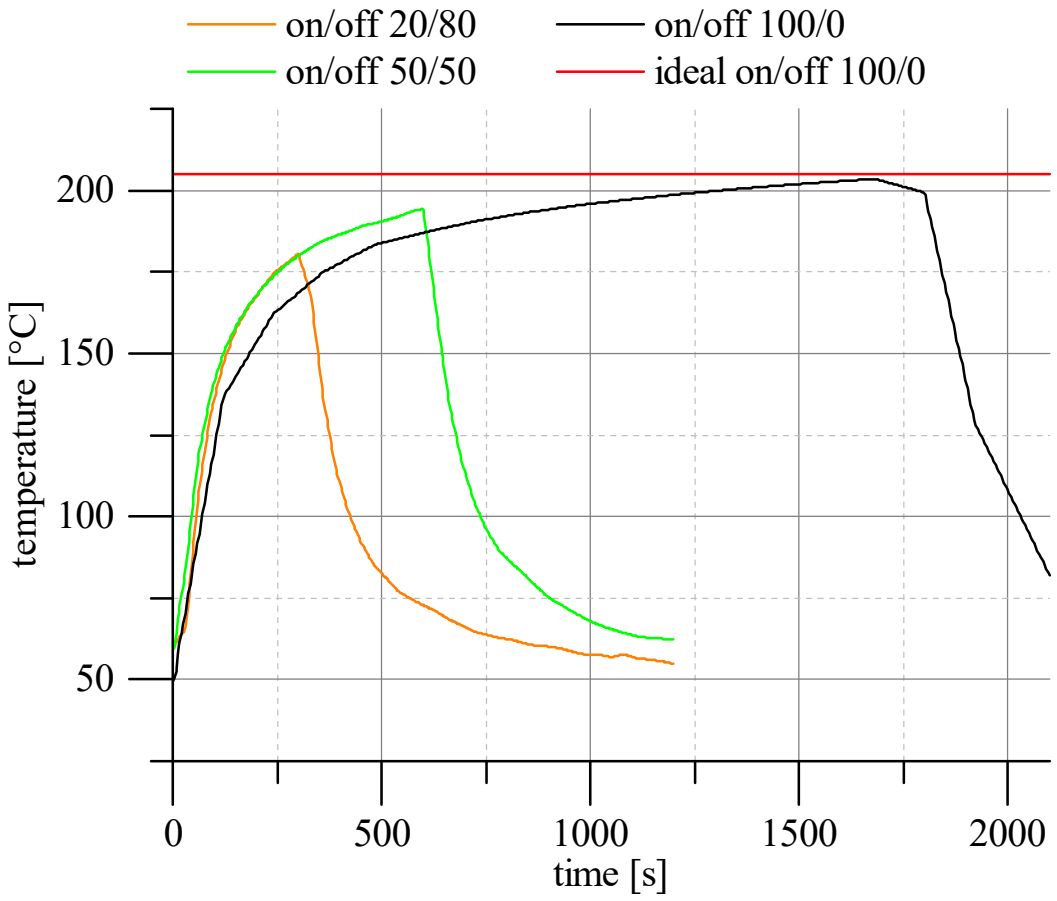

Figure 5.3: The three real measured temperature curves (black, green and orange) as well as the upper limit temperature line for the ideal steady-state full-load operation mode (red) [NeFF2015].

5.2 Cooling Control

5.2.1 Air Cooling

For the forced air cooling of the TEGs, high-end CPU cooling elements known from computer applications are used, [Scyt2015]. The CPU cooling element has a heat spreader which has direct

contact with the cold side surface of a TEG. From this heat spreader, heat pipes transfer the heat to a multitude of cooling fins which are cooled down by a controllable fan. The energy consumption of the air cooling devices is shown in Figure 5.4 as well as the possible fan speeds. They are adjustable by their duty cycle. The air cooling method uses only 2.04 W in case of maximum fan speed and normally even less for one TEG. The data of the CPU cooling element datasheet, see [Scyt2014] and [Scyt2015], have been used to create a simulation model (c.f. Chapter 3.5.3). To validate this model, the measurement data of a test set-up are compared with the corresponding simulation results, which have provided a very good match.

The simplest way of running the fans is with a constant rotating velocity set up by their duty cycle. But to increase the efficiency, a control of the fan speed has been developed with the help of the `Optimization` library of Dymola. Thereby, the optimal duty cycle and, as a consequence, the optimal fan speed is assigned to the hot side temperature of the considered TEG, see Figure 5.5. The fan speed control adapts the energy consumption in an optimal rate to the produced power of the TEG. (As mentioned in Chapter 3.5.5, this optimization curve is only valid for the chosen TEG and CPU cooling element. If other components are used, the optimization has to be done again). If there is, for example, a hot side temperature of about 125°C (ca. 400 K), the optimized duty cycle would be 55%, which results in about half the fan consumption compared to a 100% duty cycle.

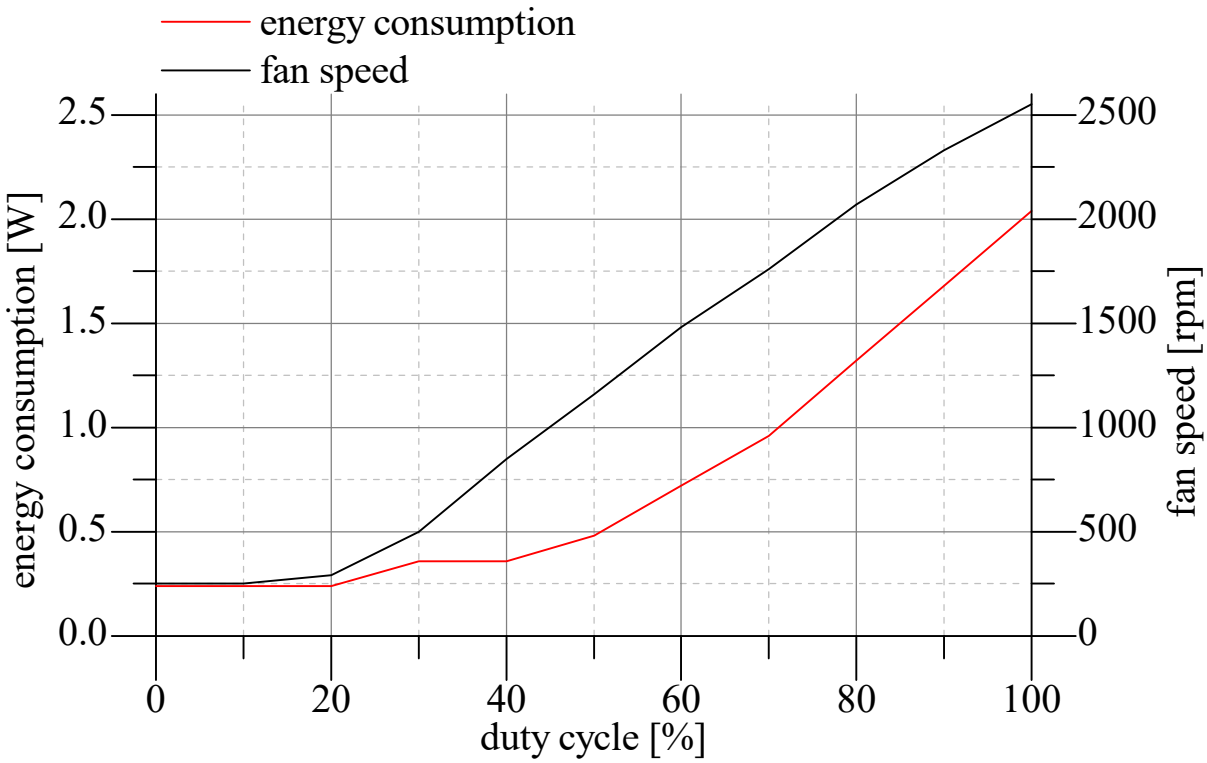

Figure 5.4: Energy consumption by fan and fan speed of air cooling elements for different duty cycles, required for modeling [Scyt2014].

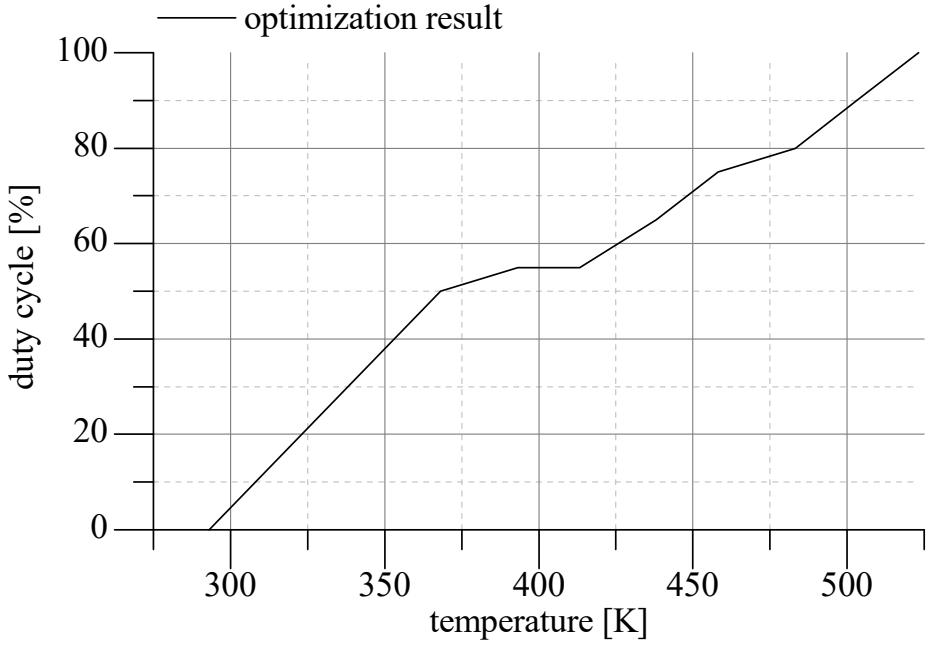

Figure 5.5: Control curve for the duty cycle of the cooling elements depending on the hot side temperature of a TEG [NeFF2014] and [NeFF2015].

5.2.2 Liquid Cooling

As mentioned in Chapter 5.1, the available liquid cooling units have only one state and consume 12.2 W. Consequently, here no control is possible like with the air cooling. The control strategy which is used for the liquid cooled system is to switch off/on a cooling unit whenever the produced power of the pTEGs, which are cooled down by the unit, is less/more than the energy consumption of the cooling unit itself.

5.3 System Reconfiguration

5.3.1 Single Thermoelectric Generators

The core idea of system reconfiguration—removing (disconnecting) and reviving (connecting) single TEGs—to increase the power output of an EHS, originates from the work of M. Chen, cf. [Chen2014a] and is also considered in the photovoltaic sector, cf. [Sp++2015]. Chen suggests removing and reviving TEGs, depending on the overall electrical energy output of the EHS, and assumes that there are single TEGs subject to completely different temperatures at different places in the system; this is the main important point. Therefore, the optimal wiring for each operating point is computed with a co-simulation between LabVIEW and Multisim. In some cases, due to the internal resistance of each single TEG, it makes more sense to disconnect detrimental TEGs or to reconnect them. This is understandable by regarding an equivalent circuit diagram of a TEG, see Figure 5.6. It is an EMF (voltage source) in series with a resistance (the internal resistance of the

TEG) and if the power loss across the internal resistance is too high, the TEG provides no contribution to the performance of the system.

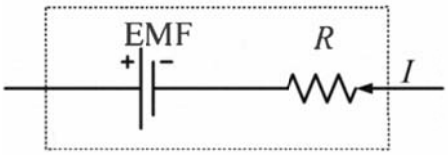

Figure 5.6: Equivalent circuit diagram of a TEG [Ch++2011].

M. Chen also considered a TEG system of eight TEGs, with four series connected pairs of two TEGs in parallel, cf. Figure 5.7. At the main line, he connected DC/DC converters and an MPPT controller and only one TEG in each parallel section can be disconnected by a switch.

With the developed `EHSTEG` library, it could be shown that this idea of removing and reviving of underheated TEGs is reproducible and understandable for this particular setup of an EHS. Figure 5.8 shows the simulation model for the same setup as in [Chen2014a] and Figure 5.9 the corresponding simulation result. Figure 5.9 above shows the different hot side temperatures for the TEGs (cold side temperature for all TEGs is the room temperature) and in Figure 5.9 below, the produced power with and without a removal and revival control concept is shown. One can see that the control concept itself works and leads to an increase in performance. The switching operation points, which are taken from the work of M. Chen, are marked with SO and a number. At the switching operation point 1 (SO1), TEG 2 and TEG 4 are disconnected, at SO2 TEG 6 is disconnected, at SO3 TEG 8 is disconnected and at SO4 the before disconnected TEGs are again connected to the EHS.

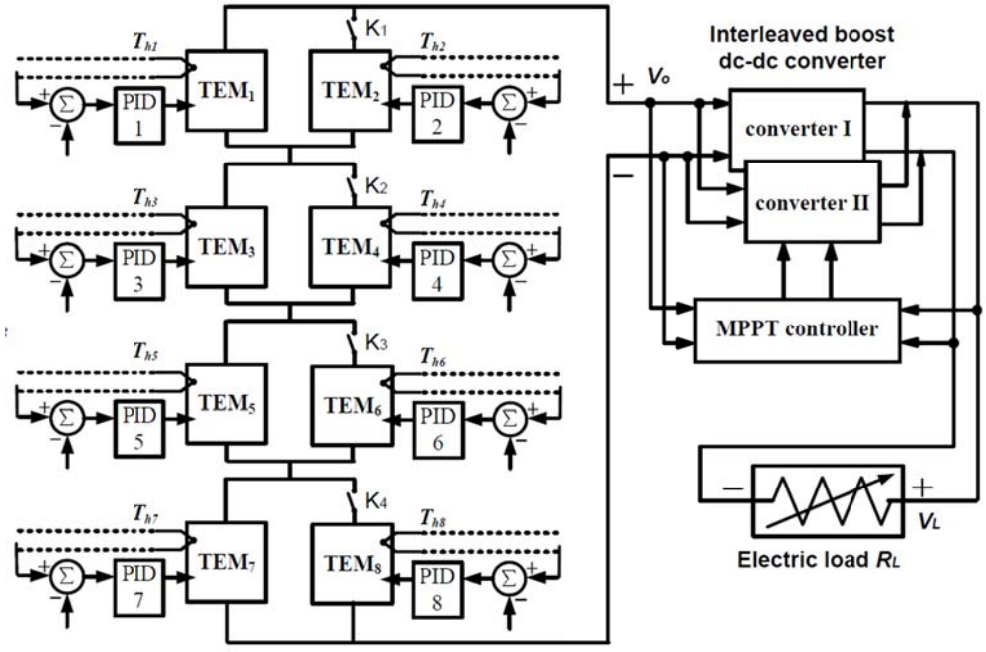

Figure 5.7: The EHS according to Chen [Chen2014a]. There are eight TEGs (here: called "TEM") and the possibility of creating different temperature conditions for each TEG (by PID-controllers).

However, the most obvious layout of a TEG-based EHS is to install pTEGs alongside a pipe (in contrast to Chen). With the exhaust gas losing heat in a downstream direction, the final pTEGs are expected to provide the least contribution to the EHS output. Even worse, those underperforming pTEGs may lower the EHS performance due to their internal electrical resistance, their low thermoelectric voltage and the energy consumption of their cooling device.

That is why Chen's concept is now modified (see also system description in Chapter 5.1):

- the cooling and its energy consumption are also taken into account, and
- the TEGs are applied to the setting of a real exhaust gas system.

The electrical wiring is obvious in Figure 5.2 (navy blue lines), and by contrast to Chen, complete pTEGs can be disconnected and reconnected as both TEGs of the same pTEG are subject to the same temperature conditions. With the help of the presented simulation model, it is possible to remove detrimental pTEGs during system design (offline) or—as in the following examples—to disconnect and to revive them at the ideal instant of time (in online mode), see following subchapter.

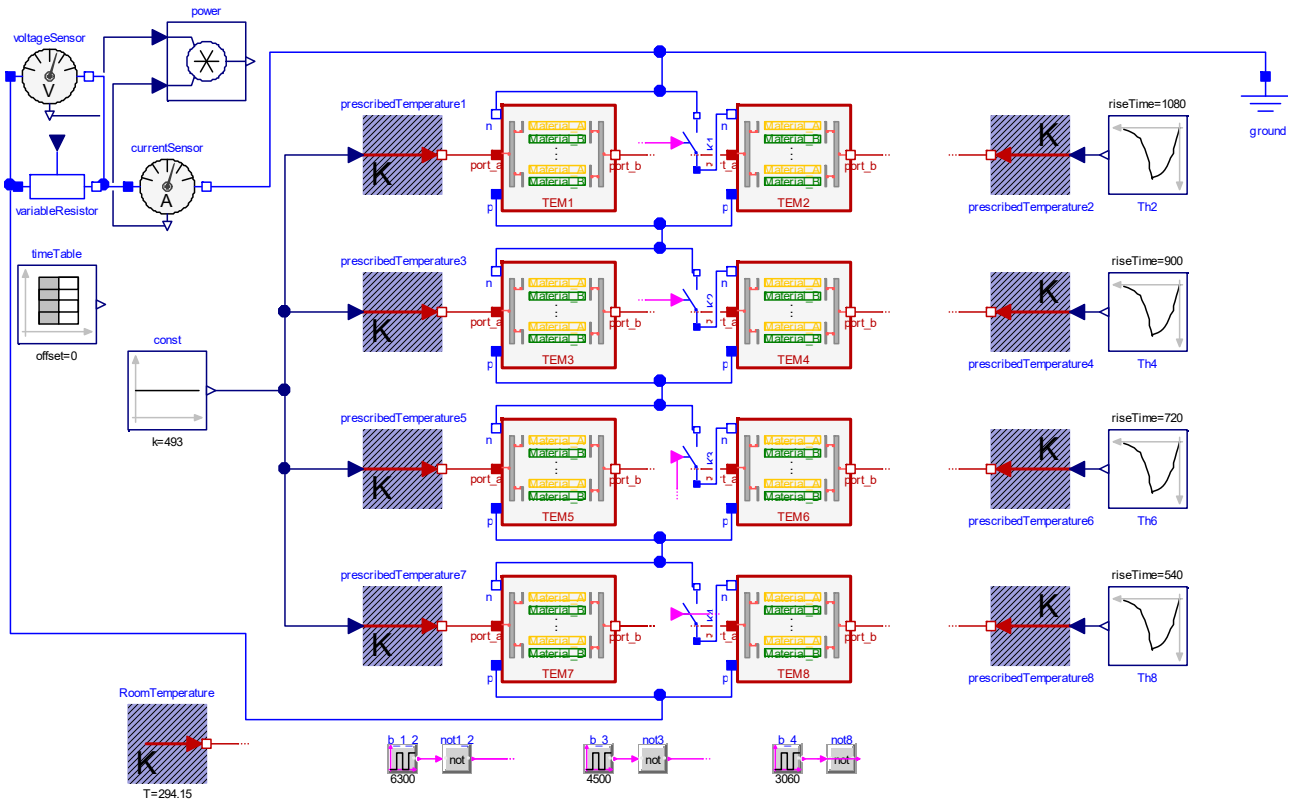

Figure 5.8: Simulation model in Modelica/Dymola for the same setup as in [Chen2014a].

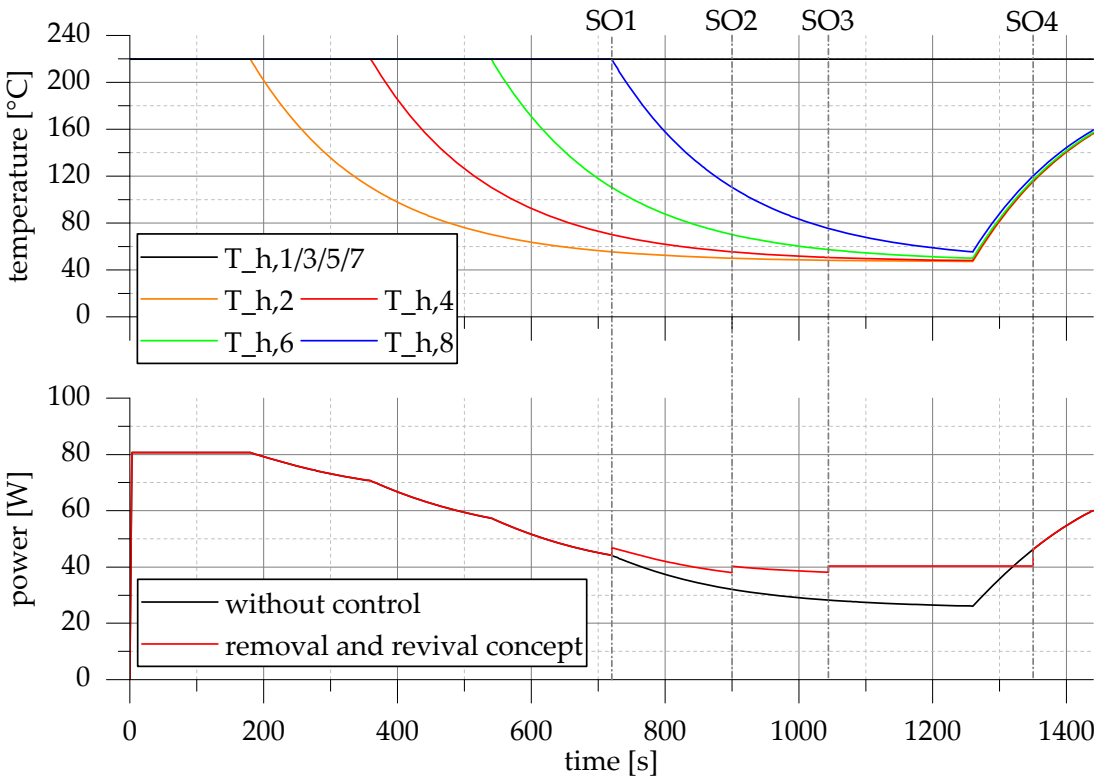

Figure 5.9: Simulation result for the simulation model of Figure 5.8; above: the hot side temperature curves of the single TEGs; below: the produced power with and without control concept. One can also see the switching operation points, which are marked with SO.

5.3.2 *Pairs of Thermoelectric Generators*

Liquid Cooled System

First, a thermoelectric EHS on a heater (see Chapter 5.1) under full-load operation and with liquid cooling is considered, cf. [NeFF2014]. In this case, the heating is turned on, run on full power for half an hour and then switched off (see black curve in Figure 5.3). The complete scenario takes 35 minutes. Figure 5.10 shows some simulation results with all pTEGs connected and without any control concept. In the upper diagram of Figure 5.10, the different pTEG temperatures for the hot and cold side of one representative TEG and the temperature of the exhaust gas coming from the heating are presented. One can see that the liquid cooling achieves a nearly constant cold TEG side. The lower diagram shows the gained power and the total energy gained from the EHS. The cooling units are running from the beginning, which is why the gained power and energy there are negative. As mentioned above, the energy consumption of the cooling units is constant and so the curve of the gained power arises from the produced power curve minus 2 × 12.2 W.

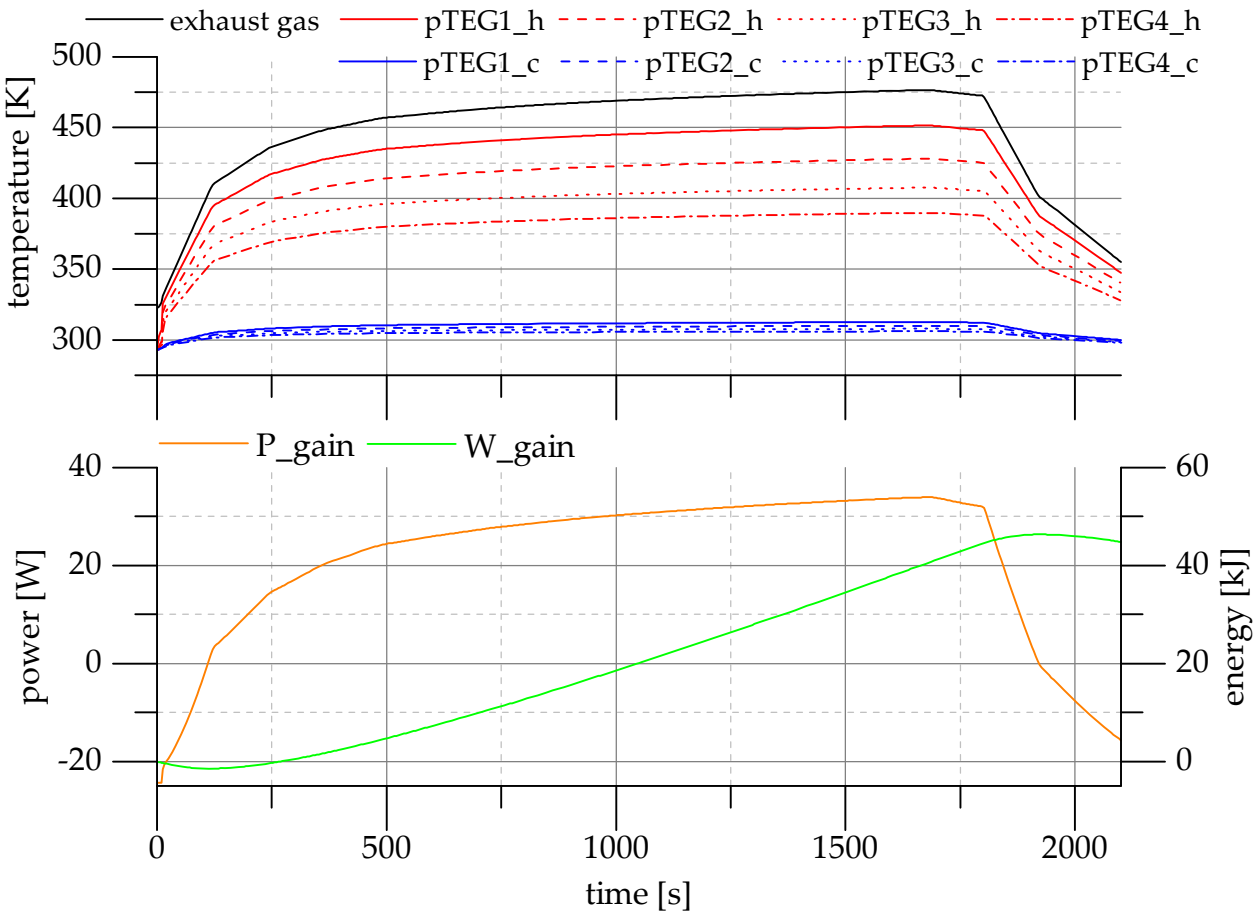

Figure 5.10: Simulation result of the uncontrolled liquid cooled EHS for full-load operation; above: Temperature of the exhaust gas coming from the heater as well as the hot (index h) and the cold (index c) temperatures of each pTEG; below: gained power and energy [NeFF2014].

Figure 5.11 shows different connection modes, e.g. only pTEG I is connected or all pTEGs I-IV are connected during the complete simulation time. In the upper diagram of Figure 5.11, one can see that the first pTEG produces the highest power and the last pTEG the lowest power, due to the lower hot side temperature of the pipe, and consequently a lower temperature difference over the TEGs (cf. Figure 5.10, above). Also shown in Figure 5.11 above, the maximum power is reached with an individual MPPT for each pTEG. As the improvement in performance is very low and the effort to build up such an EHS very high, it is suitable to use only one MPPT for the main line, in accordance with Chen.

In contrast to Chen, there is no reason to disconnect any pTEG in that test case concerning the internal resistance. Admittedly, the power output of the last pTEG is reduced, but in any case it is still a positive contribution to the EHS (see Figure 5.11, above). So, there is no negative influence based on the internal resistance of the TEG. Now, looking at the energy consumption of the cooling and finally the effective power gained by one pTEG (cf. Figure 5.11, below), it is notable that the connection of the third pTEG is very inefficient. There is only a small positive amount at the end of the steady-state area and for the remaining area even a negative influence. Also pTEG4

causes a negative contribution at the beginning and at the end. The connection of the third pTEG is so inefficient because each cooling unit supplies two pTEGs, pTEG3 and pTEG4 (the red and brown lines in Figure 5.11) are supplied by one cooling unit as well as pTEG1 and pTEG2 (the blue and cyan line) by the other one. There is only a small amount of gain in power at the end of the steady-state area, whereas the connection of the fourth pTEG provides a significant major contribution, because the cooling unit is already running.

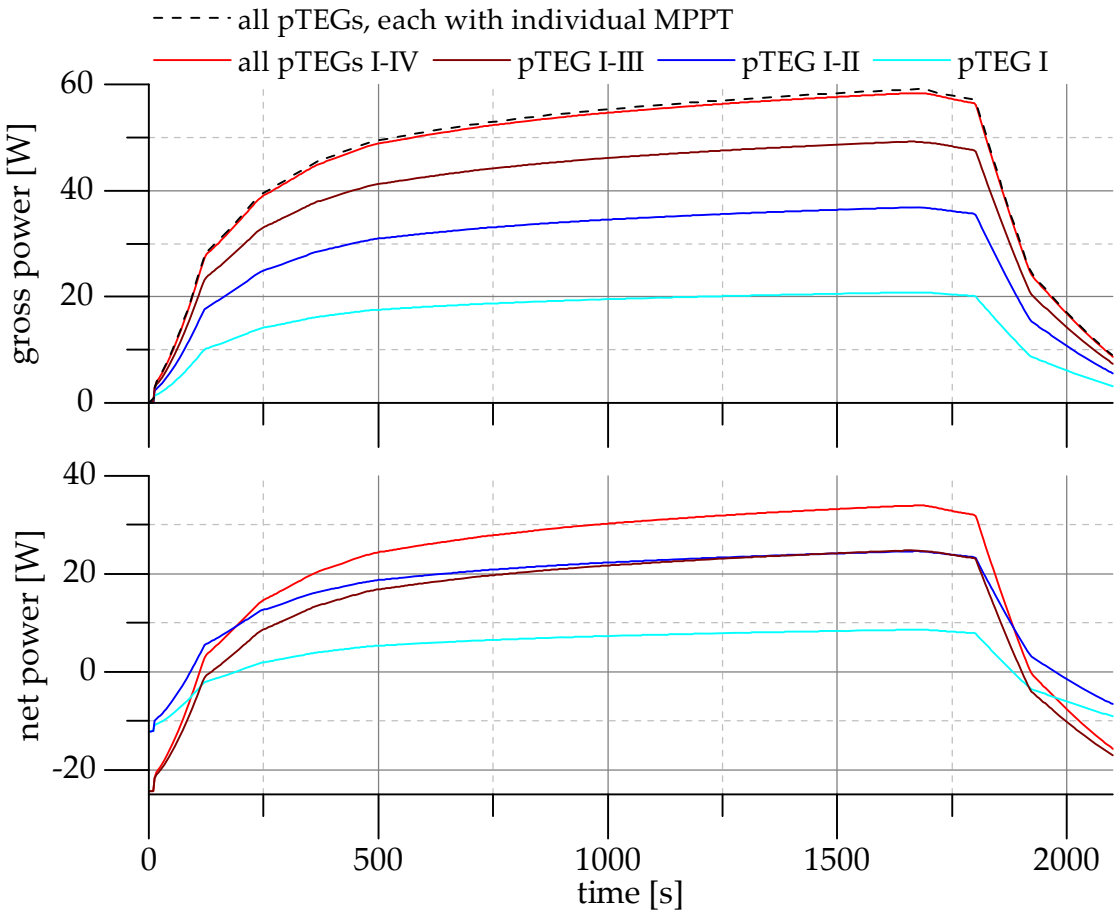

Figure 5.11: Comparison of the four different connection modes for the produced electrical power, gross power (above) and the effectively gained power, net power (below) as well as the maximum reachable power with individual MPPTs for each pTEG; concerning numbering: see Figure 5.1 [NeFF2014].

For this case, a disconnection of pTEG3 and pTEG4 at the beginning and at the end seems reasonable due to the desire of increasing the efficiency (net power). A disconnection and reconnection of pTEGs can improve the electrical power provided by the EHS and thus also increase the produced energy as depicted in Figure 5.12. The inset diagram shows the end range and it should be noted that the energy of the uncontrolled EHS—all pTEGs with running cooling systems are connected all the time—is finally 44,808 J. A disconnection of pTEG3 and pTEG4 at the beginning and the end results in a final energy delivery of 47,044 J. This is a difference of 2236 J in 35 minutes, which means enhancement plus of 5.0% for that case. The short power drop at the

beginning is caused by switching on the cooling unit, which first requires more power until the cooling effect occurs and the TEGs supply the extra power.

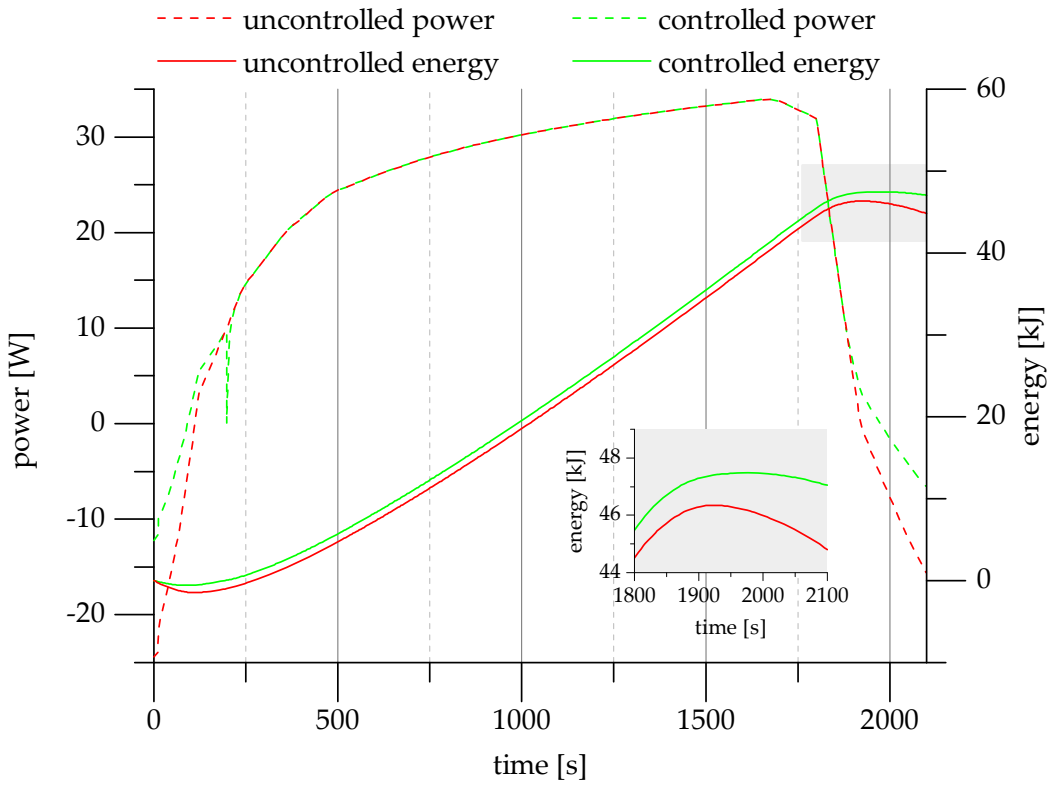

Figure 5.12: Controlled EHS (disconnection and reconnection of different pTEGs) versus uncontrolled EHS (pTEGs connected all the time) [NeFF2014].

The previous example has shown that during an almost steady-state, in full-load mode, a disconnection of pTEGs is not useful. This is because the EHS was constructed for a heater under full power and so all pTEGs have a positive contribution. However, for the start-up and the cool-down phases, the control concept of temporary removal and revival is advantageous. In real heating systems, there is often the control strategy to switch on the heating burner for a certain time and then to power off. After a definite time it will start again, so there is an on/off behavior and the burner often changes between full-load operation and idle running. Consequently, the start-up and the cool-down phases occur very often. This fact makes the suggested control concept of removing and reviving pTEGs very attractive and significantly enhances the efficiency of EHSs.

Air Cooled System

If there is an EHS with air cooling, a removing and reviving of the pTEGs would not be advantageous. There is no further power improvement with the removal/revival control concept for the air cooling option and controlled fan speeds. The fan speed control adapts the energy consumption in an optimal rate to the produced power of the pTEGs. The energy curves in Figure 5.13 show a higher energy yield for the air cooled EHS. However, this phenomenon is not referable

to the control concepts, but rather to the special test case. During boot and shutdown of the oil-fired heating, the air cooling is more efficient, whereas in the almost constant operating point at the end, the advantage is with the liquid cooling.

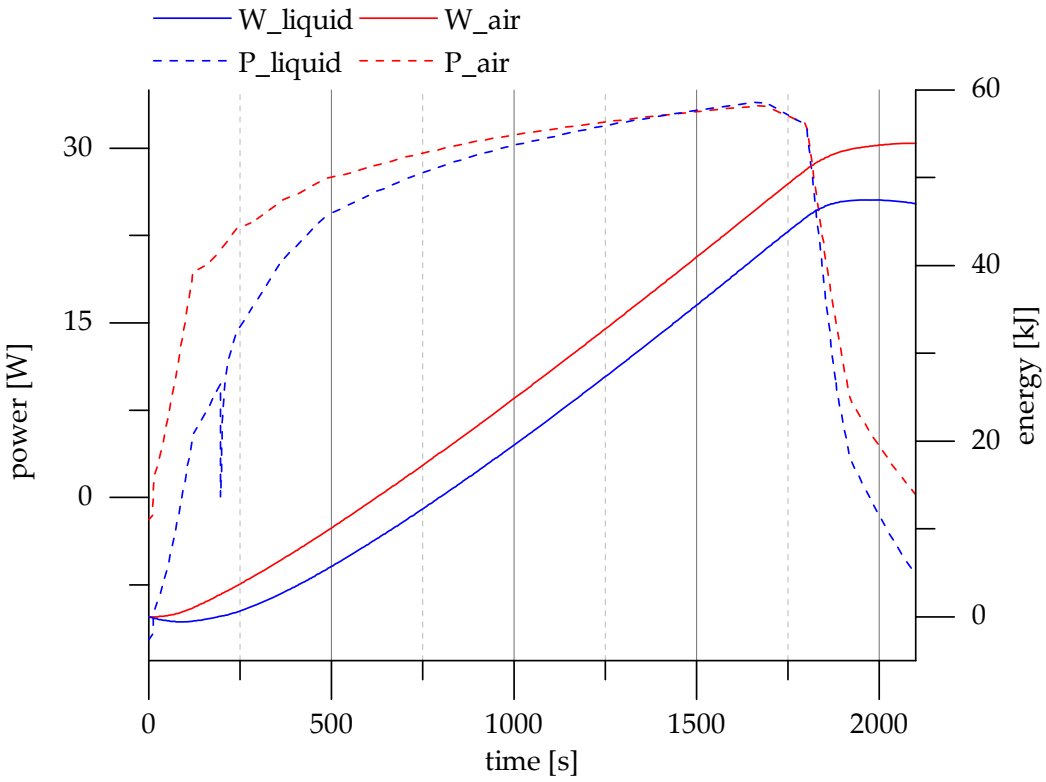

Figure 5.13: Comparing the simulation results of the controlled, liquid cooled EHS (blue lines) and the air cooled EHS (red lines) for the gained power as well as the produced energy [NeFF2014].

Consequently, the choice of the cooling option depends on the behavior of the oil burner. If it is running during a longer time than in this test case, and if the extra effort to build up a liquid cooling system is acceptable, then the preferred cooling method is liquid cooling. Otherwise, the advantage is with the air cooling. As a consequence, the cooling method also has to be considered during system design.

5.3.3 Arrays of Thermoelectric Generators

In the solar industry, it is very common to connect or disconnect complete solar modules (arrays of solar cells) 'automatically' with bypass diodes in case of partial module shading. For single TEGs or pTEGs, this solution is not possible as the inner resistance of an underheated TEG/pTEG is lower than the resistance of a bypass diode. However, if there are big TEG arrays with hundreds of elements, this concept could be adapted from the solar industry and seems to be a reasonable and simple control strategy.

5.4 Control Laws

In the previous subchapters, the control concepts mainly for the system reconfiguration of pTEGs are explained. Now, they are verbalized into the following control laws (CLs); they are opposed to the uncontrolled reference system, identified by CL0:

CL0: The cooling units run all the time. There is no control strategy applied, either for the air cooled or for the liquid cooled system.

CL1: Switch off the complete EHS as soon as the pTEGs produce less than the cooling elements consume.

CL2-L: Disconnect/connect a set of pTEGs (and the corresponding liquid cooling system) whenever the produced power is less/more than the sum of the power used for its cooling and the power loss due to its internal electrical resistance (cf. Chapter 5.3.2).

CL2-A: The air cooling elements are controlled as described in Chapter 5.2.1.

CL0 and CL1 refer to both cooling methods, whereby CL0 for the air cooled system means that the duty cycle of the fan speed is 100% and for the liquid cooled system that the units are on all the time. The CL2 is divided in one law for the liquid cooled (-L) and one for the air cooled system (-A). As described in [NeFF2014], the removing and reviving concept delivers no advantage for the air cooled system, due to the fine control of the fan speed.

In the following summary, an uncontrolled EHS means CL0 and a controlled EHS means the usage of CL1 and CL2-L/CL2-A.

5.5 Model-based System Assessment

To assess a conceived EHS construction, a simulation model as mentioned earlier is required. With the exemplary system model described in Chapter 5.1, the exhaust gas pipe of a heater, the thermoelectric elements as well as the two different cooling options are simulated. To evaluate the design and to optimize the construction for an EHS at a special heating, only the normal temperature curve of the exhaust gas at the real system is necessary. Given these measurement data, the simulation will enable the detection of the optimal number of pTEGs as well as the suitable cooling method.

There are two different cooling methods to cool down the cold side of the TEGs. One is the cooling with a liquid cooled system and the other is cooling by forced air. Moreover, there is a different control strategy for each cooling method, which was explained in Chapter 5.2.

The following figures show respectively one of the three heating behaviors as presented in Figure 5.3. Table 5-1 shows, corresponding to a steady-state scenario, the full load operation mode (100/0).

In this scenario, it is obvious that liquid cooling is more effective than air cooling and in air cooling scenarios, the controlled case is better than the uncontrolled one (for liquid cooling they are identical).

Table 5-1: The finally gained power for both cooling methods and their different control concepts for the steady-state temperature (100/0 on/off behavior) (red line in Figure 5.3). The uncontrolled and controlled liquid cooling are identical in that case [NeFF2015].

cooling method	control concept	gained power
air cooling	uncontrolled	30.7 W
	controlled	34.1 W
liquid cooling	uncontrolled	34.7 W
	controlled	34.7 W

Figure 5.14 and Figure 5.15 show the gained power (net power) for the different cooling methods in an on/off behavior of the heating. Figure 5.14 shows the 50/50 and Figure 5.15 the 20/80 ratio. In both cases, the advantage is with the controlled air cooling system and of course, in both cases, the controlled case is better than the uncontrolled. Furthermore, the different control laws mentioned in Chapter 5.4 are visible. The uncontrolled curves represent CL0. If we consider e.g. the controlled liquid curve (blue line) in Figure 5.14, CL1 keeps the system on zero (compare the beginning and the end of the curve). The peak at approx. 125 s is based on CL2-L. It is the moment when pTEG3 and pTEG4 (cf. Figure 5.1) are connected, and their corresponding cooling unit is switched on. Primarily, the cooling consumes more energy until the cooling effect of the cooling systems occurs.

As a result of the assessment with different heating loads, it can be noted that for a high constant temperature, the liquid cooling is preferable and for the other cases, on/off behavior far away from 100/0, the air cooling is preferable. The reason for this lies in the more flexible control of air cooling elements during transient phases, which was discussed in Chapter 5.2.1.

To design a thermoelectric EHS in an optimized way, the use of a simulation model is strongly recommended. Common household oil-fired heaters have an exhaust gas temperature between 120°C and 200°C. Depending on the maximum reached temperature and the temperature curve itself, an economic and reasonable EHS has to be built up. With the simulation model applied here, the number of pTEGs, the suitable cooling method and the control strategy can be determined. For this purpose, only representative curves of the exhaust gas temperature of the real oil-fired heating are necessary.

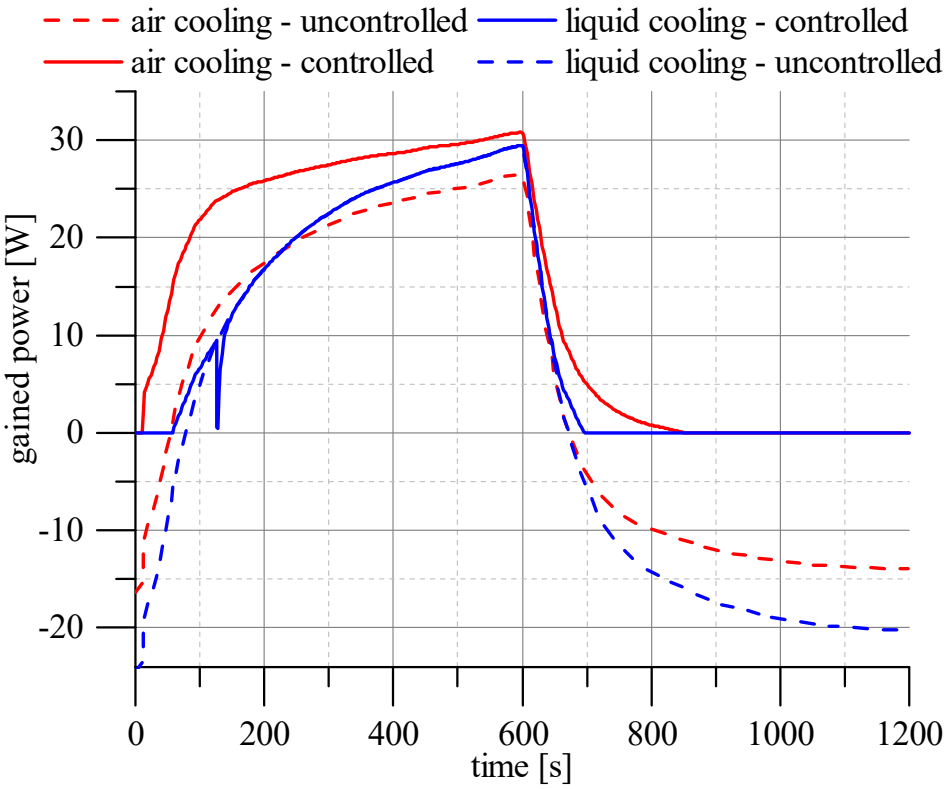

Figure 5.14: The finally gained power for both cooling methods and their different control concepts for the 50/50 on/off behavior (green line in Figure 5.3) [NeFF2015].

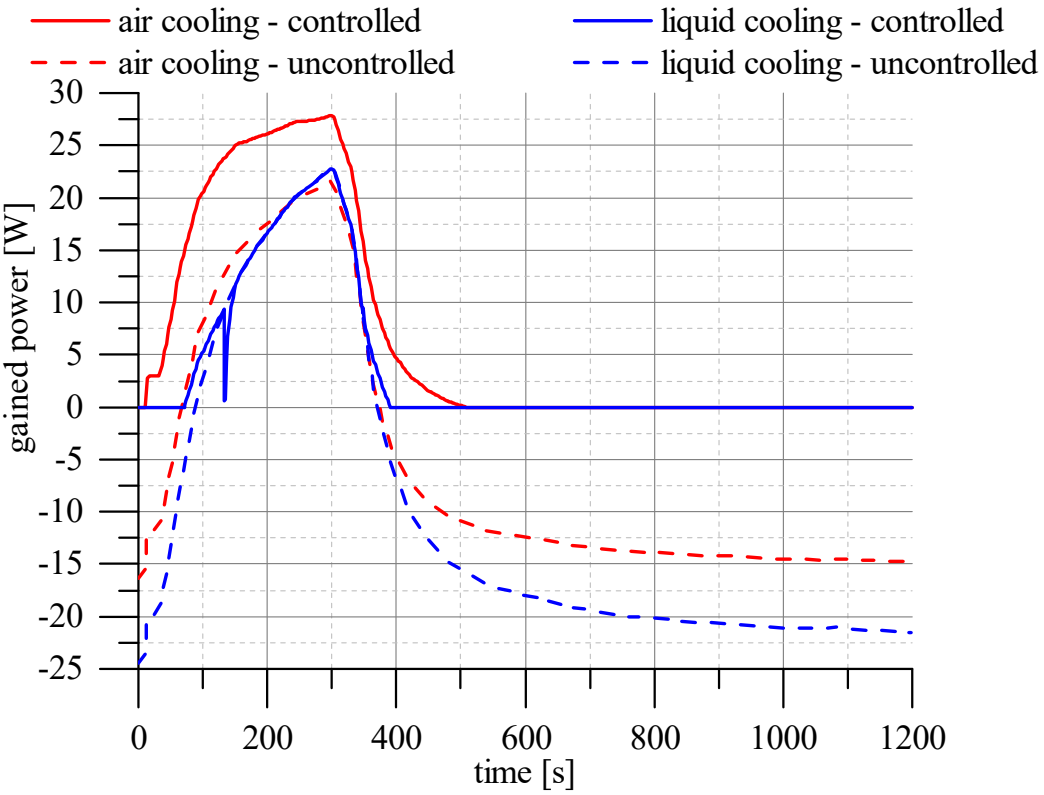

Figure 5.15: The finally gained power for both cooling methods and their different control concepts for the 20/80 on/off behavior (orange line in Figure 5.3) [NeFF2015].

If only the controlled cooling systems are considered, a further pTEG does not lower the output of the EHS. If it did, the control strategy would shut off the cooling and disconnect the pTEG from the system. The remaining question consequently concerns the economics. Theoretically, a large number of pTEGs can be attached to an exhaust gas pipe, although the last pTEGs are only connected with the system very rarely or never in the worst case (due to the applied control laws). The choice consists in determining the optimal number of pTEGs installed in the system. Therefore, the delivered extra energy of the additionally added pTEG has to be compared with the investment costs and based on that, a reasonable number of pTEGs has to be determined.

The crucial results are summarized in Table 5-2. They give practical advice concerning an appropriate TEG-based EHS depending on the boiler control on/off ratio, which is representative of the heating system considered for energy harvesting. The red arrays (-) are very bad solutions, this means they deliver a negative energy output after the simulation time and as a result they must be avoided. The orange (+) and green (++) arrays show solutions which generate a positive energy output after the simulation time, whereby the green array shows respectively the best solution for the special heating load scenario. As shown in the table, there are scenarios where a liquid cooled EHS is advantageous. This will especially be the case for heaters run under full-load operation, meaning a steady state behavior. For on/off scenarios (dynamic behaviors) the advantage is with the air-cooled EHS.

Table 5-2: Overview for different heating load scenarios; red arrays (-) deliver a negative energy output, orange (+) and green (++) arrays positive energy outputs, whereas the green arrays deliver the highest output for a certain heating load scenario [NeFF2015].

cooling method	control strategy	on/off ratio of boiler control		
		100/0 Table 5-1	50/50 Figure 5.14	20/80 Figure 5.15
air cooling	uncontrolled (CL0)	+	-	-
	controlled (CL1 + CL2-A)	+	++	++
liquid cooling	uncontrolled (CL0)	++	-	-
	controlled (CL1 + CL2-L)	++	+	+

6 Application Examples

Talking a lot about multiphysics simulation, the development process and different control concepts, this chapter finally deals with real application examples. To build up these real systems, the previously mentioned methods are applied. In total, three systems were set up, one system in the small-scale range (only a few milliwatts of generated electrical power) and two systems in the middle-scale range (about a few watts). For all three applications, the structure of the subchapters is identical. First of all, there will be a system analysis describing the original system, the goal of a possible EHS as well as preliminary investigations and calculations. Afterwards, the development of the concrete EHS is depicted concerning the used components, the design of the system, possible controlling strategies as well as a simulation model. To conclude, the results of the simulation will be compared with real measurement data of the EHS. Moreover, there will be an evaluation of the constructed system and also suggestions for improvements are given or still open problems are elaborated upon.

6.1 Thermostat

6.1.1 System Analysis

The goal of this application is to show that already today thermoelectric applications for home use may be applicable and affordable, see [NeFr2017a]. To find an application for home use, first heat sources have to be determined in the building. Apparent heat sources are the radiators in the rooms and with the upcoming interest in smart home applications, this seems very appropriate, as standard thermostats are very often replaced with electronic thermostatic valves, which themselves need energy. Of course, there are some good reasons for this smart home application. The most important one is the saving of energy by adjusting exact temperatures for explicit time intervals. Moreover, the comfort increases for the residents. Unfortunately, an electronic thermostatic valve needs electrical energy, which is normally delivered by a battery which has to be changed from time to time. The thermoelectric EHS developed here generates the electrical energy for the thermostat directly from the heating process and that is why a battery replacement is no longer necessary. The idea is that a small part of the heating energy will be converted by TEGs into electrical energy. Certainly, this energy is lost for the room heating process, but it is so little that it will be of no consequence for the room temperature.

The EHS presented here is installed in one office at our Chair and adapted to work hours; the heating mode is programmed from Monday to Friday between 7:30 and 17:30. At the other times, the thermostat is programmed to the setback temperature. Consequently, this means that enough electrical energy has to be produced in the few hours of heating to supply the thermostat 24/7.

For a preliminary consideration, the estimated power consumption of an electronic thermostatic valve has to be known as well as the maximum possible electrical energy, which can be generated by a TEG with the radiator as a heat source. Therefore, an electronic thermostatic valve is chosen, Honeywell Rondostat HR 20 [Hone2015]. First of all, the different operating modes and the corresponding power consumptions have to be listed. In total, there are three operating modes: the adaption mode, the stand-by mode and the switching operation mode. In the adaption mode—this occurs only if the thermostat is reattached to the heating valve, which is normal only during the installation—the power consumption of the electronic thermostatic valve is about 90 mW. Both other states are more relevant for the EHS. In the stand-by mode,—display is on and the internal electronics are working—the thermostat consumes approximately 0.4 mW and in the switching operation mode—time when the valve moves from one position to another—the thermostat consumes maximum 70 mW. In this test case, there is a heating scenario of 10 hours a day and with the number of heating days for this region, on average about 263 days according to [IWU2017], and the generous assumption of 240 s valve driving time per day, the total energy consumption per year of the thermostat should be approx. 17,030 J. Further analysis has shown that the highest measured surface temperature is about 55°C near the inlet valve of the radiator. The best option would be to use the heat energy in front of the inlet valve, since heat is also present there when the heater is switched off, but this is not possible in this room because of the location of the radiator. With a standard Bi_2Te_3-TEG and an approximated hot side temperature of 45°C as well as a temperature difference of 3 K, a generated electrical power of about 8 mW can be expected. This means that the produced energy will be ca. 75,740 J per year, which is more than four times higher than the calculated expected energy consumption of the thermostat (more information about the calculations can be found in Appendix **A.3**).

Furthermore, it has already been shown with a simulation model in [NeEF2014] that a TEG can generate enough energy on a heating tube, see Figure 6.1. Therefore, the Modelica example of a simplified model of a heating system was used and the hot side of the TEG was connected to a heating flange and the cold side to a simple heat sink. To reach the maximum possible output power, the TEG was connected to an MPPT. The simulation results are also shown in Figure 6.1. The TEG temperatures, the electrical output power, the electrical energy generated, and the temperature-dependent Seebeck coefficient are plotted under the assumption of active heating in the morning and in the evening. In the given simulation scenario, the generated electrical energy would be enough to cover the energy consumption by an electronic thermostat valve.

Consequently, according to the initial calculations and simulations, it seems reasonable for a thermoelectric EHS at the radiator to supply an electronic thermostatic valve.

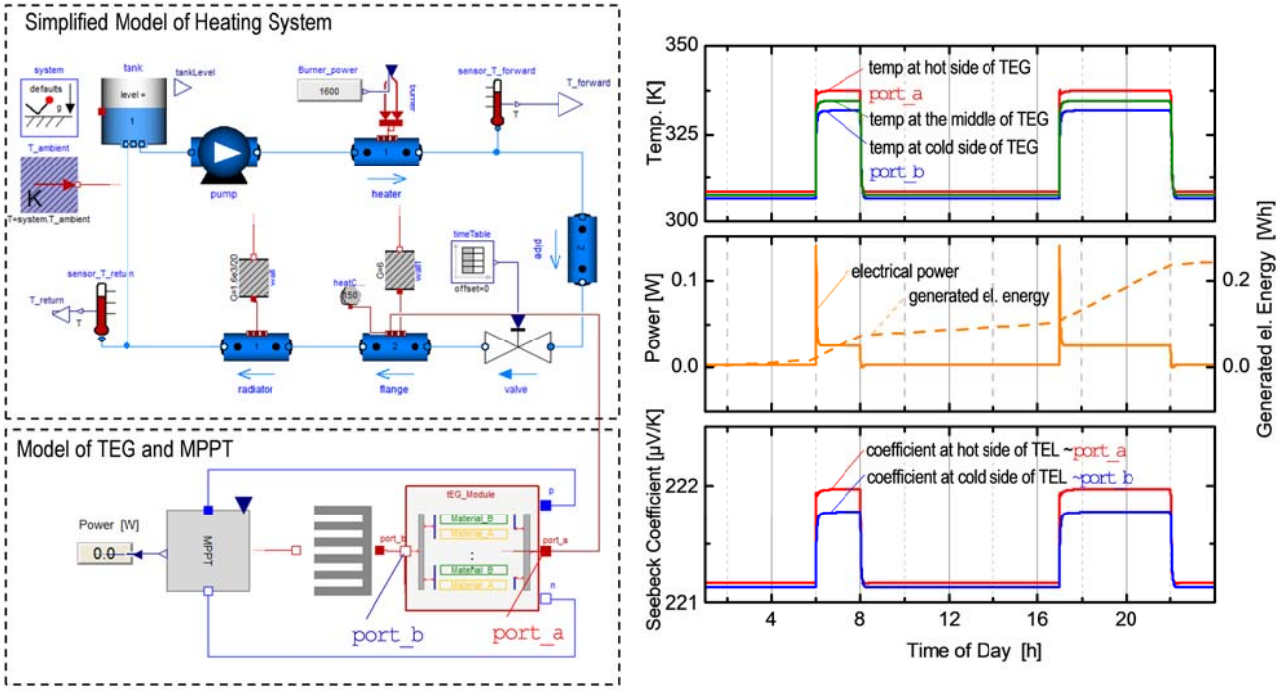

Figure 6.1: left: Modelica/Dymola diagram of a heating unit (taken from the Modelica Fluid library) with integration of a TEG model to simulate energy harvesting for an electronic thermostat valve. Right: simulation results for whole day simulation [NeEF2014].

6.1.2 Development of Energy Harvesting System

According to the development process shown in Figure 4.1, the first two steps (selection of heat source and objective) are already done in the system analysis subchapter. Now, the other six steps have to be done, which can be classified into these superordinate categories: thermal design, selection of thermoelectric device, mechanical design and electrical design, cf. Chapter 4.3 to 4.6. In Chapter 4.4, it was shown that for low temperatures, the use of TECs is preferable to TEGs. They are just as efficient as TEGs in this temperature sector, but significantly cheaper. Therefore, a TEC will be used here. Concerning the thermal and mechanical design, an aluminum half-shell will be produced, which can be directly attached to one tube of the radiator. As it is a low temperature system and should be additionally quiet and safe, the choice falls on a passive heat sink. Thus, there will also be an attachment possibility for the heat sink at the aluminum half-shell. Since the first design with only one TEC had not achieved the desired result in reality, a second one was added. The used electrical parts like an accumulator and an MPPT were purchased, whereas an MPPT specially designed for TEG-based systems was obtained. Figure 6.2 shows the final construction of the EHS from the front and the top. In the front view one can see both cooling elements at the radiator and two switching boxes. The smaller one (switching box No. 1) containing an accumulator and an MPPT, whereas the additional, bigger switching box (switching box No. 2) is necessary for measurement purposes. It contains different sensors and a micro-controller and has a direct connection with a network database. The EHS is also working without

the additional box (No. 2). The top view shows the electronic thermostat and the TECs between the aluminum half-shells, surrounding the heating tubes and the cooling elements. The two TECs are connected in series. An attempt to commercialize such a project was done by Micropelt [Micr2015]. However, the heat for the hot TEG side does not come from heating tubes like in this case, but is directly extracted from the heat in the thermostat valve with especially developed TEGs. In contrast to this, standard TEGs and mainly standard components are used here.

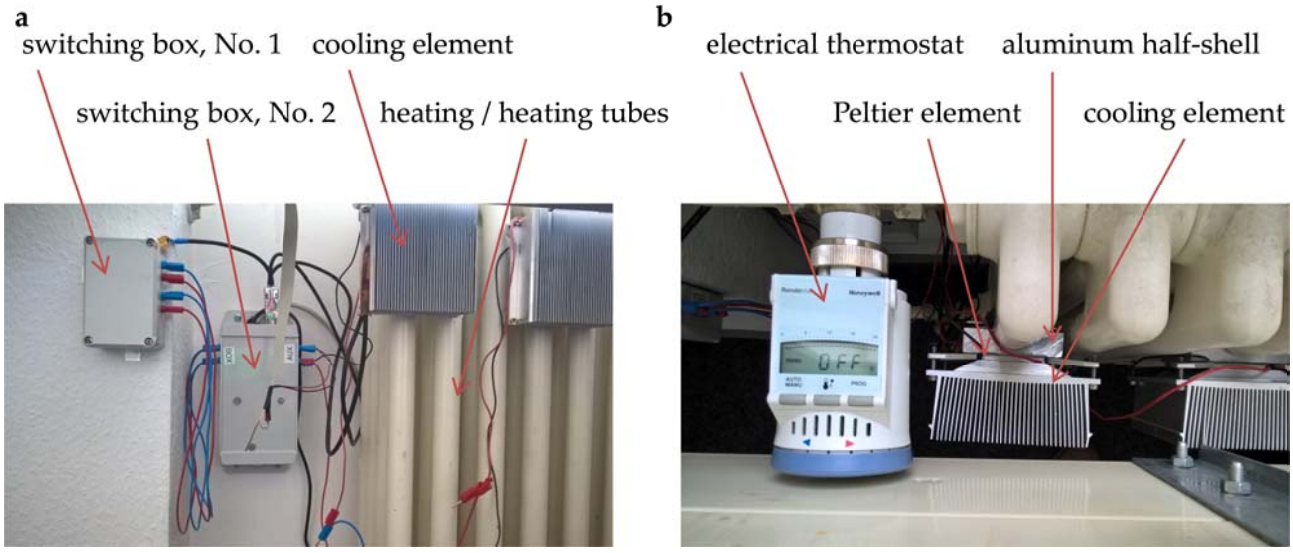

Figure 6.2: Thermoelectric EHS at a heating to supply an electronic thermostat valve: (a) front view, (b) top view [NeFr2017a].

For measurement reasons, a second switching box is needed as shown in Figure 6.2. A schematic layout of the complete system with measuring devices is shown in Figure 6.3 (for a clearly arranged overview, switching box No. 2 is not shown, only the sensors which are located inside box No. 2). Temperature sensors are directly attached at the aluminum half-shell and the cooling element and one room temperature sensor is also available, presented with thermometer symbols in Figure 6.3. Additionally, the voltage and the current coming from the TECs—equal to the produced electrical power—and the voltage and the current going from the accumulator to the thermostat—equal to the consumption—are measured. This is done in the second switching box. The measuring points are marked with an S for sensor. Thereby, it is clear that the conversion losses through the MPPT, the intermediate storage in a supercapacitor and the low-dropout regulator are not considered, as they are located behind the measuring device. All data are collected and evaluated by a micro-controller and are sent to a database.

The preliminary simulation model shown in Figure 6.1 is now adapted and extended regarding the previously described, real installed EHS system, see Figure 6.4.

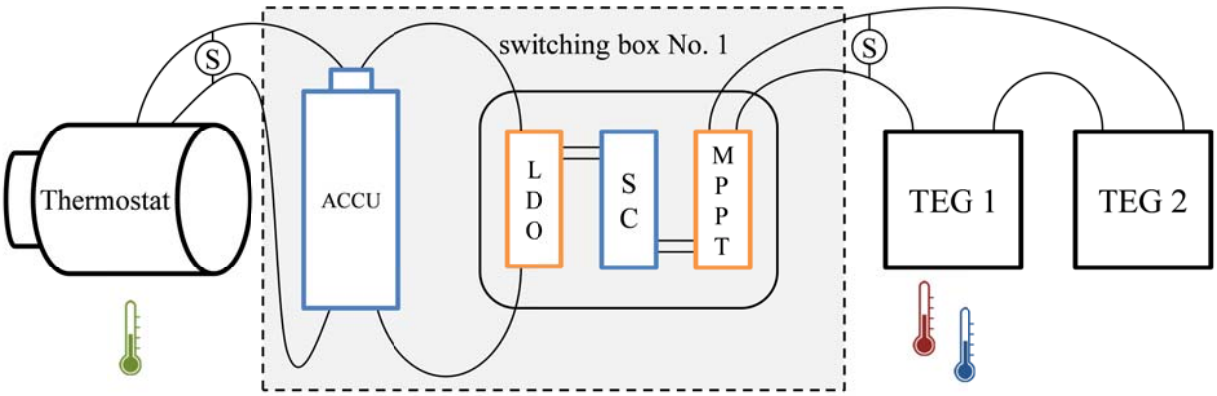

Figure 6.3: Schematic layout of the EHS at the heater. One can see the TEGs in series and the thermostat as well as the content of the first switching box—MPPT, supercapacitor (SC), low-dropout regulator (LDO) and accumulator (ACCU)—and the sensors [NeFr2017a].

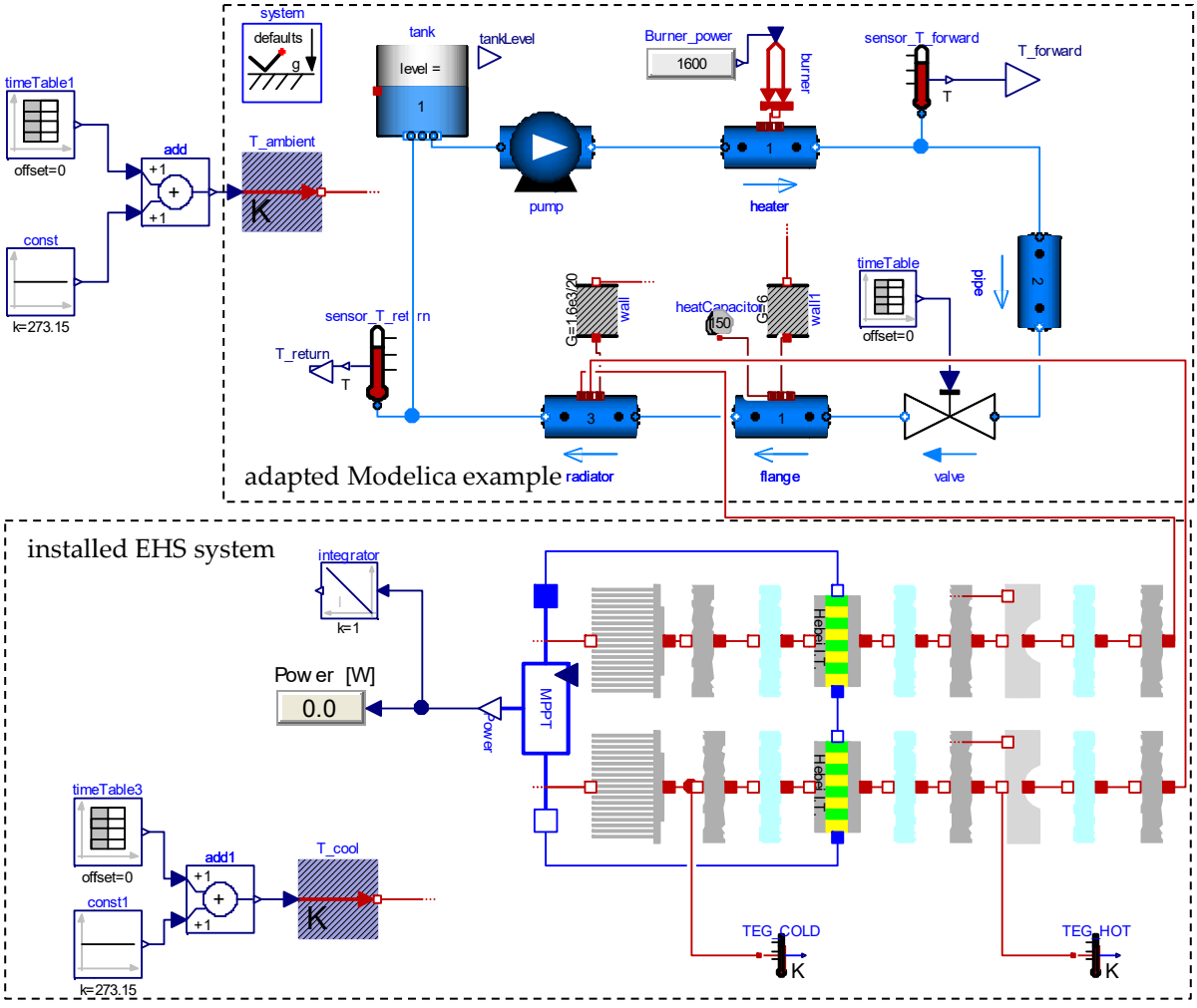

Figure 6.4: Simulation model of the real installed EHS at a heater to supply an electronic thermostatic valve as described in this section.

6.1.3 Results and Evaluation

As an example week for the winter period 2015/2016, the different temperature profiles for room temperature, the temperature of the aluminum half-shell and the cooling element temperature are shown in the upper diagram of Figure 6.5 for the week from March 21st, 2016 to March 28th, 2016. As it is the record of an office room, the heating periods on work days during work hours are visible. The maximum temperature difference between the aluminum half-shell and the cooling element is about 5 K, whereas the average value for the heating phase is between 3 and 4 K. The produced electrical power is between 3 and 4 mW on average during the heating period and is depicted in the lower diagram of Figure 6.5. In stand-by mode the consumption of the thermostat is 0.4 mW and while switching operation it can consume during this example week up to 65 mW. It is also obvious that the thermostat switches not only to the stored times, but also moves the valve very often during the heating phase and even inexplicably in the night mode or at the weekend. The right axis in the lower diagram of Figure 6.5 shows the consumed generated electrical energy during this example week, respectively. From Monday to Friday, the energies are almost balanced, but then moves over the weekend in favor of consumption. There are even weeks during this winter period with a positive energy balance on Friday afternoon, but the unexplainable high consumption of the thermostat during the weekend always leaves a negative balance at the end.

One can also see in the lower diagram of Figure 6.5 the simulation result for the produced electrical power and energy. The measurement temperatures (room temperature and cold side temperature) are given to the simulation model of the EHS in Figure 6.4. Obviously, there is an increase in power in the second half of the day, which does not occur in reality. The reason for this is the almost constant hot side temperature in the simulation model, which then leads to an increase in the temperature difference and thus a higher electrical power output. In contrast, the hot side temperature drops after a certain time in reality, as the room is more or less heated and the valve closes a little. In the simulation, the valve only has an on/off behavior and so, the simulation gives a slightly higher power output and thus, a slightly higher energy after one week. Finally, it can be noted that in the simulation, after one week the EHS delivers 759 J, whereas the real measurement data gives 707.3 J as the produced energy at the end of the week at a real energy consumption of 884 J.

In conclusion, it can be said that the EHS at the heater is not able at the moment to supply the thermostat autarkically under the current conditions. Of course, there were calculations in advance to analyze the profitability of an EHS and with the knowledge of the stand-by power of the thermostat and the necessary power to switch the valve, the planned EHS should be sufficient enough. Unfortunately, there are more switching cycles than expected. A possible solution of this

problem is to intervene in the microcontroller of the bought thermostat and to modify the switching behavior. At least the time to exchange the batteries will be extended in its current state.

The Carnot efficiency for this application is 1.6 % (for the best case of T_{high}=37.5°C and T_{low} = 32.5°C; calculation see Equation (2.1)). If a common value for ZT of Bi_2Te_3 is taken into account (ZT = 0.8; cf. Chapter 2.4.2), the efficiency of the EHS is 0.24%, see Equation (2.25). In addition, losses are also added by the MPPT, which has an electrical efficiency of up to 87%.

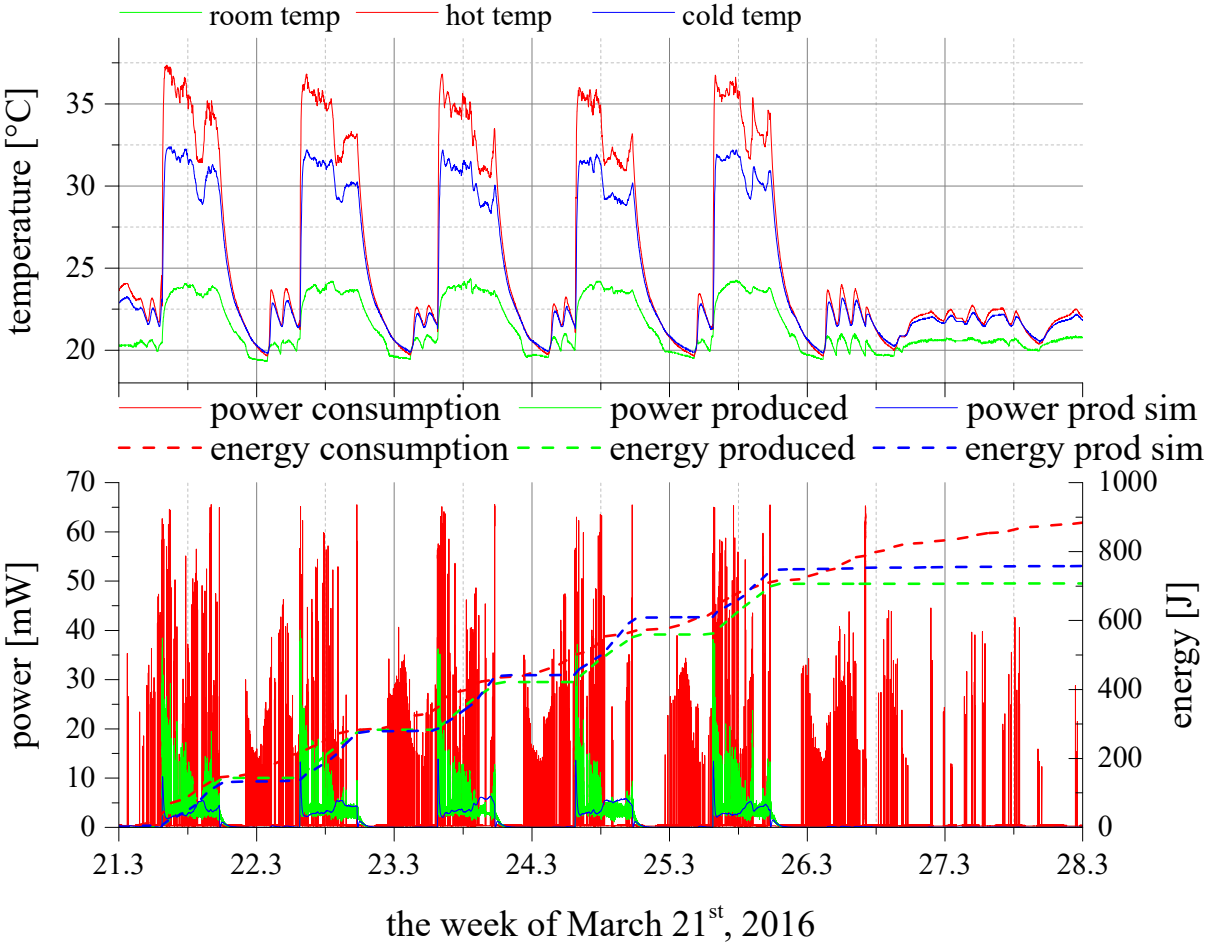

Figure 6.5: Measurement and simulation data from the week of March 21st, 2016. Above: temperature profiles during the week for the room temperature, the aluminum half-shell temperature and the temperature at the cooling element; below: power and energy consumption of the thermostat as well as power and energy production of the EHS and the simulation results for the produced power and energy, modified from [NeFr2017a].

For the future, another design can be considered which also generates electrical energy in summer and does not have such a bulky appearance [Fleu2016]. However, this approach has to be taken into account directly in the house construction process. The idea is to put the heat sinks into the exterior wall, which enclose a TEC. Thereby, one heat sink is directed to the outside and the other to the inside and thus, there is a temperature difference in winter (room temperature minus outside temperature) and in summer (outside temperature minus room temperature).

A further suggestion for improvement is the development of a charge controller. At the moment, there is an MPPT to which the TECs are connected, and which itself is connected with the accumulator and the load (thermostat). Studies on the system have shown that the MPPT can draw more energy from the TECs when the battery is not parallel to the load. During a heating phase, the battery was disconnected and consequently, the TECs deliver more energy than before. The energy output has almost doubled, but of course an accumulator is necessary for the nights, the weekends and the summer months.

6.2 Green Barbecue

6.2.1 System Analysis

The purpose is to use the heat of a fire to generate electrical energy, e.g. for charging mobile phones or loading accumulators. This could be very interesting for rural areas without electricity. With the energy gained during cooking, it is perhaps possible to replace environmentally unfriendly diesel generators or at least to reduce their usage. A prototype for an electricity-producing biomass cooking stove was presented in [O'++2015] and another thermoelectric stove for off-grid areas in [Fa++2015]. [BioL2016] has brought out a small commercial camping stove using a TEG to load a mobile device.

Here, a typical German barbecue fireplace is modified into a TEG-based EHS. The goal is to convert the thermal energy from a fire during barbecue to electrical energy. Hereby, it should be possible to charge a mobile phone, to supply an amplifier to hear music or to use a 12 V vehicle plug, e.g. to supply a small refrigerator. A further possibility is to store the generated energy in a rechargeable battery and to use it time-delayed. Therefore, a thermoelectric EHS will be attached to a commonly used fireplace for barbecue. The purpose is to use the heat of the fire, which will be lost over the outside wall of the fireplace. The preliminary stages to the current Green Barbecue were presented in [NeFr2015] (first version) and [NeFr2017a] (second version).

For a preliminary investigation, a commercial barbecue fireplace was bought and the temperatures were measured during a fire on the outer wall of the fireplace at different positions, see Figure 6.6.

As a result, it was found that the temperatures on the lower line (see Figure 6.6) are between 300 and 425°C, the temperatures on the middle line between 150 and 250°C with some outliers up to 325°C and the temperature on the upper line between 50 and 150°C. This will play a crucial role in the selection of TEGs in the next subchapter.

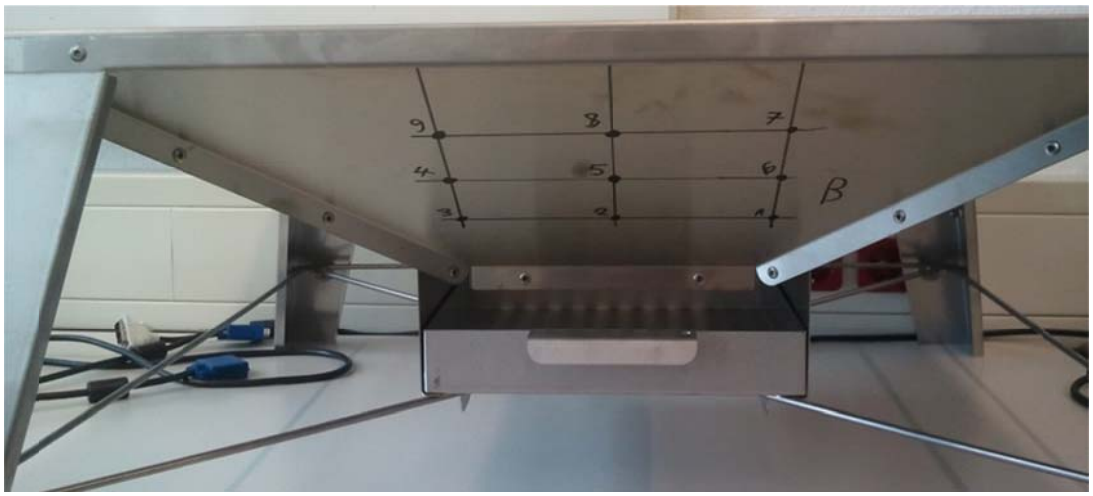

Figure 6.6: Preliminary investigation of a fireplace to find an optimal position for the EHS.

6.2.2 Development of Energy Harvesting System

For the development of the Green Barbecue, the selection of thermoelectric device, the thermal design, the mechanical design and the electrical design are again of great importance as described in Chapter 4. With the given temperature ranges from the previous subchapter, it is clear that TECs are not an option and the maximum temperatures are also too high for standard purchasable Bi_2Te_3-TEGs. This is why special TEGs are used [Hi-Z2016]. They consist of $(Bi,Sb)_2(Te,Se)_3$ and withstand intermittent temperatures up to 350°C. Therefore, they have eliminated all solders in the thermoelectric device by bonded metal conductors.

The most important thing for the mechanical setup is a very good thermal connection to the hot side as well as good heat dissipation on the cold side of the TEGs. Figure 6.7a shows the purchasable fireplace during measurements for finding out the optimal position (as described in Chapter 6.2.1). From the measurements, and with the special TEGs, the optimal place for TEG mounting is on the middle line of the outer wall. However, it was ascertained that the original material of the wall (steel) is unsuitable. The reason for this lies in the thickness of the steel wall. It is so thin that it deforms under thermal stress and thus reduces the thermal connection to the TEGs extremely. Therefore, copper insets are integrated in the four walls and serve as heat sources for the TEGs, see Figure 6.7b. The reasons for the insets are the better thermal conductivity of copper compared to steel and the thickness of the insets which prevents a deformation under thermal stress. The TEGs are directly attached at the copper insets. Also visible in Figure 6.7b is the grid on the bottom of the fire bowl. It serves for air supply to the fire and to catch the ash in the underlying ash drawer. After having the good heat transfer from the fire to the hot TEG side, a cooling method for the cold TEG side is necessary. As a liquid cooling system is excluded due to the complex structure for a portable device like the fireplace, air cooled elements are preferred. In contrast to the electrical thermostat, and to ensure a high temperature difference over the thermoelectric

devices, active cooling elements are used here, meaning that the EHS has to deliver at least the energy consumption of the cooling units to run self-sufficiently. As a cooling element, high-end CPU cooling elements known from computer applications are used [Scyt2015]. They have a heat spreader which has direct contact with the TEG. From the heat spreader there are a total of six heat pipes transferring the heat to a multitude of cooling fins, which are cooled down by a controllable fan. Figure 6.8 shows a close-up picture of a standard TEG and the cooling element in the laboratory and Figure 6.7c shows the mounted cooling elements at the fireplace. TEGs which are located between cooper insets and cooling elements are not visible. There are two TEGs and cooling elements attached at each wall side, and in total there are eight TEGs at the fireplace. Additionally, on each wall side, the hot and cold TEG side temperature is measured with Pt1000 temperature sensors, which are used for controlling purposes. To protect the fans of fat splashes, splashbacks are mounted on each side as shown in Figure 6.7d. All cables (TEG, Pt1000, fans) are collected at one corner and go from there as one wiring loom to the switch box.

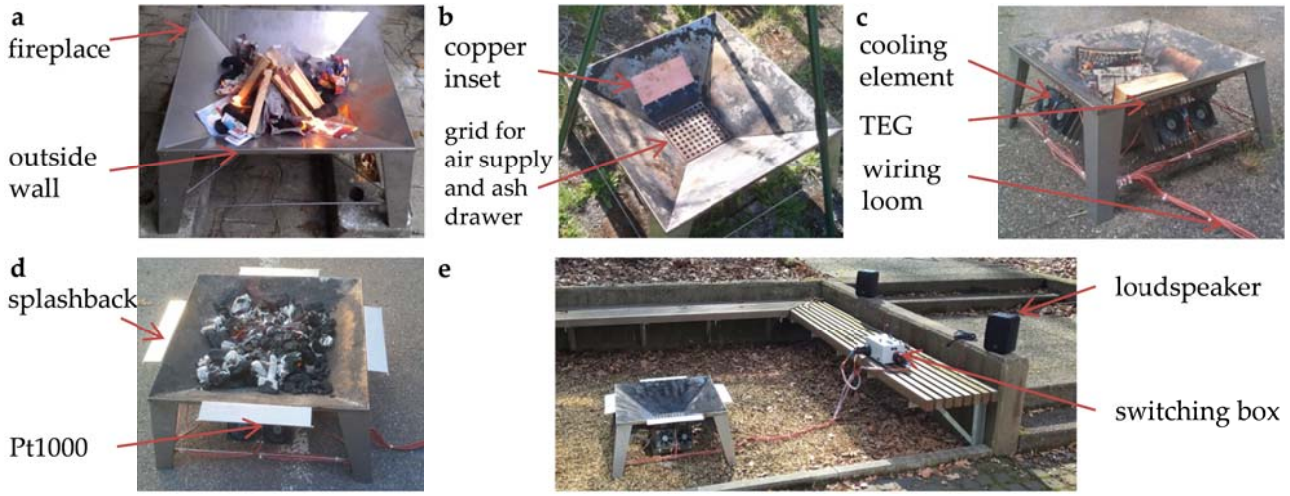

Figure 6.7: Development stages of the Green Barbecue: (a) unmodified and purchasable fireplace, (b) copper insets for a better heat transfer to the TEGs, (c) TEGs and cooling elements are attached at each side wall, (d) temperature sensors and splashbacks are mounted, (e) overall system view including the switch box [NeFr2017a].

Considering the electrical design, both TEGs of one wall side are connected in parallel, respectively, as they work under almost the same temperature conditions, and the four parallel TEG blocks are connected in series to increase the voltage level. The parallelization of two TEGs makes the green barbecue more stable against malfunctioning TEGs. The wiring loom (see Figure 6.7c) goes from the fireplace to the switch box, whereas the current version of it is depicted in Figure 6.9. There, the crucial elements of the electrical setup are marked. In the switch box, the power line of the TEGs is connected to an MPPT, which delivers a constant 12 V power output and loads an accumulator directly supplying the fans of the cooling elements, the 12 V vehicle plug and the amplifier, as well as a DC/DC converter which provides the 5 V level for the USB plug. A

picture of the overall system is shown in Figure 6.7e. Test runs have also shown that the system runs stablye without a battery, meaning the TEGs' output directly supply the electrical components. Nevertheless, the battery is needed to start the system. For temperature dependent controlling purposes a microcontroller is also installed.

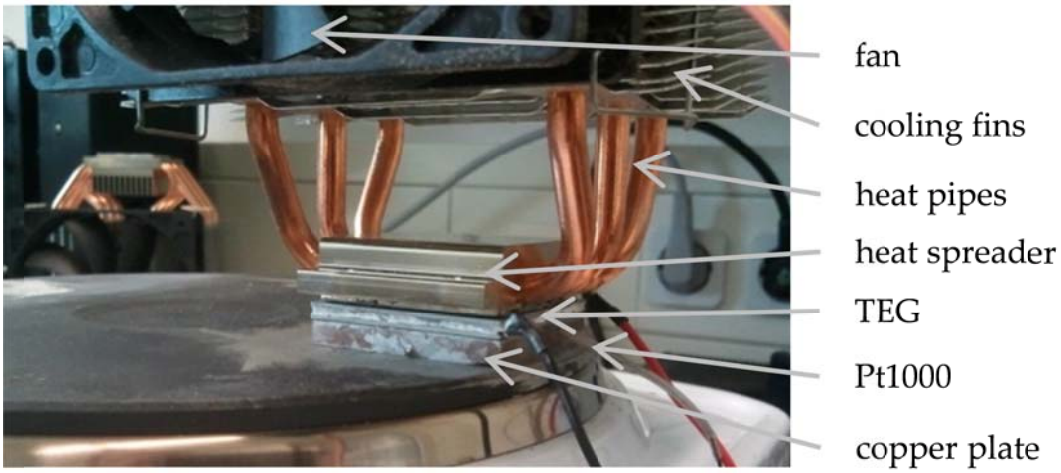

Figure 6.8: Close-up picture of a TEG and the cooling element; also visible is a PT1000 temperature sensor [NeFr2015].

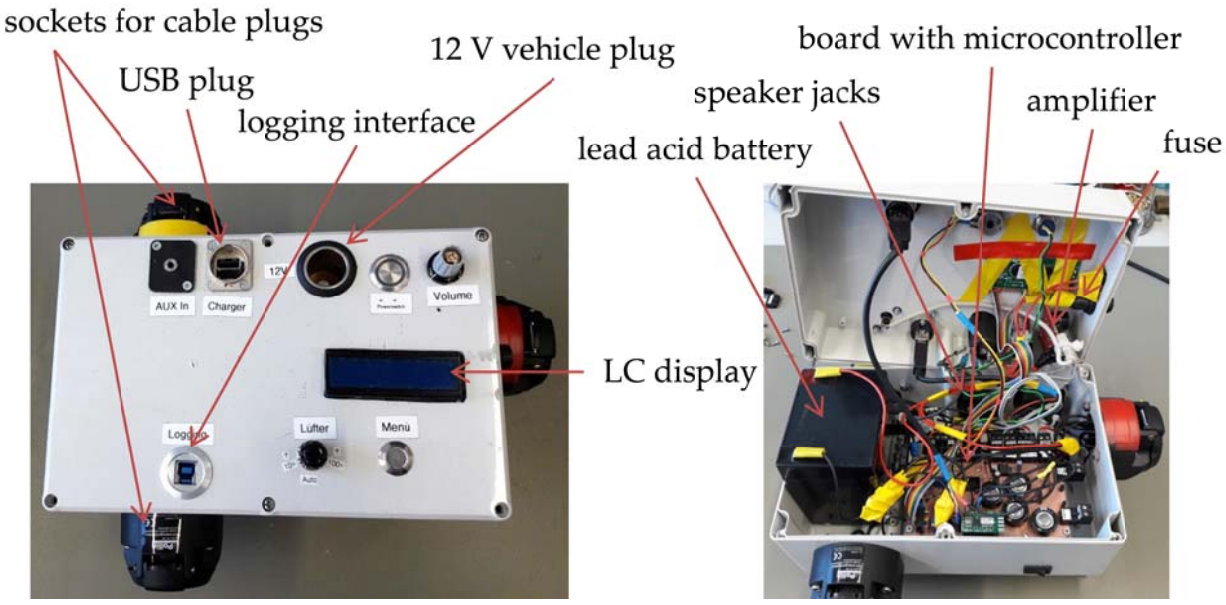

Figure 6.9: View of the switch box and inside it; all important elements are marked.

Measurement data on the Green Barbecue can be directly logged via the logging interface, see Figure 6.9. They contain a time stamp, the four hot and the four cold side temperatures, the voltage of the TEG power line, the current coming from the TEGs into the MPPT as well as the voltage level of the accumulator, the current going from the accumulator to the loads and the duty cycle of the fans, which can be a controlled parameter by the intern microcontroller or a manual set parameter. The schematic layout is shown in Figure 6.10. The measuring points are marked with an S and the temperature measuring points are presented with thermometer symbols.

The corresponding simulation model is shown in Figure 6.11, in which the installed EHS is modeled, but not the firing process itself. Instead, the real measured hot side wall temperatures are given as simulation input values.

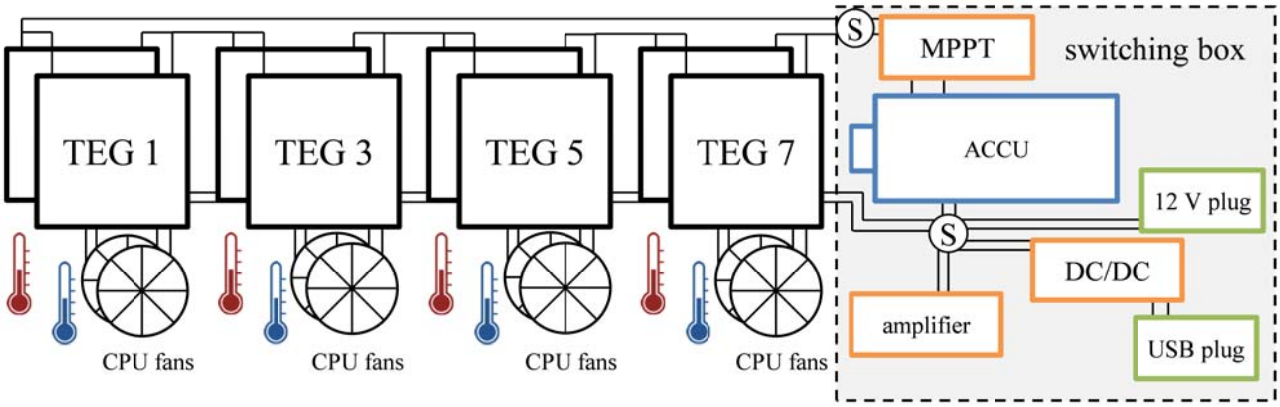

Figure 6.10: Schematic layout of the EHS at the fireplace: The connection of the TEGs is visible, as well as the structure of the switch box and the loads which are supplied.

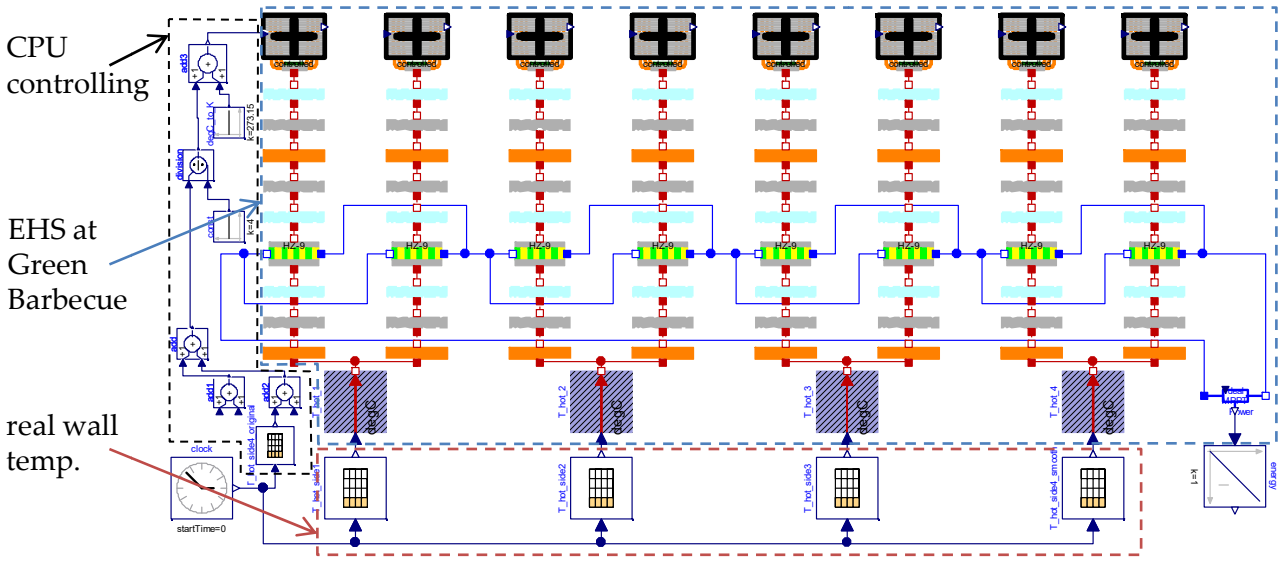

Figure 6.11: Simulation model of the Green Barbecue with the measured hot side wall temperatures as simulation input.

6.2.3 *Results and Evaluation*

Measurement data of the green barbecue were recorded during different barbecues in 2016. Figure 6.12 shows the measurement results for an exemplary barbecue, which took place on March 22nd, 2016. During this experiment, a mobile phone was charged via the USB interface of the switch box and music was played. The upper diagram shows the different temperature curves, where the hot and cold temperatures on each wall side were measured. However, it is notable that one temperature sensor (Cold 2) did not work and that there were temporary signal errors for a second temperature sensor (Hot 4). The maximum temperature reached was about 350°C at the hot wall side 1 and it is clearly visible that the fire is not uniform in the fireplace as there are high

differences between the hot side temperatures. The maximum temperature difference is temporary 200 K on the wall side 1 at 12:50pm. The lower diagram of Figure 6.12 shows the produced and consumed power and energy. In total the produced and consumed energy is nearly equal (about 70 kJ). The high power consumption at the beginning is traced back to the supplying of the fans and the amplifier, which are switched on directly, although there is yet no energy delivered from the TEGs. This energy comes from the integrated accumulator.

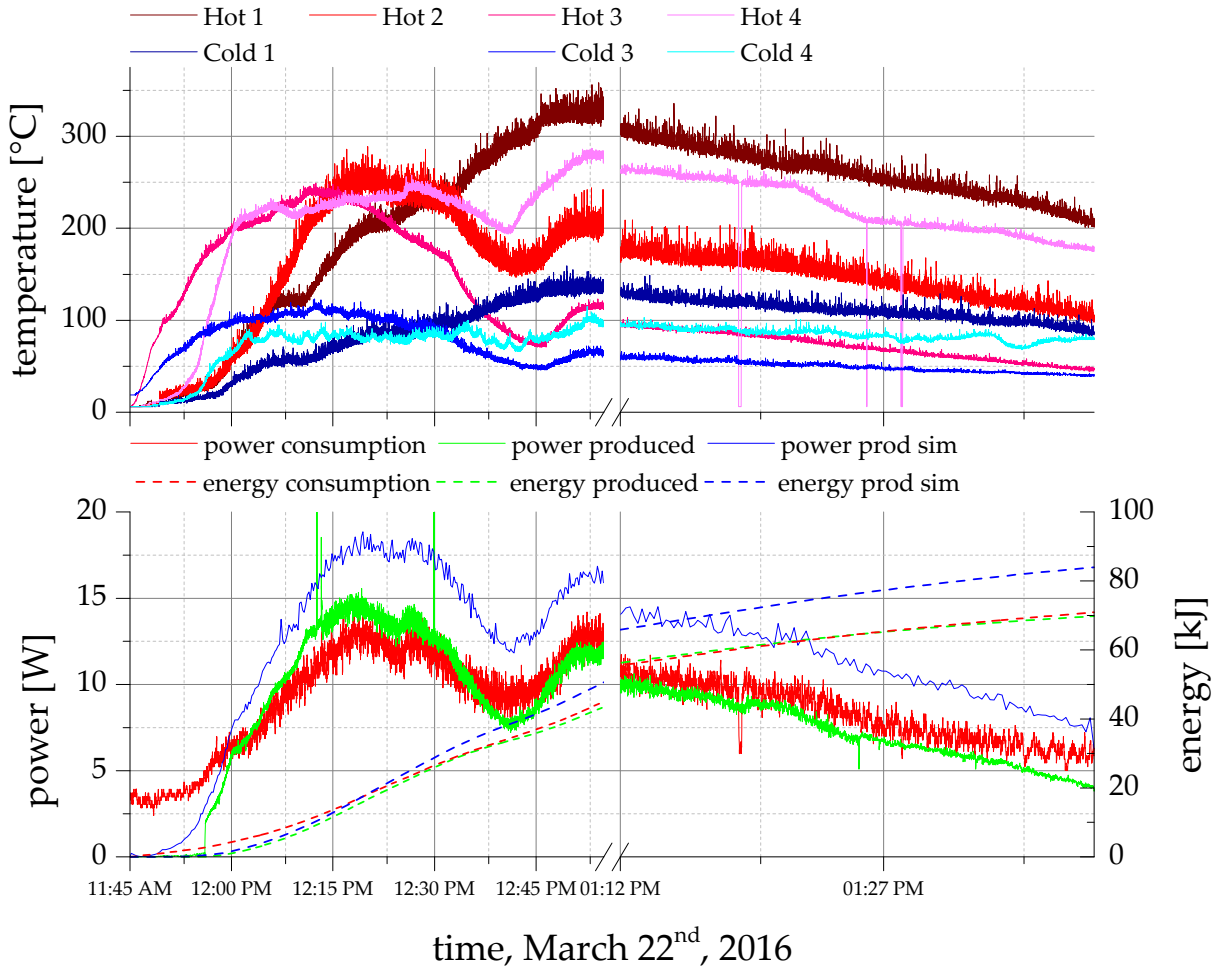

Figure 6.12: Measurement and simulation data for the Green Barbecue at a barbecue on March 21st, 2016 between 11:45am and 1:39pm. Above: temperature curves of each wall side for hot and cold temperature, below: power and energy consumption of the Green Barbecue as well as power and energy production of the EHS and the simulation results for the produced power and energy, modified from [NeFr2017a].

Also shown in Figure 6.12 are the simulation results for the energy and power production of the EHS at the fireplace. The hot side temperatures are given to the simulation model presented in Figure 6.11, where the values for the area of the signal errors of temperature sensor Hot 4 are interpolated. The trend of the simulation results fit quantitatively to the real measured values, but the simulated power is up to 20% higher and the final energy yield (ca. 83.9 kJ) is about 18% higher than for the real system. The reason for this is probably the material data of the TEGs. In the simulation, Bi_2Te_3 was assumed as the thermoelectric material, but the TEGs used in the green

barbecue consist of $(Bi,Sb)_2(Te,Se)_3$ to withstand higher temperatures, as mentioned at the beginning of this subchapter. However, since there was no freely available data of this material, Bi_2Te_3 had to be used for the simulation.

In order to be able to say something about the efficiency of the EHS, the time 12:19pm is considered. Here, the power production is 16 W, which means an average of 2 W per TEG. The temperature difference is on average 150 K over the devices and with the given geometric and the thermal conductivity, see [Hi-Z2016], the heat flow through one device can be calculated to 163.05 W according to Equation (2.7). Thus, the efficiency of one TEG is 1.23% (see Equation (2.24)), whereas the Carnot efficiency is 28.67% for these temperature levels (Equation (2.1)). If the cooling is now also considered, the efficiency of the EHS will be reduced. One cooling unit consumes 1.5 W at this instance of time (average hot side temperature is 223°C and consequently, the adjusted duty cycle is 85%) and thus, the total efficiency of this thermoelectric EHS will be 0.3%. As the sensors are placed in front of the MPPT, there are also additional losses of the used MPPT, which in this case has an electrical efficiency between 90 and 97 %.

Finally it can be said that the EHS at the fireplace runs autarkically and is capable of supplying the extra loads and thus represents a successful thermoelectric EHS. Moreover, the simulation has shown that with the current setup the maximum energy yield is almost reached. To increase beyond the produced power, the construction has to be changed, which means a better connection especially of the cooling element on the cold TEG side, which is now the performance-determining factor. A further possibility to increase the energy yield is a separate control of the fans, as each TEG block has its own temperature levels. Consequently, there is an optimal duty cycle for the fans on each side. The usage of four MPPTs, one per each TEG block, would also slightly increase the power output, but in contrast significantly increase the costs of the system and is therefore not recommended.

6.3 Heating Mockup

6.3.1 System Analysis

A further idea for an EHS is the use of the heat in an exhaust gas pipe—to not disturb the regular heating process—of a gas or oil-fired heating system. A heating system is installed in almost every German household and so there is a big potential for EHS, all the more considering that 86.8% of heating energy used in Germany (2015) comes from fossil sources [BMWi2016], and an estimated 71% of those heating systems (2013) have inadequate efficiencies [BDBo2014]. The gained energy should be used as a primary goal for a variety of DC home applications. Moreover, as a secondary goal, it may supply the heating system; so it will be autarkical and operational during a blackout as well. According to [Quad2016], in Germany in 2015 there was an average power failure per

customer (considering also force majeure) of 15.3 minutes; without force majeure of 11.9 minutes. In general, the main electrical consumers in gas or oil-fired heating systems for space heating and domestic hot water preparation are the blower of the boiler, the electronics and the different pumps. In these systems, there are generally two main pumps. One to supply the heat emission system (in this case radiators), which is now called 'space heating pump', as well as the pump for charging a domestic hot water storage, called 'domestic hot water pump'. Additionally, for comfort reasons and to ensure water hygiene and legionella prophylaxis, in many systems an additional 'hot water circulation pump' is installed, which circulates the heated tapping water in the circulation circuit permanently or with defined control and e.g. night shut-off.

The exhaust pipe of the heating system can of course be representative for other possible exhaust pipes, e.g. in industry or in automobiles. Related test benches on heating systems are already described in [QiHa2009] and [QiHa2011].

As the main objectives are now formulated, data has to be collected from heating systems to calculate first whether or not such an EHS is promising. That is why a measurement system was installed in one building at our university, where an oil-fired heating system is available. In order not to disturb the real heating system, only temperature sensors were attached and the following temperatures were measured: room and ambient temperature, outside pipe temperature at the beginning and in the middle of the exhaust gas pipe as well as inside pipe temperature (equal to medium temperature) at the beginning and in the middle. The data are stored in a database and can be seen via a web interface. A typical curve progression is shown exemplary for the 15th of November, 2016 between 08:42am and 10:22am in Figure 6.13.

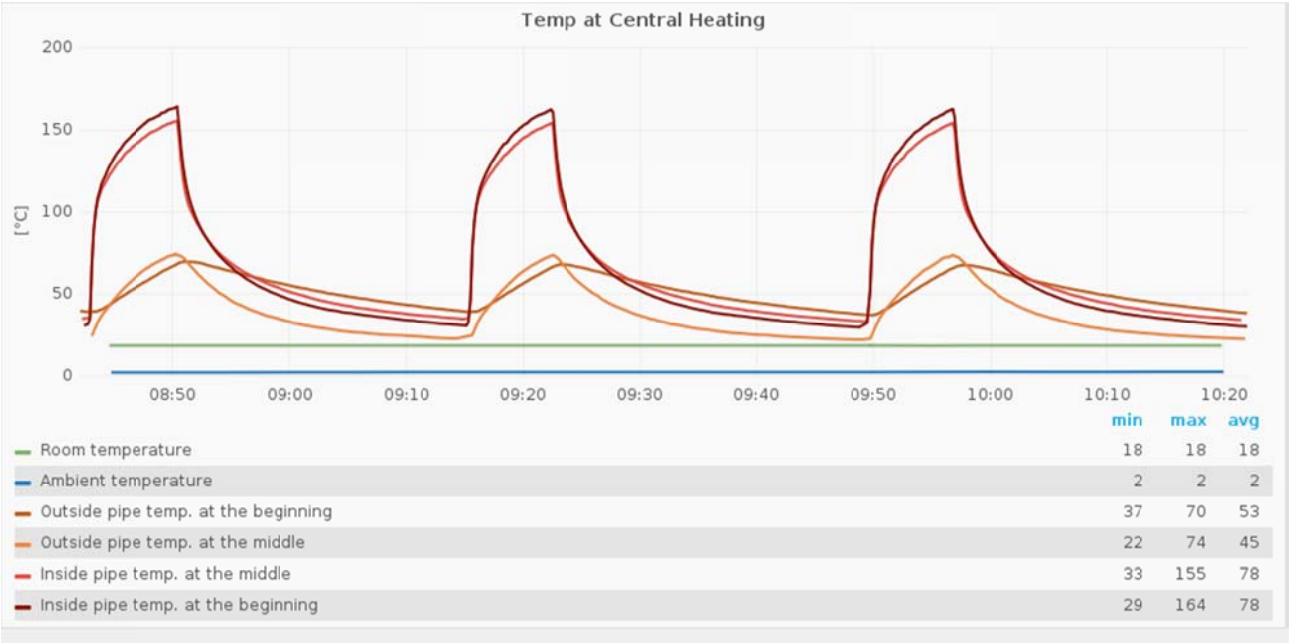

Figure 6.13: Measured temperatures at the oil-fired heater on the campus, illustrated by the web interface.

The aforementioned temperatures are visible and as already described in the control chapter, Chapter 5, the approximately 20/80 heating load. The outside temperatures of the pipe have their maximum at about 74°C, whereas the inside pipe temperatures reach a temperature of 163°C. For the time being, the temperature levels seem to be appropriate to install a TEG-based EHS.

A second measurement system was installed in a private house. This building represents a normal one-family house and besides different temperatures, also the energy consumption of the pumps as well as the temperatures of a tiled stove in the living room are measured. Figure 6.14 shows a typical behavior for the 23rd of January, 2016 between 12:00am and 11:59pm. The measured data are again stored in a database and can be seen via the web interface.

Figure 6.14: Measured temperatures at a heater and a tiled stove in a private house as well as power consumption of the pumps in the heating, illustrated by the web interface.

In the upper diagram of Figure 6.14, the temperatures are depicted and in the lower diagram the power consumptions. The central gas-fired condensing boiler recovers the latent heat of vaporization, which is reflected in the low maximum exhaust gas temperatures of about 75°C. Therefore, a TEG-based EHS is not suitable for new condensing boilers as the exhaust temperatures there are too low. Nevertheless, the on/off behavior of the boiler is also recognizable for this heating system. The power consumption of the pumps are on average 45 W for the domestic hot water pump (runs only a few times a day), 6 W for the space heating pump (runs all day) and 2 W for the hot water circulation pump (runs almost continuously between 5:30am and 11:30pm). The consumption of the other components (like blower and the heating electronics) is about 23 W, which results from the overall consumption minus the pump consumptions. In addition to that, the gas consumption of the heater is also measured (diagram is not shown in Figure 6.14) and during the on phase of the boiler, there is an average gas consumption of about 30 kW (the gas volume consumed is measured and then multiplied by the calorific value for natural gas, $10\,\frac{\mathrm{kWh}}{\mathrm{m}^3}$). An investigation based on the German BImSchV regulation has yielded an efficiency of 93.4%, after which 6.6% of the energy used is lost as waste heat. If the measured gas consumption is taken as the basis, the exhaust gas has a residual energy of 1.98 kW.

A first simulation model for preliminary investigations of a TEG-based EHS at a oil-fired heating was published in [NeFr2014].

6.3.2 Development of Energy Harvesting System

Regarding the development process, the selection of the heat source and the settings of the objectives are already done in the previous chapter. As the first simulation model shows good results with an ideal heat transfer from the outside wall and appears not to disturb the real heating process, an EHS was attached around the pipe with a liquid cooled system as shown in Figure 5.1. Specially manufactured aluminum half-shells were attached to the pipe to finally ensure a smooth surface for attaching the TEGs. Unfortunately, the results were unsatisfactory, as not enough heat could be extracted from the system. To collect more heat for the TEG-based EHS, the heat in the exhaust pipe (heat of the medium) must be tapped. This step is of course an intervention in the real process and that is why a heating mockup was planned and finally build-up in our laboratory. A preliminary investigation was made in the Bachelor's thesis of M. Bernat [Bern2016]. Consequently, all following results are valid for a hot flowing medium in a pipe, but cannot be transferred directly to a real system, e.g. a real heater, before doing more studies on the influence for the real process.

As a heat source for the heating mockup, an industrial hot air blower is used, at which the temperature and the velocity of the air can be controlled. Real heating data are measured for two different heaters, as mentioned in the previous subchapter, and are stored in a database. With a

self-written LabVIEW program, it is now possible to control the heating mockup. For the heat source, there are two main options: to control the airflow (temperature and velocity) manually or automatically. The automatic mode is again divided into three options: to control the heating mockup according to the live data of the oil-fired heating on campus, to give a special time range for the stored data in the database which will then be reproduced by the heating mockup, or to give a txt-file as a temperature profile.

Concerning the thermal design, a segment cooling aggregate [Fisc2015], which is originally designed to cool down a flowing medium, is installed in the exhaust gas pipe. It is built from cooling elements which penetrate into the medium, collect the heat and transport it to the outer side of the pipe, see Figure 4.11b. There, the TEGs and the corresponding cooling units can be easily attached. First, measurements with a real heating behavior and without TEGs and cooling units are shown in Figure 6.15. The temperatures for each section of the segment cooling aggregate—in total there are four sections—are measured, cf. Figure 6.16c. It is therefore apparent that TEGs should be used for the first two sections and TECs can be used for the third and fourth sections, cf. Chapter 4.4. In total, there are always four thermoelectric devices for one section, which are consequently under the same temperature conditions.

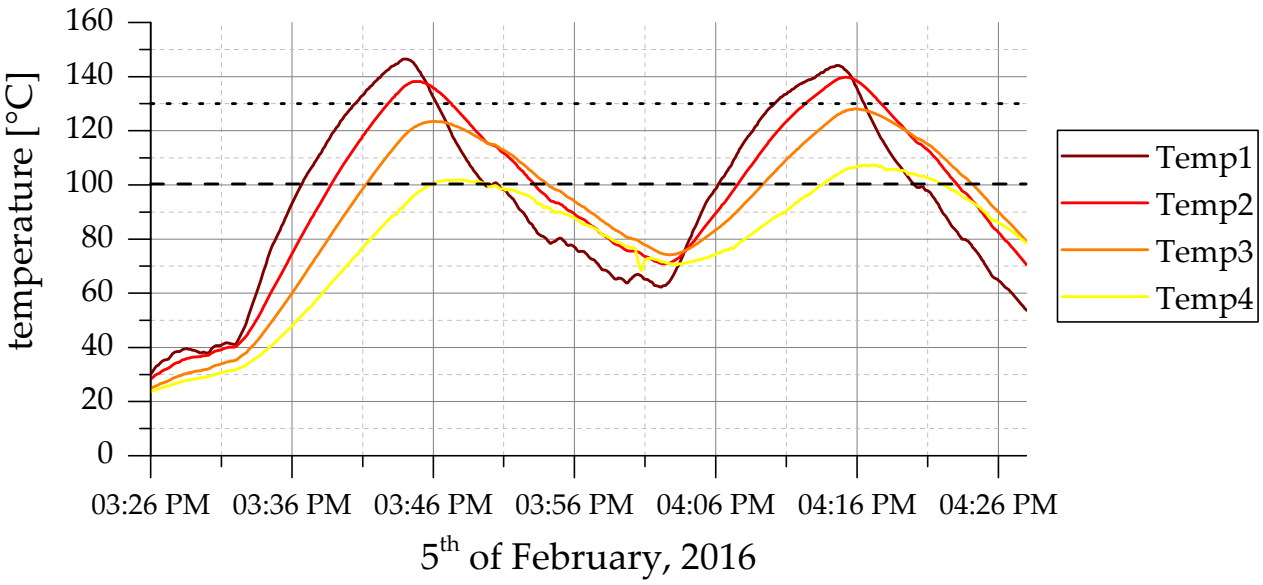

Figure 6.15: Temperature measurement of each section of the segment cooling aggregate for a 20/80 heating load.

As described in Chapter 5.5, for a real heater with an on/off scenario of 20/80, liquid cooling elements are not suggested, but controlled air forced cooling elements should be used. Due to the lack of space, special small CPU cooling elements are attached and the fans of the cooling elements are only mounted at the outside on the first and the fourth sections. The fans on the first section blow air through the heat sinks and the fans on the last section pull the air from the heat sinks. So,

there is airflow from the first section to the fourth. The mechanical setup of the heating mockup is shown in Figure 6.16. There, the four sections are visible as well as the temperature sensors for these sections, the inside pipe temperature sensor at the beginning, the cooling elements and the fans for sections 1 and 4. The blue arrow in Figure 6.16b shows the air flow direction through the cooling elements.

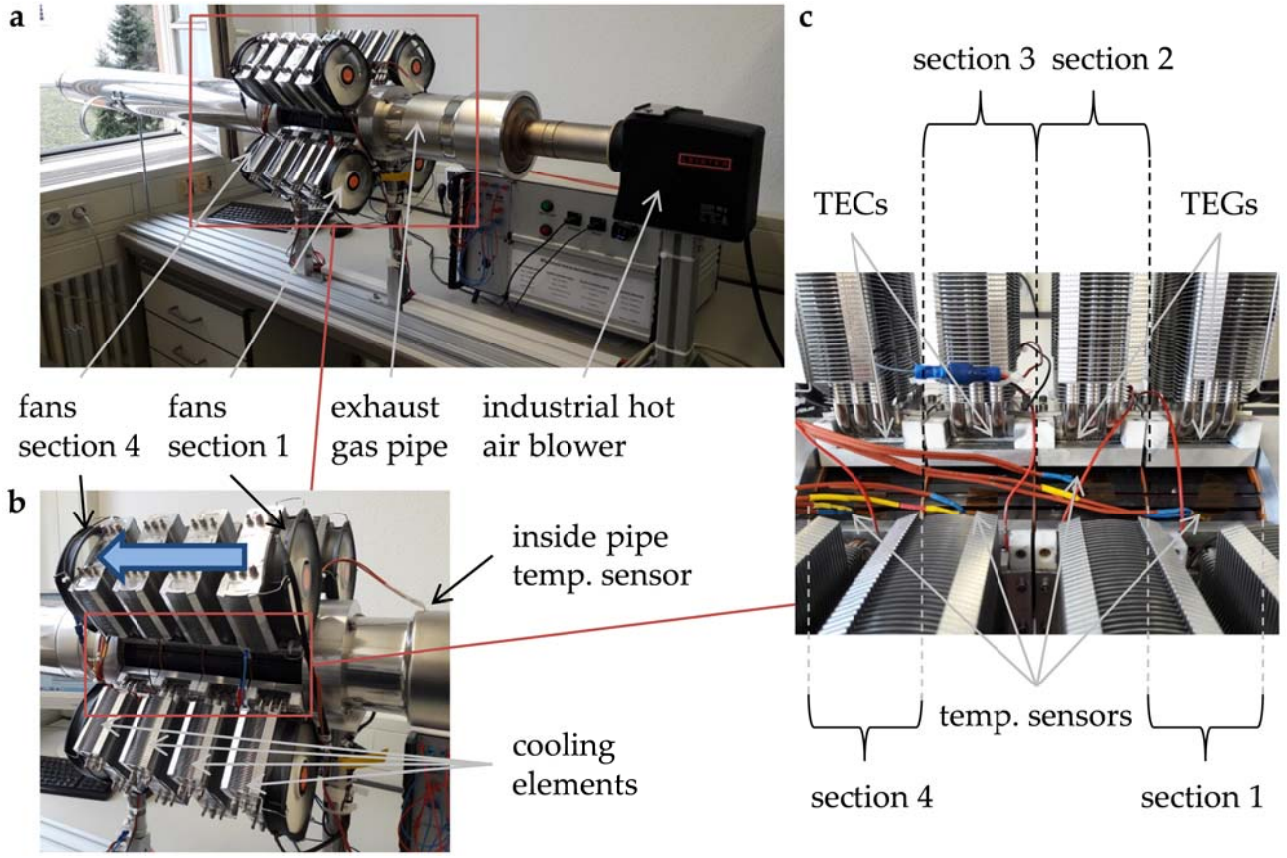

Figure 6.16: Heating Mockup with attached thermoelectric EHS; a) shows the complete setup, b) shows an enlargement of a partial excerpt of a, c) shows an enlargement of a partial excerpt of b.

Regarding the last point of the development process, the electrical design, the prospective was to be very flexible. That is why a switch cabinet with a front panel was built up, see Figure 6.17a. As the thermoelectric devices of one section have the same temperature differences, they are connected in parallel. The individual blocks can then be individually interconnected, see front panel in Figure 6.17b. There are different connection possibilities, e.g. TEG/TEC blocks in series or in parallel or a mixture of both, connecting them to one or two MPPTs, connecting some TEG/TEC blocks with the fans or supplying the fans over a 12 V power supply, see Appendix **A.4**. Beneath the front panel, the switch cabinet also includes an industrial PC to control the hardware setup via the LabVIEW program, an accumulator, the two MPPTs, the 12 V power supply, some relays (for system reconfiguration during operation mode; condition: all TEG/TEC blocks in series and between the relays), a vehicle plug to connect different loads as well as different measurement

devices. All the measurement data are also written in the database and can be illustrated by the previously mentioned web interface.

The following measurements are carried out:

- Temperatures: at first/second/third/fourth section, inside pipe beginning, inside pipe end
- Voltages: Input MPPT1/MPPT2, Output MPPTs (equal to accumulator voltage), hot air blower
- Current: Input MPPT1/MPPT2, Output MPPTs, hot air blower

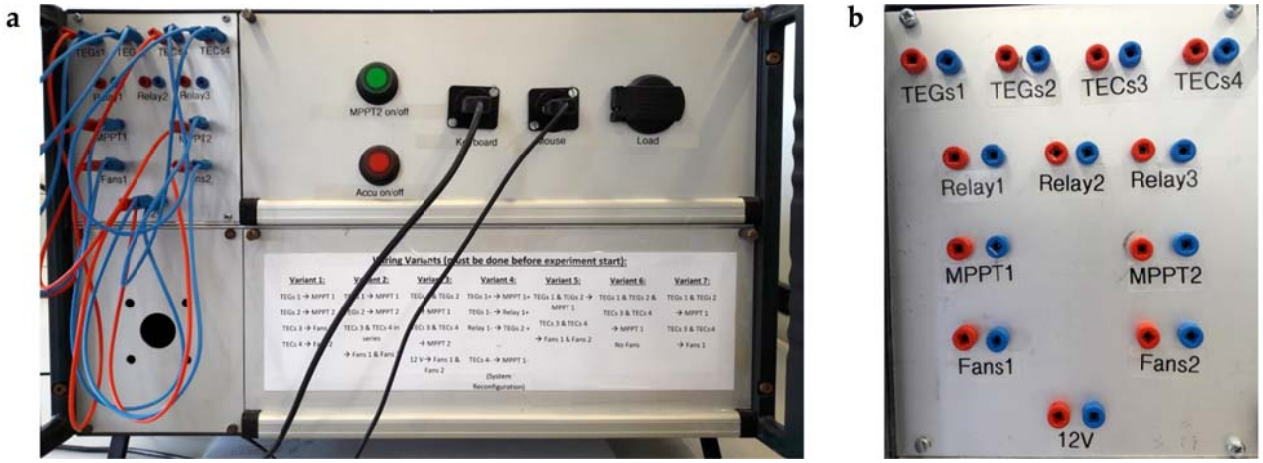

Figure 6.17: Switch cabinet of the Heating Mockup; a: complete switch cabinet; b: Enlargement of the front panel to realize different wiring structures

The corresponding simulation model is shown in Figure 6.18. There, the measured hot medium temperatures of the real heater, which are stored in the database, act as simulation input.

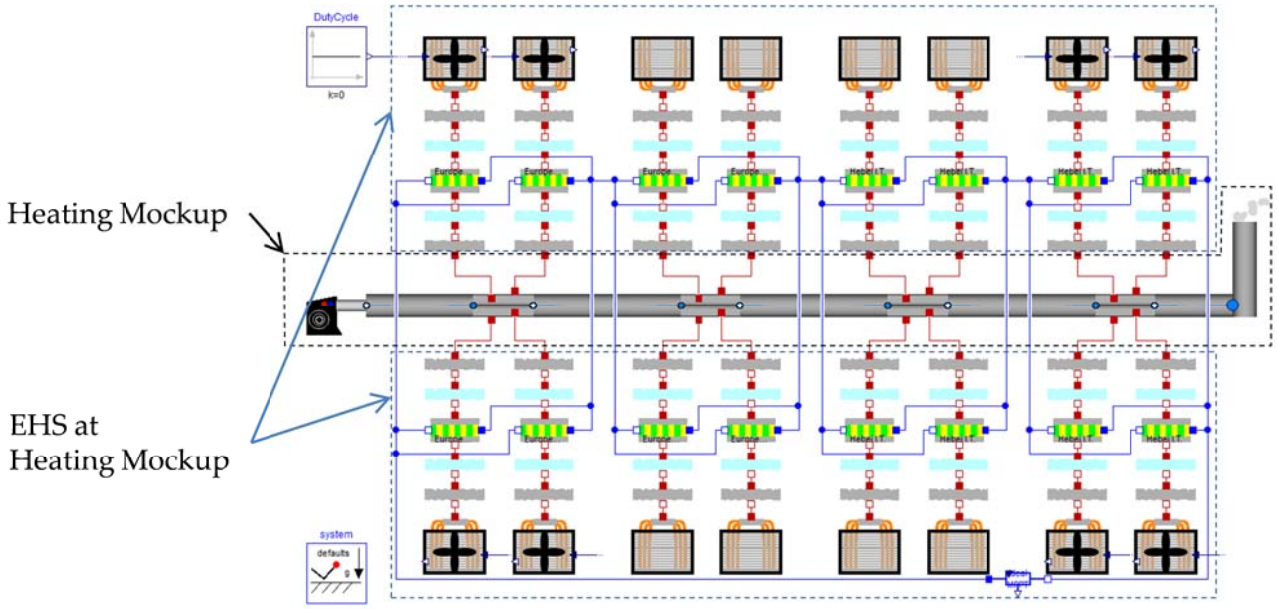

Figure 6.18: Simulation model of the thermoelectric EHS at the Heating Mockup

6.3.3 *Results and Evaluation*

To test the prospective EHS for a real heating scenario, the real heating data for the oil-fired heating on campus on November 15th, 2016 between 8:42am and 10:22am are given to the Heating Mockup, cf. Figure 6.13. Thereby, the following was selected as the connection variant because it gives the best result: TEG blocks 1 and 2 are connected in series and then to MPPT1, whereas TEC blocks 3 and 4 are also connected in series and supply the fans of section 1. Thus, in this scenario, a fan control over the duty cycle is not necessary, as the fan velocity will be self-controlled by the energy supported from TEC blocks 3 and 4. Consequently, the power delivered from TEG blocks 1 and 2 can be completely considered as gained power of the system. The measurements as well as the simulation results are shown in Figure 6.19, where the upper diagram shows the measured temperatures as well as the set temperature inside the pipe and the lower diagram the measured gained power and energy as well as the simulated ones. As there are no additional consumers connected and the fans are directly supplied by TEC blocks 3 and 4, there is no direct power consumption (contrary to the Thermostat and the Green Barbecue).

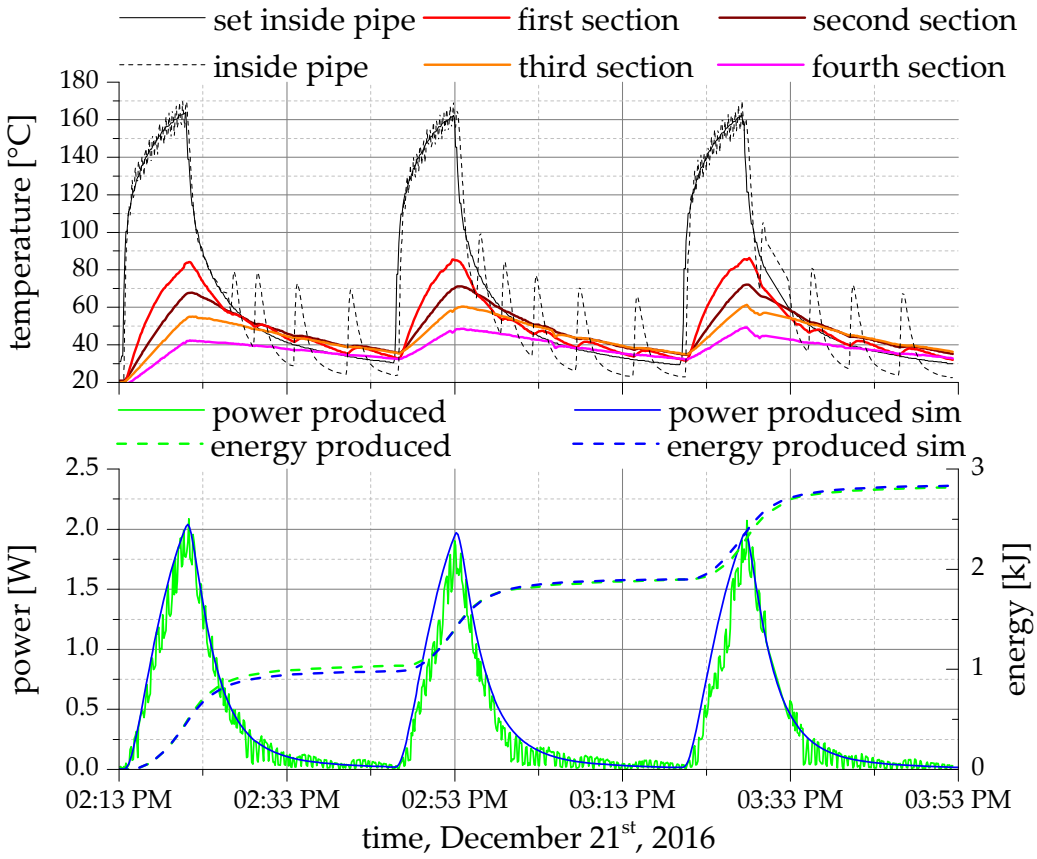

Figure 6.19: Measurement and simulation data for the Heating Mockup: heating scenario of the oil-fired heating on campus on November 15th, 2016 between 8:42am and 10:22am, executed on December 21st, 2016 at the Heating Mockup. Above: temperature curves of each section as well as the set and real inside pipe temperature at the beginning; below: produced power and energy of the EHS and the corresponding simulation results

In the upper diagram of Figure 6.19, one can see that the reproduced inside pipe temperature of the medium fits very well with the set temperature of the medium (which is also the real measured temperature) for temperatures over 80°C. However, for lower temperatures there are some overshoots which are related to the setting options of the hot air blower—it can only be adjusted for temperatures over 80°C and due to that fact, it turns on briefly and then off again to control lower temperatures. Moreover, it is obvious that the temperatures of the single sections (now, with the attached EHS) are all under 90°C, for the last section even only around 50°C. Consequently, the produced power is very low, which is visible in the lower diagram of Figure 6.19. The maximum gained power is around 2 W, which also matches the simulation result. Since the oil-fired heating starts about 39 times a day, the daily energy output is approx. 36.4 kJ, which is about 10 Wh a day. Concerning the 263 heating days per year, this will be 2.63 kWh per year.

To calculate the efficiency of the EHS, Figure 6.20 represents the system consideration relating to the heat flow rates. The energy balance is given by

$$0 = \dot{Q}_1 - \dot{Q}_2 - \dot{Q}_{\text{use}} - \dot{Q}_{\text{lost}} \,, \tag{6.1}$$

where $\dot{Q}_1$ is the inflow heat rate, $\dot{Q}_2$ the outflow heat rate, $\dot{Q}_{\text{use}}$ the useful heat rate and $\dot{Q}_{\text{lost}}$ the lost heat rate. With the assumption of no heat losses, the useful heat rate can be calculated by

$$\dot{Q}_{use} = \dot{Q}_1 - \dot{Q}_2 = \dot{m} \cdot c_p \cdot (T_1 - T_2) \,. \tag{6.2}$$

The temperatures T_1 and T_2 as well as the mass flow rate $\dot{m}$ are measured or calculated values, whereas the specific heat capacity c_p of the medium can be taken from the simulation. Thus, the useful heat rate here is approx. 560 W at the peaks, cf. Figure 6.19. The produced power is 2 W and so the efficiency is about 0.36%, according to Equation (2.24).

Figure 6.20: Schematic system consideration of the heat flow rates for the EHS at the Heating Mockup

To conclude, it can be said that the presented EHS can harvest electrical energy from the exhaust gas of a heater. The first objective of supplying small DC applications is possible and also the second objective of supplying the heating and their components during a short blackout can be done. However, for this purpose, it is necessary to use an accumulator to save the electrical energy over the year—which could also be loaded by the electrical grid.

To improve the EHS and to increase the efficiency of the heater, the water to be heated could be used as cooling medium and thus, the water will be preheated (less energy input of the heating is necessary) and the thermoelectric devices will produce more electrical power.

The high power outputs as presented in the simulation in Chapter 5.5 are not possible with these exhaust gas temperatures, but the system can also be integrated in industry pipes with higher temperatures and thus comes closer to the aforementioned example.

7 Conclusions and Outlook

The two main goals of this work, which are essential for a model-based development of thermoelectric energy harvesting systems (EHS), were successfully achieved. This includes on the one hand the developing of different Modelica Libraries, namely the `ThermoelectricGenerator`, the `HeatPipe` and the `EHSTEG` library, and on the other hand the elaboration and presentation of a development process for thermoelectric EHSs. Concerning the libraries and according to the V-model approach, the designs of the main important components were explained and afterwards validated. Lastly, the application of the libraries for complete EHSs was shown for the three examples: Thermostat, Green Barbecue and Heating Mockup. In addition to that, the elaborated development process, which will be supported by multi-physics simulation based on the previously developed libraries, was described in detail. The process itself can be subdivided into five categories: the thermal design, the selection of thermoelectric device, the mechanical design, the electrical design and the control concepts. The single categories were specified in this work, specifically the control concepts having been a major focus. In total there are two control possibilities, namely the control of the cooling elements as well as the control of the system due to system reconfiguration. Regarding cooling control, air cooling elements can be controlled over an optimized setting of the fans duty cycle, depending on the hot side temperatures of the thermoelectric generators (TEG), and the liquid cooling elements must be switched on and off smartly. Concerning the system reconfiguration, there is the possibility of reconfiguration for single TEGs, pairs of TEGs or even an array of TEGs, mainly depending on their inner resistance/power production and the power consumption of the corresponding cooling elements.

The three presented application examples have shown that even today, with currently purchasable components, thermoelectric EHSs can be built and can produce a positive amount of electrical energy. The efficiency of the entire system is currently not very high—the efficiency in the case of the thermostat is 0.24%, in the case of the Green Barbecue 0.3% and in the case of the heating mockup 0.36%—, however, since the waste heat is normally unused, such systems can be worthwhile. Especially if there is a need for a robust, maintenance free and reliable power supply and the investment costs do not matter, thermoelectric EHS are highly recommended; compare the usage in space applications. To increase the energy yield, the number of TEGs or the temperature difference applied over the thermoelectric devices has to be enhanced. Furthermore, an adapted control strategy is very important, so as not to further reduce the efficiency unnecessarily.

In summary, this work has provided a broad insight into the optimized design and set-up of thermoelectric EHSs. It was shown that the usage of a thermoelectric EHS is a very promising approach and can already be installed successfully today, but unfortunately with hardly any real

applications at the moment. The systems are working fine, but the low efficiency and the high investment costs—which did not matter in this work, since it was about the principle of functioning—currently dominate the advantages. Above all, there are very good alternatives to use the waste heat. Either one uses the waste heat directly for heat supply or converting it into electrical energy. For example, this is possible with Stirling engines or ORC processes, which have a higher efficiency than TEG-based systems and are more mature. Therefore, there is really a great need for new thermoelectric materials, which on the one hand are significantly more efficient and on the other hand can be produced more cost-effectively. So, here is still a lot of potential for scientific research.

As a future prospect, it can be said that some further studies for the systems could be carried out. First of all, it would be interesting to know how stable the cycle strength of the TEGs is, especially for the Green Barbecue and the Heating Mockup. Moreover, as with the real heating behavior in the Heating Mockup, there are only temperatures about 80°C at the hot sides of the TEGs, and the Heating Mockup could be run with higher temperatures like those found in automotive exhaust pipes or industrial applications, to investigate further control strategies.

Appendix

A.1: Adjusted parameters for the steady-state and dynamic validation of the three heat pipe model approaches.

Model Approach	Adjusted Parameters	Description
single resistance approach	$R_{th} = 0.1 \frac{\mathrm{K}}{\mathrm{W}}$	thermal resistance given by datasheet
thermal equivalent network	Medium_SaturationLine = WaterIF97_R4ph	working fluid at saturation line
	Medium = Water: IdealSteam	working fluid as vapor
	$l = 0.4$ m	total length of pipe
	$l_e = 0.04$ m	length of evaporator zone
	$l_c = 0.04$ m	length of condenser zone
	$r_{p_{out}} = 0.004$ m	outer radius of heat pipe wall
	$r_{w_{out}} = 0.0036$ m	outer radius of wick; equal to inner radius of heat pipe wall
	$r_v = 0.00335$ m	radius of vapor space; equal to inner radius of wick
	$\lambda_p = k_p = 400 \frac{\mathrm{W}}{\mathrm{m\,K}}$	thermal conductivity of heat pipe material
	$\lambda_w = k_w = 400 \frac{\mathrm{W}}{\mathrm{m\,K}}$	thermal conductivity of wick material
Physical approach	Medium = WaterIF97_pT	Working fluid
	$l = 0.4$ m	total length of pipe
	$l_e = 0.04$ m	length of evaporator zone
	$l_c = 0.04$ m	length of condenser zone
	$r_{out} = 0.004$ m	outer radius of pipe shell
	$r_{in} = 0.0036$ m	inner radius of pipe shell; equal to outer radius of wick
	$r_v = 0.00335$ m	radius of vapor space; equal to inner radius of wick
	$\varphi = 0$	angle between heat pipe and horizontal
	Inclination = false	true if evaporator part higher than condenser part, otherwise false
	$\lambda_p = k_p = 400 \frac{\mathrm{W}}{\mathrm{m\,K}}$	thermal conductivity of heat pipe material
	$\vartheta = 0.74$ rad	wetting angle (estimated)
	$w = 0.0005$ m	groove width (estimated)
	$d = 0.0003$ m	diameter of wire (estimated)
	$\epsilon = 0.739$	porosity of wick structure (estimated)
	$x = 1$	vapor quality

A.2: Structure of the `HeatPipe` library

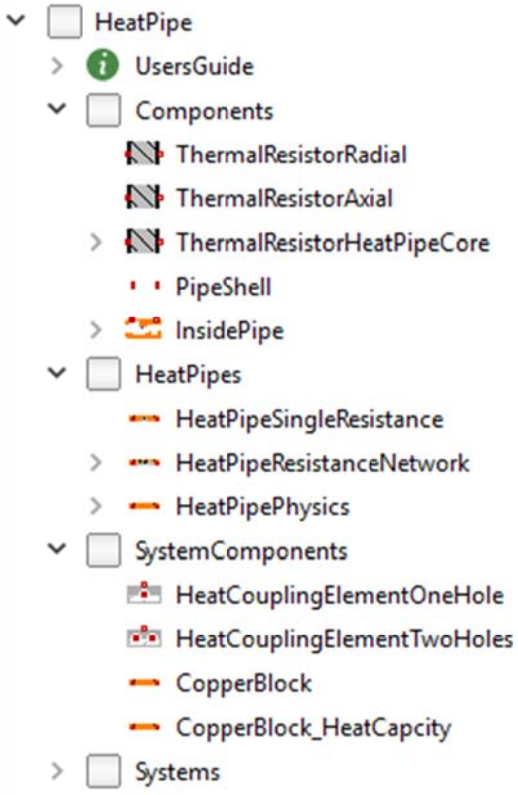

A.3: Preliminary calculations for the EHS at the radiator (thermostat)

Consumption of the Thermostat:

- Adaption mode: about 90 mW
- Stand-by mode: approx. 0.4 mW
- Switching operation mode: max. 70 mW

In this test case:

- Heating per day: 10 h
- Heating days per year: on average about 263
- Valve driving time per day (assumption): 240 s

Calculations for energy consumption:

- Energy consumption of µ-Controller per year:

$$E_{\mu} = 0.4\ \text{mW} \cdot 365\ \frac{\text{d}}{\text{y}} \cdot 24\ \frac{\text{h}}{\text{d}} \cdot 60\ \frac{\text{min}}{\text{h}} \cdot 60\ \frac{\text{s}}{\text{min}} = 12\,614.4\ \frac{\text{J}}{\text{y}}$$

- Energy consumption of valve driving per year:

$$E_{\text{vd}} = 263\ \frac{\text{d}}{\text{y}} \cdot 240\ \frac{\text{s}}{\text{d}} \cdot 70\ \text{mW} = 4\,418.4\ \frac{\text{J}}{\text{y}}$$

- **Total energy consumption per year:**

$$\boldsymbol{E_{\text{tc}} = 12\,614.4\ \frac{\text{J}}{\text{y}} + 4\,418.4\ \frac{\text{J}}{\text{y}} = 17\,032.8\ \frac{\text{J}}{\text{y}}}$$

Estimated conditions for TEG:

- Estimated hot side temperature: 45°C
- Estimated temperature difference: 3 K
- Generated electrical power according to `calculation sheet` of Thermalforce: 8 mW

Calculations for energy production:

- Energy production per day:

$$E_{\text{TEG,d}} = 10\ \frac{\text{h}}{\text{d}} \cdot 60\ \frac{\text{min}}{\text{h}} \cdot 60\ \frac{\text{s}}{\text{min}} \cdot 8\ \text{mW} = 288\ \frac{\text{J}}{\text{d}}$$

- **Energy production per year:**

$$\boldsymbol{E_{\text{TEG,y}} = 263\ \frac{\text{d}}{\text{y}} \cdot 288\ \frac{\text{J}}{\text{d}} = 75\,744\ \frac{\text{J}}{\text{y}}}$$

A.4: Tested wiring variants for the Heating Mockup

Variant 1:

- TEGs 1 → MPPT 1
- TEGs 2 → MPPT 2
- TECs 3 → Fans 1
- TECs 4 → Fans 2

Variant 2:

- TEGs 1 → MPPT 1
- TEGs 2 → MPPT 2
- TECs 3 & TECs 4 in series → Fans 1 & Fans 2

Variant 3:

- TEGs 1 & TEGs 2 in series → MPPT 1
- TECs 3 & TECs 4 in series → MPPT 2
- 12 V power supply → Fans 1 & Fans 2

Variant 4 (system reconfiguration):

- TEGs 1+ → MPPT 1+
- TEGs 1- → Relay 1+
- Relay 1- → TEGs 2+
- …
- TECs 4- → MPPT 1-

Variant 5:

- TEGs 1 & TEGs 2 in series → MPPT 1
- TECs 3 & TECs 4 in series → Fans 1 & Fans 2

Variant 6:

- TEGs 1 & TEGs 2 & TECs 3 & TECs 4 in series → MPPT 1
- No Fans

Variant 7:

- TEGs 1 & TEGs 2 in series → MPPT 1
- TECs 3 & TECs 4 in series → Fans 1

List of Figures

List of Tables

List of Abbreviations

Bi_2Te_3	Bismuth Telluride
BINE	Bürger-Information Neue Energietechniken (German)
CHP	Combined Heat and Power
CTEL	Connected Thermoelectric Legs
DC	Direct Current
DLR	German Aerospace Center
DTG	German Thermoelectric Society
ECT	European Conference on Thermoelectrics
EHS	Energy Harvesting System
EHSTEG	Energy Harvesting Systems based on Thermoelectric Generators (Modelica Library)
EMF	Electromotive Force
ETS	European Thermoelectric Society
GUI	Graphical User Interface
HiL	Hardware-in-the-Loop
ICT	International Conference on Thermoelectrics
IoT	Internet of Things
ITS	International Thermoelectric Society
MiL	Model-in-the-Loop
MMRTG	Multi-Mission Radioisotope Thermoelectric Generator
MPPT	Maximum Power Point Tracker
NAPE	National Action Plan on Energy Efficiency
ORC	Organic Rankine Cycle
PbTe	Lead Telluride
PhD	Doctor of Philosophy
pTEG	Pairs of TEGs

PVC	Polyvinyl Chloride
PWM	Pulse Width Modulation
RFID	Radio-frequency Identification
RTG	Radioisotope Thermoelectric Generator
StAP	Static Averaged-properties Model
TEC	Thermoelectric Cooler (Peltier Element)
TEG	Thermoelectric Generator
TEL	Thermoelectric Leg
TrDP	Transient Distributed-properties Model
$TrDP_{\alpha Int}$	Transient Distributed-properties α-Integrals Model

List of Symbols

Latin letters

A	(Cross-sectional) Area	m^2
$A_{\mathrm{v,\,a}}$	Vapor cross-sectional area	m^2
c	Specific heat capacity	$\frac{\mathrm{J}}{\mathrm{kg\,K}}$
c_p	Specific heat capacity at constant pressure	$\frac{\mathrm{J}}{\mathrm{kg\,K}}$
d	Length, distance	m
d	Diameter	m
d_v	Hydraulic diameter	m
$\boldsymbol{E}$	Electric field strength vector	$\frac{\mathrm{V}}{\mathrm{m}}$
$\boldsymbol{E}_{\mathrm{EMF}}$	Electric field strength vector of electromotive force	$\frac{\mathrm{V}}{\mathrm{m}}$
g	Gravity constant	$\frac{\mathrm{m}^3}{\mathrm{kg\,s}^2}$
h	Height	m
Δh_v	Latent heat of vaporization	$\frac{\mathrm{kJ}}{\mathrm{mol}}$
I	Electrical current	A
I_l	Load current	A
I_s	Short-circuit current	A
$\boldsymbol{J}$	Current density vector	$\frac{\mathrm{A}}{\mathrm{m}^2}$
K	Permeability of wick structure	m^2
l	Length	m
L	Length	m
L_{eff}	Effective length	m
$\dot{m}$	Mass flow rate	$\frac{\mathrm{kg}}{\mathrm{s}}$
N	Scaling factor	-
Δp_{c}	Capillary pressure difference	Pa

Δp_l	Liquid pressure difference	Pa
$\Delta p_\mathrm{l,\,h}$	Hydrostatic pressure difference	Pa
$\Delta p_\mathrm{l,\,s}$	Flow pressure loss	Pa
Δp_v	Vapor pressure difference	Pa
P_el	Actual gained electrical power	W
$P_\mathrm{el,\,max}$	Maximum electrical power	W
P_J	Resistive power loss	W
$\dot{q}$	Heat flux density	$\frac{\mathrm{W}}{\mathrm{m}^2}$
$\dot{\boldsymbol{q}}$	Heat flux density vector	$\frac{\mathrm{W}}{\mathrm{m}^2}$
$\dot{Q}$	Rate of heat flow	W
$\dot{Q}_\mathrm{C,h/c}$	Rate of heat flow by conduction (hot or cold side)	W
$\dot{Q}_J$	Rate of heat flow by resistive power losses	W
$\dot{Q}_\mathrm{lost}$	Lost rate of heat flow	W
$\dot{Q}_\mathrm{P,h/c}$	Rate of heat flow by Peltier heat (hot or cold side)	W
$\dot{Q}_T$	Rate of heat flow by Thomson effect	W
$\dot{Q}_\mathrm{use}$	Useful rate of heat flow	W
r	Electrical resistivity (equal to ρ)	Ω m
r_i	Inner radius	m
r_o	Outer radius	m
r_v	Vapor radius	m
R	Electrical resistor	Ω
R_i	Inner resistance	Ω
R_jk	Thermal resistance	$\frac{\mathrm{K}}{\mathrm{W}}$
R_L	Load resistance	Ω
R_va	Thermal resistance for the axial heat transfer of the vapor	$\frac{\mathrm{K}}{\mathrm{W}}$
R_vc	Thermal resistance of vapor-liquid surface at condensation zone	$\frac{\mathrm{K}}{\mathrm{W}}$

R_{ve}	Thermal resistance of vapor-liquid surface at evaporation zone	$\frac{K}{W}$
S	Discretization	-
∇T	Temperature gradient	$\frac{K}{m}$
ΔT	Temperature difference (= $T_{high} - T_{low}$, = $T_h - T_c$)	K
ΔT_{TE}	Temperature difference over thermoelectric	K
ΔT_{supply}	Temperature difference over EHS	K
t	Time	s
T_c	Cold temperature	K
T_h	Hot temperature	K
T_{high}	High temperature	K
T_{low}	Low temperature	K
T_v	Vapor temperature	K
U	Voltage	V
U_L	Load voltage	V
U_{OC}	Open-circuit voltage	V
U_R	Voltage drop over resistance	V
$U_{S,n/p}$	Seebeck voltage (n- or p-type)	V
U_{th}	Thermal voltage (equivalent to Seebeck voltage)	V
V	Volume	m^3
w	Groove width	m
x	position	m
ZT	Figure of merit	-

Greek Letters

α	Seebeck coefficient	$\frac{V}{K}$
ϵ	Porosity of wick structure	%
η_{Carnot}	Carnot efficiency	%

η_{TE}	Thermoelectric efficiency	%
η_{TEG}	TEG efficiency	%
η_{max}	Maximum efficiency	%
ϑ	Wetting angle	°
Θ	Thermal resistance	$\frac{K}{W}$
Θ_{Hx}	Combined thermal resistance of hot and cold heat exchanger	$\frac{K}{W}$
λ	Heat conductivity	$\frac{W}{K\,m}$
μ_v	Dynamic viscosity	Pa s
ν_l	Kinematic viscosity	$\frac{m^2}{s}$
π	Peltier coefficient	V
ρ	Electrical resistivity	Ω m
ρ	Density	$\frac{kg}{m^3}$
ρ_v	Vapor density	$\frac{kg}{m^3}$
σ	Electrical conductivity	$\frac{S}{m}$
σ	Surface tension	$\frac{N}{m}$
τ	Thomson coefficient	$\frac{V}{K}$
φ	Angle between heat pipe and horizontal	°

Indices

1/2	Point 1/2
a/*c*/*e*	Adiabatic/condensation/evaporation
h/*c*	Hot/cold
p/*n*	P-type/n-type material
p/*v*/*w*	Pipe/vapor/wick
sim	Simulated
TE	Thermoelectric

Bibliography

Publications of the Author

[Fe++2014] Felgner, F.; Exel, L.; Nesarajah, M.; Frey, G.: Component-Oriented Modeling of Thermoelectric Devices for Energy System Design. In IEEE Transactions on Industrial Electronics, 2014, 61; pp. 1301–1310.

[NeEF2014] Nesarajah, M.; Exel, L.; Frey, G.: Modelica® Library for Dynamic Simulation of Thermoelectric Generators. In (Amaldi, A.; Tang, F. Eds.): Proceedings of the 11th European Conference on Thermoelectrics. Springer International Publishing, Cham, 2014; pp. 213–217.

[NeFF2014] Nesarajah, M.; Felgner, F.; Frey, G.: Modeling and simulation of a thermoelectric Energy Harvesting System for control design purposes: 16th International Conference on Mechatronics - IEEE Mechatronika (ME), 2014; pp. 170–177.

[NeFF2015] Nesarajah, M.; Felgner, F.; Frey, G.: Model-Based System Assessment of Thermoelectric Energy Harvesting from the Exhaust Gas Pipe of Oil-fired Heatings. In MM Science Journal, 2015; pp. 570–575.

[NeFr2014] Nesarajah, M.; Frey, G.: Object-Oriented Modeling of an Energy Harvesting System Based on Thermoelectric Generators. In (Oral, A. Y.; Bahsi, Z. B.; Ozer, M. Eds.): International Congress on Energy Efficiency and Energy Related Materials (ENEFM2013). Springer International Publishing, Cham, 2014; pp. 211–216.

[NeFr2015] Nesarajah, M.; Frey, G.: Energy Harvesting from Open Fireplaces. In (Oral, A.; Bahsi Oral, Z.; Ozer, M. Eds.): 2nd International Congress on Energy Efficiency and Energy Related Materials (ENEFM2014). Springer International Publishing, Cham, 2015; pp. 525–531.

[NeFr2016a] Nesarajah, M.; Frey, G.: Thermoelectric power generation: Peltier element versus thermoelectric generator: IECON 2016 - 42nd Annual Conference of the IEEE Industrial Electronics Society, 2016; pp. 4252–4257.

[NeFr2016b] Nesarajah, M.; Frey, G.: Multiphysics Simulation in the Development of Thermoelectric Energy Harvesting Systems. In Journal of Electronic Materials, 2016, 45; pp. 1408–1411.

[NeFr2017a] Nesarajah, M.; Frey, G.: Thermoelectric Applications for Home Use: Thermostat and Green Barbecue 2.0. [accepted]: Materials Today: Proceedings. 14th European Conference on Thermoelectrics (ECT 2016), 2017.

[NeFr2017b] Nesarajah, M.; Frey, G.: Modeling of a Heat Pipe for Using in Thermoelectric Energy Harvesting Systems. In (Oral, A. Y.; Bahsi Oral, Z. B. Eds.): 3rd International Congress on Energy Efficiency and Energy Related Materials (ENEFM2015). Springer International Publishing, Cham, 2017; pp. 183–190.

References

[Alph2014] Alphabet Energy: Thermoelectrics History Timeline. http://www.alphabetenergy.com/thermoelectrics-timeline/.

[AlRa2013] Alam, H.; Ramakrishna, S.: A review on the enhancement of figure of merit from bulk to nano-thermoelectric materials. In Nano Energy, 2013, 2; pp. 190–212.

[AnKu2012] Anatychuk, L. I.; Kuz, R. V.: Materials for Vehicular Thermoelectric Generators. In Journal of Electronic Materials, 2012, 41; pp. 1778–1784.

[AnLo2005] Antonova, E. E.; Looman, D. C.: Finite elements for thermoelectric device analysis in ANSYS: ICT 2005. 24th International Conference on Thermoelectrics, 2005; pp. 215–218.

[BaAs2009] Baghbani, R.; Ashoorirad, M.: A Power Generating System for Mobile Electronic Devices Using Human Walking Motion: 2009 Second International Conference on Computer and Electrical Engineering, 2009; pp. 385–388.

[BDBo2014] BDH; Bosch Thermotechnik GmbH: Zwei Drittel aller Heizungen veraltet. (engl.: two-thirds of all heaters are obsolete, translation by Marco Nesarajah). https://www.effizienzhaus-online.de/zwei-drittel-aller-heizungen-veraltet.

[Benn1995] Bennett, G. L.: Space Applications. In (Rowe, D. M. Ed.): CRC handbook of thermoelectrics. CRC Press, Boca Raton, FL, 1995; pp. 515–537.

[Bern2016] Bernat, M.: Aufbau eines Energy Harvesting Systems. (engl.: buildup an energy harvesting system, translation by Marco Nesarajah). Bachelorarbeit, Saarbrücken, 2016.

[Bhan1995] Bhandari, C. M.: Thermoelectric Transport Theory. In (Rowe, D. M. Ed.): CRC handbook of thermoelectrics. CRC Press, Boca Raton, FL, 1995; pp. 27–42.

[BioL2016] BioLite: Homepage of BioLite. http://www.biolitestove.com/.

[Bits2009] Bitschi, A.: Modelling of thermoelectric devices for electric power generation. ETH, Zürich, 2009.

[BMWi2014] BMWi: Making more out of energy. National Action Plan on Energy Efficiency, 2014.

[BMWi2016] BMWi: Immer mehr erneuerbare Wärme. (engl.: more and more renewable heat, translation by Marco Nesarajah). https://www.bmwi-energiewende.de/EWD/Redaktion/Newsletter/2016/07/Meldung/infografik.html.

[Br++2015] Briand, D. et al. Eds.: Micro Energy Harvesting. Wiley-VCH, Weinheim, 2015.

[BrDr1995] Bröhl, A.-P.; Dröschel, W.: Das V-Modell. Oldenburg-Verlag, München, Wien, 1995.

[Ch++2011] Chen, M.; Junling Gao; Zhengdong Kang; Jianzhong Zhang; Qungui Du; Suzuki, R. O.: Design methodology of large-scale thermoelectric generation: A hierarchical modeling approach in SPICE: 2011 IEEE Industry Applications Society Annual Meeting, 2011; pp. 1–7.

[Chen2009] Chen, M.: Design, modeling and utilization of thermoelectrical materials and devices in energy systems. Institut for Energieteknik, Aalborg Universitet, Aalborg, 2009.

[Chen2012] Chen, M.: Realistic optimal design of thermoelectric battery bank under partial lukewarming: 2012 IEEE/IAS Industrial & Commercial Power Systems Technical Conference (I&CPS), 2012; pp. 1–4.

[Chen2014a] Chen, M.: Adaptive Removal and Revival of Underheated Thermoelectric Generation Modules. In IEEE Transactions on Industrial Electronics, 2014, 61; pp. 6100–6107.

[Chen2014b] Chen, M.: Reconfiguration of Sustainable Thermoelectric Generation Using Wireless Sensor Network. In IEEE Transactions on Industrial Electronics, 2014, 61; pp. 2776–2783.

[Conr2015] Conrad Electronic: HeatPipe QY-SHP-D8-400SA. http://www.conrad.de/ce/de/product/182587/Heatpipe-02-KW-x-L-8-mm-x-400-mm-QuickCool-QY-SHP-D8-400SA.

[Da++2014] Date, A.; Date, A.; Dixon, C.; Akbarzadeh, A.: Theoretical and experimental study on heat pipe cooled thermoelectric generators with water heating using concentrated solar thermal energy. In Solar Energy, 2014, 105; pp. 656–668.

[Dono2013] Donovan, J.: New Application for Energy Harvesting. In Mouser Electronics, 2013.

[Eb++2009] Ebling, D.; Jaegle, M.; Bartel, M.; Jacquot, A.; Böttner, H.: Multiphysics Simulation of Thermoelectric Systems for Comparison with Experimental Device Performance. In Journal of Electronic Materials, 2009, 38; pp. 1456–1461.

[Eb++2016] Ebling, D. G.; Krumm, A.; Pfeiffelmann, B.; Gottschald, J.; Bruchmann, J.; Benim, A. C.; Adam, M.; Labs, R.; Herbertz, R. R.; Stunz, A.: Development of a System for Thermoelectric Heat Recovery from Stationary Industrial Processes. In Journal of Electronic Materials, 2016, 45; pp. 3433–3439.

[eFun2016] eFunda Inc.: Thermoelectric Sensitivity. http://www.efunda.com/designstandards/sensors/thermocouples/thmcple_theory.cfm?Orderby=Seebeck0C#Sensitivity.

[El++2013] Elefsiniotis, A.; Kiziroglou, M. E.; Wright, S. W.; Toh, T. T.; Mitcheson, P. D.; Becker, T.; Yeatman, E. M.; Schmid, U.: Performance evaluation of a thermoelectric energy harvesting device using various phase change materials. In Journal of Physics: Conference Series, 2013, 476; pp. 1–5.

[Euro2016] European Thermodynamic Limited: Datahseet - GM250-127-14-10.

[Fa++2014] Fateh, H.; Baker, C. A.; Hall, M. J.; Shi, L.: High fidelity finite difference model for exploring multi-parameter thermoelectric generator design space. In Applied Energy, 2014, 129; pp. 373–383.

[Fa++2015] Favarel, C.; Champier, D.; Kousksou, T.; Rozis, J.-F.; Bédécarrats, J. P.: Thermoelectricity - A Promising Complementarity with Efficient Stoves in Off-grid-areas. In Journal of Sustainable Development of Energy, Water and Environment Systems, 2015, 3; pp. 256–268.

[Fa++2016] Favarel, C.; Bédécarrats, J.-P.; Kousksou, T.; Champier, D.: Experimental analysis with numerical comparison for different thermoelectric generators configurations. In Energy Conversion and Management, 2016, 107; pp. 114–122.

[Fe++2014] Felgner, F.; Exel, L.; Nesarajah, M.; Frey, G.: Component-Oriented Modeling of Thermoelectric Devices for Energy System Design. In IEEE Transactions on Industrial Electronics, 2014, 61; pp. 1301–1310.

[FeEF2012] Felgner, F.; Exel, L.; Frey, G.: Model-based design and validation of waste heat recovery systems: 2012 IEEE International Energy Conference (ENERGYCON 2012), 2012; pp. 265–270.

[Fisc2015] Fischer Elektronik GmbH & Co. KG: Segment cooling aggregate. LA 1. http://www.fischerelektronik.de/web_fischer/en_GB/heatsinks/D03/Segment%20cooling%20aggregates/PG/LA1/search.xhtml.

[Fleu2016] Fleurial, J.-P.: Discussion of the author's poster at ECT2016. oral, Lisbon, Portugal, 2016.

[Ga++2012] Gao, J.; Sun, K.; Ni, L.; Chen, M.; Kang, Z.; Zhang, L.; Xing, Y.; Zhang, J.: A Thermoelectric Generation System and Its Power Electronics Stage. In Journal of Electronic Materials, 2012, 41; pp. 1043–1050.

[Gaug1944] Gaugler, R. S.: Heat transfer device. Google Patents, 1944.

[Gerw2015] Gerwin Möbus GmbH: Kleines Heizungs-ABC. (engl.: basics of heaters, translation by Marco Nesarajah). http://www.gerwinmoebus.de/wissenswertes/kleines-heizungs--abc/index.html.

[Gold2010] Goldsmid, H. J.: Introduction to thermoelectricity. Springer, Heidelberg, New York, 2010.

[Hall1995] Hall, W. C.: Generator Applications. In (Rowe, D. M. Ed.): CRC handbook of thermoelectrics. CRC Press, Boca Raton, FL, 1995; pp. 503–513.

[Hebe2016] Hebei I. T. (Shanghai) Co, Ltd: Datasheet - TEC1-12706.

[Hi-Z2016] Hi-Z Technology, I.: Datasheet of HZ-9. http://www.hi-z.com//wp-content/uploads/2016/09/Hi-Z-Data-Sheet-HZ-9-1.pdf.

[Hone2015] Honeywell: Rondostat HR 20, 2015.

[Hs++2011] Hsu, C.-T.; Huang, G.-Y.; Chu, H.-S.; Yu, B.; Yao, D.-J.: Experiments and simulations on low-temperature waste heat harvesting system by thermoelectric power generators. In Applied Energy, 2011, 88; pp. 1291–1297.

[IWU2017] IWU: Gradtagszahlen_Deutschland.xls, Datenquelle: Deutscher Wetterdienst (DWD). (engl.: degree day count Germany, data source: German weather service , translation by Marco Nesarajah)., 2017.

[Ju++2008] Junior, C.; Richter, C.; Tegethoff, W.; Lemke, N.; Köhler, J.: Modeling and Simulation of a Thermoelectric Heat Exchanger using the Object-Oriented Library TIL. In Modelica 2008, 2008, March 3rd-4th; pp. 437–445.

[Juni2010] Junior, C.: Analyse thermoelektrischer Module und Gesamtsysteme. (engl.: analysis of thermoelectric modules and overall systems , translation by Marco Nesarajah). Eul, Lohmar, Köln, 2010.

[Kabe2006] Kabelac, S.: VDI-Wärmeatlas. [Berechnungsunterlagen für Druckverlust, Wärme- und Stoffübergang]. Springer-Verlag Berlin Heidelberg, Berlin, Heidelberg, 2006.

[Ki++2014] Kiziroglou, M. E.; Wright, S. W.; Toh, T. T.; Mitcheson, P. D.; Yeatman, E. M.: Design and Fabrication of Heat Storage Thermoelectric Harvesting Devices. In IEEE Transactions on Industrial Electronics, 2014, 61; pp. 302–309.

[Kö++2016] König, J. D.; Bartholomé, K.; Böttner, H.; Jänsch, D.; Klein Altstedde, M.; Köhne, M.; Nurnus, J.; Roch, A.; Tarantik, K.: Thermoelektrik: Stom aus Abwärme. Thermoelektrische Generatoren machen Systeme energieautark und sparen Energie (engl.: Thermoelectric: electricity from waste heat, translation by Marco Nesarajah). In BINE-Themeninfo, 2016.

[Köni2016] König, J.: Energy Harvesting. Abwärmenutzung mit Thermoelektrik. http://www.ipm.fraunhofer.de/de/gf/funktionelle-materialien-systeme/anw/energyharvesting.html.

[Kü++2010] Kühne, I.; Frey, A.; Seidel, H.; Kreusel, J.: Energieautarke Mikrosysteme unter Ausnutzung mikromechanischer Energiewandler. (engl.: Energy-efficient microsystems using micromechanical energy converters, translation by Marco Nesarajah)., 2010.

[LaLu2011] Laird, I.; Lu, D. D.: SPICE steady state modelling of thermoelectric generators involving the Thomson effect: IECON 2011 - 37th Annual Conference of IEEE Industrial Electronics, 2011; pp. 1584–1589.

[Li++2010] Li, P.; Cai, L.; Zhai, P.; Tang, X.; Zhang, Q.; Niino, M.: Design of a Concentration Solar Thermoelectric Generator. In Journal of Electronic Materials, 2010, 39; pp. 1522–1530.

[Li++2017] Liu, T.; Wang, T.; Luan, W.; Cao, Q.: Optimal Number of Thermoelectric Couples in a Heat Pipe Assisted Thermoelectric Generator for Waste Heat Recovery. In Journal of Electronic Materials, 2017, 46; pp. 3137–3144.

[LiBe2007] Lineykin, S.; Ben-Yaakov, S.: Modeling and Analysis of Thermoelectric Modules. In IEEE Transactions on Industry Applications, 2007, 43; pp. 505–512.

[Ma++2014] Maganga, O.; Phillip, N.; Burnham, K. J.; Montecucco, A.; Siviter, J.; Knox, A.; Simpson, K.: Hardware Implementation of Maximum Power Point Tracking for Thermoelectric Generators. In Journal of Electronic Materials, 2014, 43; pp. 2293–2300.

[MaBu1995] Marlow, R.; Burke, E.: Module Design and Fabrication. Thermoelectric Module Fabrication. In (Rowe, D. M. Ed.): CRC handbook of thermoelectrics. CRC Press, Boca Raton, FL, 1995; pp. 605–606.

[Maxi2015] Maxim Integrated Inc.: Glossary Definition for Energy Harvesting. Glossary Term: Energy Harvesting.

https://www.maximintegrated.com/en/glossary/definitions.mvp/term/Energy%20Harvesting/gpk/1144.

[McNa1995] McNaughton, A. G.: Commercially Available Generators. In (Rowe, D. M. Ed.): CRC handbook of thermoelectrics. CRC Press, Boca Raton, FL, 1995; pp. 459–469.

[MeLi2000] Merz, R.; Litz, L.: Objektorientierte mathematische Modellierung. (engl.: object-oriented mathematical modeling, translation by Marco Nesarajah). In Informatik-Spektrum, 2000, 23; pp. 90–99.

[Mich2004] Michael Klotsche: Entwicklung, Fertigung und experimentelle Untersuchung von kostengünstigen Hochtemperatur-Heatpipes. (engl.: development, manufacturing and experimental investigation of cost-effective high-temperature heatpipes, translation by Marco Nesarajah). Diplomarbeit, München, 2004.

[Micr2015] Micropelt: Der energieautarke Heizkörperstellantrieb. (engl.: The self-powered radiator actuator, translation by Marco Nesarajah). http://micropelt.de/downloads/itrv_heft.pdf.

[Miks2011] Miksch, B.: Energy Harvesting. Energieautarke Systeme, Stuttgart, 2011.

[Mode2016] Modelica Association: Modelica Homepage. https://modelica.org/.

[MoKK2015] Montecucco, A.; Knox, A.; Knox, A. R.: Maximum Power Point Tracking Converter Based on the Open-Circuit Voltage Method for Thermoelectric Generators. In IEEE Transactions on Power Electronics, 2015, 30; pp. 828–839.

[MoKn2014] Montecucco, A.; Knox, A. R.: Accurate simulation of thermoelectric power generating systems. In Applied Energy, 2014, 118; pp. 166–172.

[MoSK2012] Montecucco, A.; Siviter, J.; Knox, A. R.: Simple, fast and accurate maximum power point tracking converter for thermoelectric generators, 2012; pp. 2777–2783.

[Nard2011] Narducci, D.: Do we really need high thermoelectric figures of merit? A critical appraisal to the power conversion efficiency of thermoelectric materials. In Applied Physics Letters, 2011, 99; pp. 1–3.

[NeEF2014] Nesarajah, M.; Exel, L.; Frey, G.: Modelica® Library for Dynamic Simulation of Thermoelectric Generators. In (Amaldi, A.; Tang, F. Eds.): Proceedings of the 11th European Conference on Thermoelectrics. Springer International Publishing, Cham, 2014; pp. 213–217.

[NeFF2014] Nesarajah, M.; Felgner, F.; Frey, G.: Modeling and simulation of a thermoelectric Energy Harvesting System for control design purposes: 16th International Conference on Mechatronics - IEEE Mechatronika (ME), 2014; pp. 170–177.

[NeFF2015] Nesarajah, M.; Felgner, F.; Frey, G.: Model-Based System Assessment of Thermoelectric Energy Harvesting from the Exhaust Gas Pipe of Oil-fired Heatings. In MM Science Journal, 2015; pp. 570–575.

[NeFr2014] Nesarajah, M.; Frey, G.: Object-Oriented Modeling of an Energy Harvesting System Based on Thermoelectric Generators. In (Oral, A. Y.; Bahsi, Z. B.; Ozer, M. Eds.): International Congress on Energy Efficiency and Energy Related Materials (ENEFM2013). Springer International Publishing, Cham, 2014; pp. 211–216.

[NeFr2015] Nesarajah, M.; Frey, G.: Energy Harvesting from Open Fireplaces. In (Oral, A.; Bahsi Oral, Z.; Ozer, M. Eds.): 2nd International Congress on Energy Efficiency and Energy Related Materials (ENEFM2014). Springer International Publishing, Cham, 2015; pp. 525–531.

[NeFr2016a] Nesarajah, M.; Frey, G.: Thermoelectric power generation: Peltier element versus thermoelectric generator: IECON 2016 - 42nd Annual Conference of the IEEE Industrial Electronics Society, 2016; pp. 4252–4257.

[NeFr2016b] Nesarajah, M.; Frey, G.: Multiphysics Simulation in the Development of Thermoelectric Energy Harvesting Systems. In Journal of Electronic Materials, 2016, 45; pp. 1408–1411.

[NeFr2017a] Nesarajah, M.; Frey, G.: Thermoelectric Applications for Home Use: Thermostat and Green Barbecue 2.0. [accepted]: Materials Today: Proceedings. 14th European Conference on Thermoelectrics (ECT 2016), 2017.

[NeFr2017b] Nesarajah, M.; Frey, G.: Modeling of a Heat Pipe for Using in Thermoelectric Energy Harvesting Systems. In (Oral, A. Y.; Bahsi Oral, Z. B. Eds.): 3rd International Congress on Energy Efficiency and Energy Related Materials (ENEFM2015). Springer International Publishing, Cham, 2017; pp. 183–190.

[Nowo2003] Nowotka, F.: Abgastemperatur bei Öl-Heizkesseln. (engl.: exhaust gas temperature for oil-fired heating boiler, translation by Marco Nesarajah). http://www.heiz-tipp.de/ratgeber-88-abgastemperatur.html.

[O'++2015] O'Shaughnessy, S. M.; Deasy, M. J.; Doyle, J. V.; Robinson, A. J.: Adaptive design of a prototype electricity-producing biomass cooking stove. In Energy for Sustainable Development, 2015, 28; pp. 41–51.

[Onot2008] Ong, K. S.; others: Heat pipes. In Jurutera, 2008.

[Otte2013] Otter, M.: Modelica Overview, 2013.

[Pasc2015] Paschotta, R.: Abgastemperatur. (engl.: exhaust gas temperature, translation by Marco Nesarajah). https://www.energie-lexikon.info/abgastemperatur.html.

[Ph++2013] Phillip, N.; Maganga, O.; Burnham, K. J.; Ellis, M. A.; Robinson, S.; Dunn, J.; Rouaud, C.: Investigation of Maximum Power Point Tracking for Thermoelectric Generators. In Journal of Electronic Materials, 2013, 42; pp. 1900–1906.

[Poll1995] Pollock, D. D.: General Principles and Theoretical Considerations. In (Rowe, D. M. Ed.): CRC handbook of thermoelectrics. CRC Press, Boca Raton, FL, 1995.

[QiHa2009] Qiu, K.; Hayden, A.: A Natural-Gas-Fired Thermoelectric Power Generation System. In Journal of Electronic Materials, 2009, 38; pp. 1315–1319.

[QiHa2011] Qiu, K.; Hayden, A. C. S.: Development of Thermoelectric Self-Powered Heating Equipment. In Journal of Electronic Materials, 2011, 40; pp. 606–610.

[Quad2016] Quadflieg, D.: FNN-Störungsstatistik 2015. (engl.: FNN-fault statistics, translation by Marco Nesarajah)., Berlin, 2016.

[Quas2010] Quaschning, V.: Erneuerbare Energien und Klimaschutz. Hintergründe - Techniken - Anlagenplanung - Wirtschaftlichkeit (engl.: Renewable Energy and Climate Protection, translation by Marco Nesarajah). Hanser, München, 2010.

[ReMK2014] Reay, D. A.; McGlen, R.; Kew, P. A.: Heat pipes, 2014.

[Reut2009] Reuters: Norway opens world's first osmotic power plant. https://www.cnet.com/news/norway-opens-worlds-first-osmotic-power-plant/.

[RoMa1995] Rowe, D. M.; Matsuura, K.: Low-Temperature Heat Conversion. In (Rowe, D. M. Ed.): CRC handbook of thermoelectrics. CRC Press, Boca Raton, FL, 1995; pp. 573–593.

[Sche2007] Schedlinski, R.: Häufigste Ursachen für Ausfälle von TEG. (engl.: most common causes for failures of TEG, translation by Marco Nesarajah). http://www.thermalforce.de/de/download/haeufigste_ursachen_fuer_ausfaelle_von_thermogeneratoren.pdf.

[Schw2014] Schwager, J.: Informationsportal für Energy Harvesting. (engl.: information portal for energy harvesting, translation by Marco Nesarajah). http://www.harvesting-energy.de/.

[Scyt2014] Scythe EU GmbH: Specifications of the fan. E-Mail, Saarbrücken, 2014.

[Scyt2015] Scythe Co. LTD.: Scythe Katana 4. product page. http://www.scythe-eu.com/unternehmen/firmenprofil.html.

[Seik2012] Seiko: SEIKO World's First. http://www.seikowatches.com/heritage/worlds_first.html.

[Shab2010] Shabany, Y.: Heat transfer. Thermal management of electronics. CRC Press, Boca Raton, 2010.

[SnTo2008] Snyder, G. J.; Toberer, E. S.: Complex thermoelectric materials. In Nature Materials, 2008, 7; pp. 105–114.

[Snyd2004] Snyder, G. J.: Application of the compatibility factor to the design of segmented and cascaded thermoelectric generators. In Applied Physics Letters, 2004, 84; pp. 2436–2438.

[Snyd2008] Snyder, G. J.: Thermoelectric Energy Harvesting. In (Priya, S.; Inman, D. J. Eds.): Energy harvesting technologies. Springer, New York, London, 2008.

[Snyd2016] Snyder, G. J.: Brief History of Thermoelectrics. http://thermoelectrics.caltech.edu/thermoelectrics/history.html.

[Sp++2015] Spagnuolo, G.; Petrone, G.; Lehman, B.; Ramos Paja, Carlos Andres; Zhao, Y.; Orozco Gutierrez, Martha Lucia: Control of Photovoltaic Arrays: Dynamical Reconfiguration for Fighting Mismatched Conditions and Meeting Load Requests. In IEEE Industrial Electronics Magazine, 2015, 9; pp. 62–76.

[Stei2008] Steingart, D.: Power Sources for Wirless Sensor Networks. In (Priya, S.; Inman, D. J. Eds.): Energy harvesting technologies. Springer, New York, London, 2008.

[Step2006] Stephan, P.: Wärmerohre. (engl.: Heat pipes).: VDI-Wärmeatlas. CD-ROM 3.0. Springer, Berlin, Heidelberg, 2006.

[Stev2001] Stevens, J. W.: Optimal design of small ΔT thermoelectric generation systems. In Energy Conversion and Management, 2001, 42; pp. 709–720.

[Su++2015] Suzuki, R. O.; Fujisaka, T.; Ito, K. O.; Meng, X.; Sui, H.-T.: Dimensional Analysis of Thermoelectric Modules Under Constant Heat Flux. In Journal of Electronic Materials, 2015, 44; pp. 348–355.

[TECT2014] TECTEG MFR: Video post about Differences Between TEC and TEG. http://thermoelectric-generator.com.

[Ther2015] Thermalforce: Datasheet - TEG 199-200-5. http://www.thermalforce.de/de/product/thermogenerator/TG199-200-5k.pdf.

[Ther2016] Thermonamic Electronics Corp., Ltd: Thermonamic Homepage. www.thermonamic.com.

[TrSu2006] Tritt, T. M.; Subramanian, M. A.: Thermoelectric Materials, Phenomena, and Applications: A Bird's Eye View. In MRS Bulletin, 2006; pp. 188–198.

[TsLi2010] Tsai, H.-L.; Lin, J.-M.: Model Building and Simulation of Thermoelectric Module Using Matlab/Simulink. In Journal of Electronic Materials, 2010, 39; pp. 2105–2111.

[VDE2016] VDE: Auf dem Weg in ein neues Energiezeitalter. (engl.: On the way to a new energy era; translated by Marco Nesarajah). In VDE dialog, 2016, 01; pp. 30–31.

[Vini2009] Vining, C. B.: An inconvenient truth about thermoelectrics. In Nature Materials, 2009, 8; pp. 83–85.

[Zerv2016] Zervos, H.: Thermoelectric Energy Harvesting 2016-2026. Technologies, devices & applications for thermoelectric generators, 2016.

[Zh++2011] Zhu, J.; Gao, J.; Chen, M.; Zhang, J.; Du, Q.; Rosendahl, L. A.; Suzuki, R. O.: Experimental Study of a Thermoelectric Generation System. In Journal of Electronic Materials, 2011, 40; pp. 744–752.

[Zi++2010] Ziolkowski, P.; Poinas, P.; Leszczynski, J.; Karpinski, G.; Müller, E.: Estimation of Thermoelectric Generator Performance by Finite Element Modeling. In Journal of Electronic Materials, 2010, 39; pp. 1934–1943.